ARCHIVES OF ACOUSTICS
25, 3, 275–281 (2000)

IMPULSIVENESS OF DISCOTHEQUE EXPOSURES

A. JAROSZEWSKI and A. JAROSZEWSKA

Laboratory of Music Acoustics,
F. Chopin Academy of Music
(00-368 Warszawa, ul. Okólnik 2, Poland)

Long term average spectra, cumulative distribution functions and impulsiveness in terms of $L_{peak} - L_{eq}$ and in terms of kurtosis were determined for 8 Warsaw discotheques. The results are discussed with reference to hearing damage risk.

1. Introduction

In one of the Medical Research Council reports [17], a number of discotheque attenders in the United Kingdom is estimated at 2 to 6 mln. These persons spend in the discotheques from 156 to 234 hrs in a year, over a period of 5 to 7 years on the average. The equivalent sound pressure level L_{eq} (A) for a year amounts in these discotheques from 80 to 95 dB. In the polish society of youngsters attending the discotheques, a number of visits to the discotheque amounts on the average to 30 in a year. This number gives from 120 to 220 hrs of the discotheque exposure in a year at an equivalent sound pressure level L_{eq} (A) for a year amounting from 84 to 97 dB. The number of discotheque attenders in Poland is unknown but estimated at 3 mln approximately.

The effects of such exposures were investigated by many researchers but the results of these investigations are in substantial measure controversial. Fearn and Hanson in numerous investigations carried out over a period of 27 years, FEARN and HANSON [4, 6–9]. FEARN [5, 10, 11], reported substantial hearing loss of 10 dB in the whole auditory range, 15 dB or more at 4 kHz and 20 dB or more at 6 kHz in large proportion of the tested persons (7–30%) in the examined samples in age categories of mainly 11–25 years.

In the samples of musicians working in the discotheques and youth clubs a proportion of persons with such hearing loss reaches 50.5% according to FEARN [11]. These data are in agreement with the data from AXELSSON and LINDGREN [2] for example, who found hearing loss in 13–30% of the exposed subjects, and the data from AXELSSON *et al.* [1] who found hearing loss of 20 dB or more at various frequencies in 15% of the examined sample, while WEST and EVANS [21] found poorer frequency resolution in 15% of the sample of exposed subjects. In the data from JAROSZEWSKI *et al.* [13] hearing loss of

18.8 dB on average at 6 kHz was found in 60% of the examined sample of 98 musicians, while JAROSZEWSKI and RAKOWSKI [12] found hearing loss 20 to 50 dB deep in the whole sample of the tested group of pop/rock musicians.

On the other hand CARTER *et al.* [3] in investigation carried out in Australia and MEYER–BISCH [16] in France did not observe differences between audiometric data from exposed and unexposed persons. However, their opinion was based on estimation of the averages in large samples of the examined population. Here an observation from FEARN and HANSON [6] should be cited: "*What we are concerned with is the top 5 – 10% of the affected population. For this purpose the average is too insensitive for judgement.*" It should also be noted that in the results from Carter and Meyer–Bisch, hearing loss of from 9.4 dB at 6 kHz to 13 dB at 12 kHz is present in the data from both exposed and control group of subjects.

A distinct disproportion appears in comparison of the depth of the measured hearing loss with the measures of exposures from which this loss resulted. Namely, these losses are substantially larger than those predicted on the grounds of the measures of the exposition and number of years of exposure. In many cases hearing loss of 10 – 15 dB in the upper part of auditory range, and selective hearing loss of V-dip type (notch) of 15 – 40 dB, are found after only 25 to 70 exposures in the discotheques in a period of only one to two years. It should be stressed however, that this observation does not pertain to averages for the tested samples, but only to from 15 to 25% of the affected.

According to the working hypothesis larger damaging effect of the discotheque exposures than this predicted on the grounds of the equal energy hypothesis and equivalent sound pressure levels may result from partially impulsive character of these exposures. This possibility was been pointed out in the earlier publication, JAROSZEWSKI *et al.* [14] in which "impulsiveness" was determined for ten Warsaw discotheques, a measure never applied to the discotheque exposures before. The present report is a continuation of this investigation and contains statistical analysis of the impulsiveness of sound pressure levels in discotheques in terms of $L_{\text{peak}} - L_{\text{eq}}$ and in terms of kurtosis.

2. Procedure and apparatus

Material used in the analysis was obtained from 8 routine presentations in 8 Warsaw discotheques. The duration of these presentations typically equalled to from 4 ½ to 9 hrs, usually without breaks or with very short breaks of 1 to 2 min. All presentations were recorded full length on magnetic tape using digital magnetic recorder DAT SONY type TCD-D10 PRO-II and omnidirectional condenser microphone Bruel & Kjaer type 4155. Sound pressure levels were determined with the use of Bruel & Kjaer Precision Integrating Sound Level Meter type 2230 with 1/2" condenser microphone type 4155.

The raw data containing 4 hrs of recorded music was next analysed typologically with the use of computerised procedure. With that procedure 63 selections of the recorded music, 5 min each were selected, characteristic for the whole presentations in all discotheques examined. For these selections of recorded music, long term average spectra (LTAS) in 1/3 octave bands, sound pressure levels L_{50}, L_1, L_{eq} and the impulsiveness

distribution functions, defined as a difference $I = L_{peak} - L_{eq}$ were determined. Also were determined distribution functions of the instantaneous sound pressure levels and the values of kurtosis as an alternative measure of the impulsiveness.

Statistical analysis and spectral analysis were carried out with the use of HP class PC minicomputer and of the MATLAB program procedures. Kurtosis was determined with the use of WaveStat program prepared in this laboratory.

3. Results

The results of the analysis in terms of LTAS, and cumulative distribution functions are presented in Fig. 1 to Fig. 3 for the discotheque with the largest equivalent sound pressure levels and in Fig. 4 to Fig. 6 for the discotheque with the smallest sound pressure levels. Distribution functions of the instantaneous sound pressure levels and the values of the kurtosis are given in Fig. 7 and Fig. 8. Statistical characteristics of the presentations in eight examined discotheques are given in Table 1.

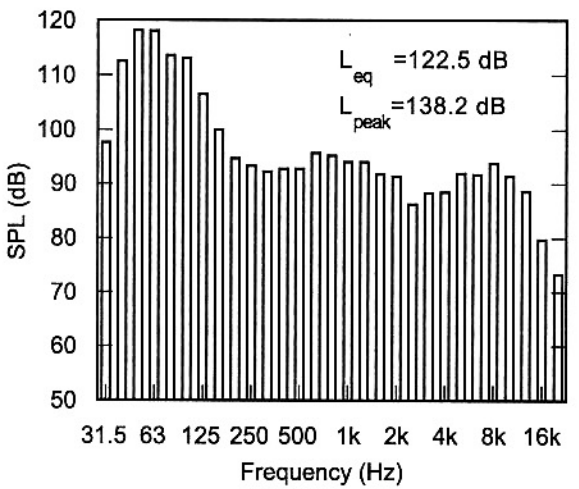

Fig. 1. The averaged 1/3 octave sound pressure spectrum for the discotheque with the largest equivalent sound pressure level.

Table 1. Statistical characteristics of presentations in 8 Warsaw discotheques.

Discotheque	L_{eq} (dB)	L_{peak} (dB)	β_2	L_1 (dB)	L_{10} (dB)	L_{50} (dB)	CF* (dB)	I (dB)
Akwarium	112.8	133.9	5.5 – 6.3	122.7	117.2	106.5	9.9	21.1
Colosseum	122.5	138.2	3.5 – 5.2	132.2	127.1	116.8	9.7	15.7
Hades	113.5	131.6	3.1 – 5.6	123.0	117.8	108.8	9.5	18.1
Hybrydy	113.7	133.6	3.6 – 5.5	123.7	118.1	107.8	10.0	19.9
Klub Medyka	109.0	130.1	4.2 – 6.0	119.9	112.9	102.2	10.9	21.1
Park	108.7	135.3	4.4 – 5.8	119.3	112.9	102.0	10.6	26.6
Remont	117.3	139.0	3.4 – 8.0	127.4	121.4	111.6	10.1	21.7
Stodoła	112.5	129.4	4.0 – 5.7	122.7	116.6	107.2	10.2	16.9
Mean over all	116.1	139.0	3.1 – 8.0	127.9	119.5	107.8	11.8	22.9

* CF – crest factor

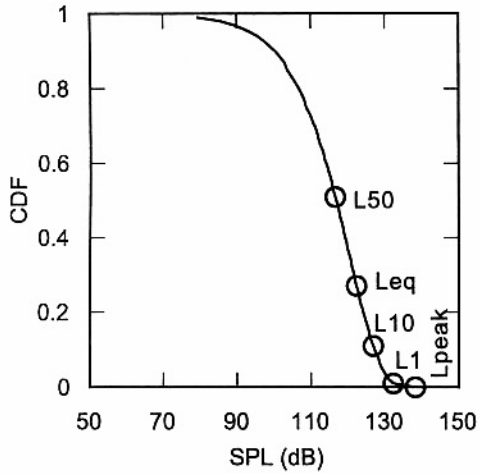

Fig. 2. Cumulative distribution function of the instantaneous sound pressure levels for the discotheque with the largest equivalent sound pressure level.

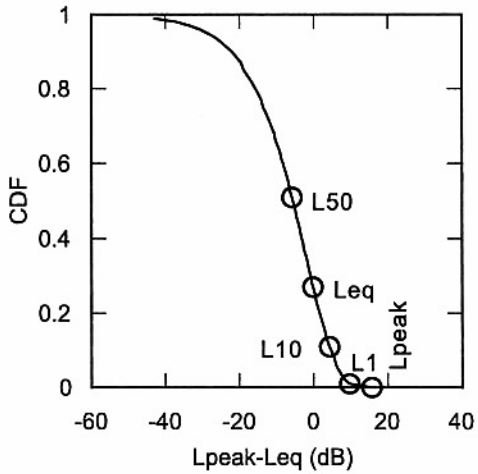

Fig. 3. Impulsiveness in the discotheque with the largest equivalent sound pressure level.

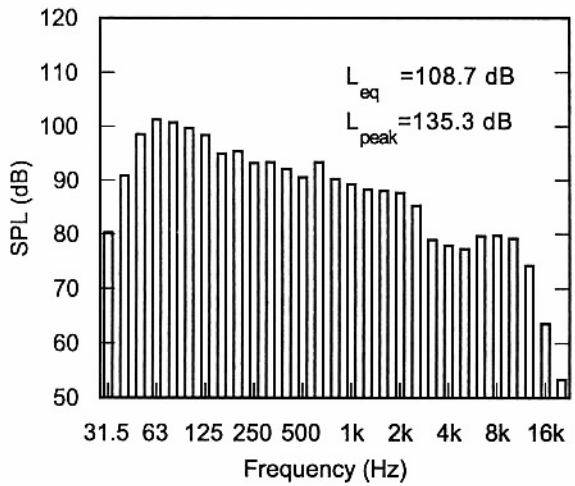

Fig. 4. The averaged 1/3 octave sound pressure spectrum for the discotheque with the smallest equivalent sound pressure level.

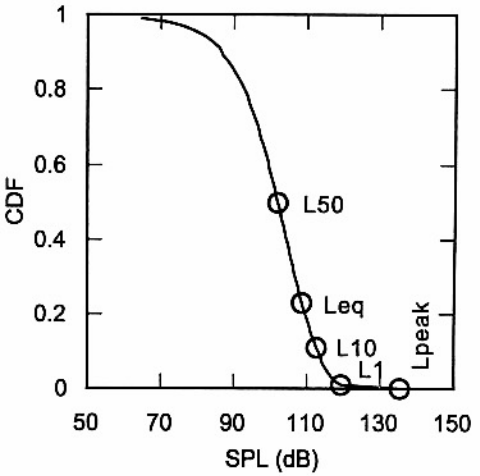

Fig. 5. Cumulative distribution function of the instantaneous sound pressure levels for the discotheque with the smallest equivalent sound pressure level.

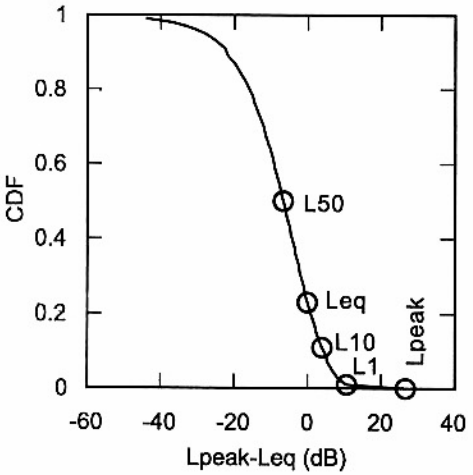

Fig. 6. Impulsiveness in the discotheque with the smallest equivalent sound pressure level.

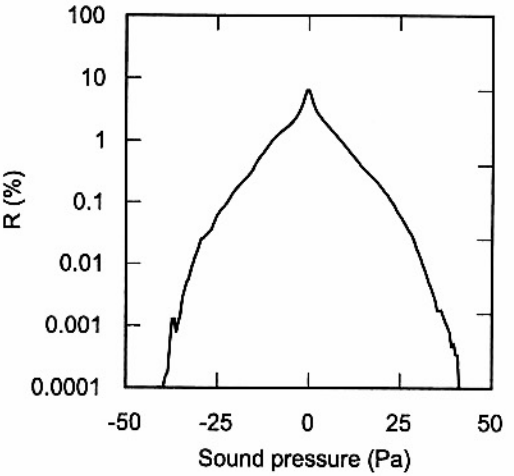

Fig. 7. Distribution of the instantaneous sound pressure levels in the sample recorded in the discotheque with the largest equivalent sound pressure level, kurtosis $\beta_2 = 4.8$.

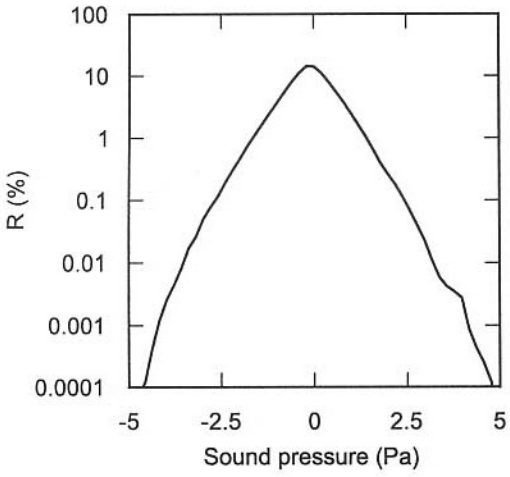

Fig. 8. Distribution of the instantaneous sound pressure levels in the sample recorded in the discotheque with the smallest equivalent sound pressure level, kurtosis $\beta_2 = 4.7$.

4. Discussion and conclusion

In the results obtained the impulsiveness was found to be at a level of 20 – 26 dB in terms of $L_{\text{peak}} - L_{\text{eq}}$ determinant, and at a level of 4.7 in terms of kurtosis. These values correspond to the values of impulsiveness, which in industrial exposures are recognised as leading to hearing damage larger than those from the stationary continuous noise, e.g. THIERY and MEYER–BISCH [20]. It should be observed however, that Thiery and Meyer–Bisch determined damaging effects of the partially impulsive exposures at a level of 87 – 90 dB (A), whilst in the case of Warsaw discotheques the sound pressure levels amount to from 100 to 110 dB (A). Thus the damaging effect may be larger in spite of the relatively lower values of impulsiveness.

In estimation of the results presented it should be recognised that the measurements were carried out with the use of apparatus and tools functioning in the range of frequencies up to only 20 kHz. From the recent reports by ROGOWSKI *et al.* [18, 19] and JAROSZEWSKI *et al.* [15] it appears that the examination of the impulsiveness in the music material should be performed in the frequency range up to 100 kHz at least, because a power spectral density for cymbals for example remains at a level of 90 dB up to approximately 60 kHz. The preliminary experimental data by the present authors indicate that the supersonic components of the spectrum may have substantial contribution in the damaging effects of the exposure. Therefore, the results presented supply only preliminary estimation of the effects of impulsive exposure in the discotheques.

Acknowledgements

This work was supported by grant T 07B 051 15 from the State Committee for Scientific Research.

References

[1] A. AXELSSON, T. JERSON, U. LINDBERG and F. LINDGREN, *Early noise-induced hearing loss in teenage boys*, Scand. Audiology, **10**, 91–96 (1981).

[2] A. AXELSSON and F. LINDGREN, *Does pop music cause hearing damage?*, Audiology, **16**, 432–437 (1977).

[3] N.L. CARTER, R.L. WAUGH, K. KEEN, N. MURRAY and V.G. BULTEAU, *Amplified music and young people's hearing*, Medical Journal of Australia, August 7, 125–128 (1982).

[4] R.W. FEARN and D.R. HANSON, *Hearing acuity in young people exposed to pop music and other noise*, The Lancet, August 5th, 203–205 (1975).

[5] R.W. FEARN, *Hearing loss caused by different exposures to amplified pop music*, J. of Sound and Vibration, **47**, 454–456 (1976).

[6] R.W. FEARN and D.R. HANSON, *Hearing level measurements of students aged 18–25 years exposed to amplified pop music*, J. of Sound and Vibration, **94**, 591–595 (1984).

[7] R.W. FEARN and D.R. HANSON, *Hearing level measurements of schoolchildren aged 9–16 exposed to amplified pop music*, J. of Sound and Vibration, **95**, 430–434 (1984).

[8] R.W. FEARN and D.R. HANSON, *Hearing level of young subjects exposed to amplified music*, J. of Sound and Vibration, **128**, 509–512 (1989).

[9] R.W. FEARN and D.R. HANSON, *Hearing threshold of young people aged 11–25 years: A review and overall assessment*, J. of Sound and Vibration, **138**, 155–161 (1990).

[10] R.W. FEARN, *Serial audiometry in young subjects aged 11–25 years exposed to amplified music*, J. of Sound and Vibration, **150**, 350–355 (1991).

[11] R.W. FEARN, *Hearing loss in musicians*, J. of Sound and Vibration, **163**, 372–378 (1993).

[12] A. JAROSZEWSKI and A. RAKOWSKI, *Loud music induced thresholds shifts and damage risk prediction*, Archives of Acoustics, **19**, 311–321 (1994).

[13] A. JAROSZEWSKI, T. FIDECKI, P. ROGOWSKI and R. MONIAK, *Exposures and hearing thresholds in loud pop/rock music* [in Polish], [in:] Akustyka w Technice Medycynie i Kulturze, Institute of Fundamental Technological Research, Polish Academy of Sciences, (Ed.), 291–300 (1995).

[14] A. JAROSZEWSKI, T. FIDECKI and P. ROGOWSKI, *Sound pressure level distributions in 10 Warsaw discotheques and TTS_2 in attendants and performers*, Proceedings of the 1997 International Congress on Noise Control Engineering, Budapest, 25–27.VIII.1997, Vol. II, 1163–1166 (1997).

[15] A. JAROSZEWSKI, P. ROGOWSKI and A. RAKOWSKI, *Statistical analysis of the sound pressure levels in emission of percussion instruments during training sessions* [in Polish], Proc. of the XLVI Open Seminar on Acoustics, Kraków – Zakopane, 14–17.09.1999, Polish Acoustical Society, (Ed.), 169–174 (1999).

[16] C. MEYER–BISCH, *Epidemiological evaluation of hearing damage related to strongly amplified music (personal cassette players, discotheques, rock concerts) — high-definition audiometric survey on 1364 subjects*, Audiology, **35**, 121–142 (1996).

[17] MRC, Medical Research Council, Institute of Hearing Research, *Damage to hearing arising from leisure noise*, Brit. Journal of Audiology, **20**, 157–164 (1986).

[18] P. ROGOWSKI, A. RAKOWSKI and A. JAROSZEWSKI, *High frequency hearing loss in percussion players*, Proc. 11th International Conference on Noise Control, 2–4 June, Krynica 1998, 163–170, 1998.

[19] P. ROGOWSKI, A. RAKOWSKI and A. JAROSZEWSKI, *High frequency hearing loss in percussion players*, Archives of Acoustics, **24**, 119–127 (1999).

[20] L. THIERY and C. MEYER–BISCH, *Hearing loss due to partly impulsive industrial noise exposure between 87 and 90 dB (A)*, J. Acoust. Soc. Amer., **84**, 651–659 (1988).

[21] P.D.B. WEST and E.F. EVANS, *Early detection of hearing damage in young listeners resulting from exposure to amplified music*, Brit. Journal of Audiology, **24**, 89–103 (1990).

ARCHIVES OF ACOUSTICS
25, 3, 283–289 (2000)

SOUND PRESSURE LEVELS IN EMISSION OF PERCUSSION INSTRUMENTS DURING TRAINING SESSIONS

A. JAROSZEWSKI, P. ROGOWSKI and A. RAKOWSKI

Laboratory of Music Acoustics,
F. Chopin Academy of Music
(00-368 Warszawa, ul. Okólnik 2, Poland)

Sounds of selected percussion instruments played in individual training sessions of students-percussion players were recorded and analysed. In statistical signal analysis the "impulsiveness" in terms of $L_{max} - L_{eq}$ and in terms of kurtosis, as an alternative measure were determined. Signal recording and spectral analysis were performed in the frequency range up to 96 kHz.

1. Introduction

The effects of exposure to sounds of percussion instruments were observed already in early investigations pertaining to the hearing damage risk in musicians, e.g. JAHTO and HELLMAN [8], GRYCZYŃSKA and CZYŻEWSKI [6], AXELSSON and LINDGREN [1]. These observations were next confirmed by the data from KARLSSON *et al.* [10], OSTRI *et al.* [11] and recently by the data from remarkable work by FEARN [5]. However, also conflicting data were reported, e.g. WESTMORE and EVERSDEN [15], JOHNSON *et al.* [9], in which no correspondence was found between the instrument type and hearing loss.

It should be noted, that in all the investigations cited, except for that by JOHNSON *et al.* [9], hearing thresholds were determined in the frequency range from 0.25 or 0.5 kHz to 8 kHz only. Also, hearing losses up to 30 dB (without correction for the loss specific for the given age) were, as it seems, underestimated, KARLSSON *et al.* [10], ROYSTER *et al.* [13]. Selective hearing loss (V-dip type) of the order of 20 dB at 4 or 6 kHz (KARLSSON *et al.* [10]) or high frequency sloping hearing loss reaching 28 dB (over 10 dB after correction for age, ROYSTER *et al.* [13]) should not be neglected either.

In a remarkable work by FEARN [5] percussion players were identified as exposed to probably the highest peak sound pressure levels in music exposures, reaching 140 – 146 dB or even 148 dB (depending on instrument type, room characteristics etc.) and thus experiencing the highest risk of hearing damage. In the examined sample of musicians aged 16 – 30, Fearn found hearing loss over 15 dB at 4 kHz or 20 dB at 6 kHz in 46% of percussion players, while in musicians playing brass, woodwinds and strings the proportion

with hearing loss was significantly lower. It should be noted according to FEARN [5], that extreme sound pressure levels are present in the orchestra in the neighbourhood of percussion and brass section. In these places, often second violins, violas and violoncellos are situated, sometimes also woodwinds. Hence, the effects of exposure to percussion sounds pertain to a high degree also to other musicians, a fact which very often is disregarded. SCHACKE [14] in turn, found supernormal hearing loss in 60% in a sample of percussion players examined.

Examination of the hearing thresholds in young percussion players in the frequency range up to 16 kHz presented in the earlier paper, ROGOWSKI *et al.* [12] estimated the specific high frequency sloping hearing loss as 24 dB higher on the average than in musicians who were less exposed to percussion sounds. In that paper a preliminary analysis of the selected xylophone sounds is given; an instrument that is recognised as very annoying by percussion players themselves. In some selected xylophone sounds the determined rise time was lower than 10 μs, with the resultant very high frequency components, HAMERNIK *et al.* [7].

It may be worthwhile to note that small rise times and high values of the sound pressure level in acoustic pulses may result in a hearing loss of specific character. Such loss is often moderate in the range of low and mid frequencies and reaches the largest values in the frequency range between 8 and 20 kHz, i.e. in the range where normal audiometric examination is executed only occasionally, FAUSTI *et al.* [4].

Earlier observations (ROGOWSKI *et al.* [12]) indicated the need of performing the analysis of the emission of percussion instruments in the frequency range up to 96 kHz. Preliminary results of that analysis are given in the present report.

2. Procedure and apparatus

The analysis was performed on the sounds of selected percussion instruments, namely: xylophone, snare drum, A-Due cymbals, tube bells, orchestral bells, kettledrum and a set of drums. The measurements were carried out in the practice rooms of the Academy of Music. Music selections typical for practice sessions isolated sounds and orchestral music selections played with various different drumsticks were recorded.

Sound signal was picked up from the acoustic field using 1/4″ condenser microphone Brüel & Kjær type 4135 with follower Brüel & Kjær type 2669. The microphone was situated on a tripod near the instrument at a distance corresponding to the position of the head of the musician. This signal, amplified in a Brüel & Kjær amplifier type 2690 "NEXUS" was sampled at frequency 192 kHz with the use of 12-bit A/D converter Quatech DAQ1201 and recorded on a hard drive of a class IBM PC. Spectral analysis of the recorded signals was performed with the use of the MATLAB program procedures. Statistical analysis and computation of kurtosis was done using WaveStat program prepared by the second author. Kurtosis is a ratio of the fourth moment of the distribution to the square of the second moment (DWEYER [2]). It is a measure of the "peakedness" of the distribution and was used as a measure of impulsiveness (ERDREICH [3]).

3. Results

The results of spectral analysis of short (120 s) music selections played on a xylophone, marimba, snare drum and cymbals are presented in Fig. 1. The spectra were calculated using Hanning window 1024 samples long and 50% overlapping. The distribution of the instantaneous sound pressures for the same music selections are represented in Fig. 2. The results of statistical analysis of music selection played on eight percussion instruments are given in Table 1. In case of xylophone the results are for two different kinds of drumsticks.

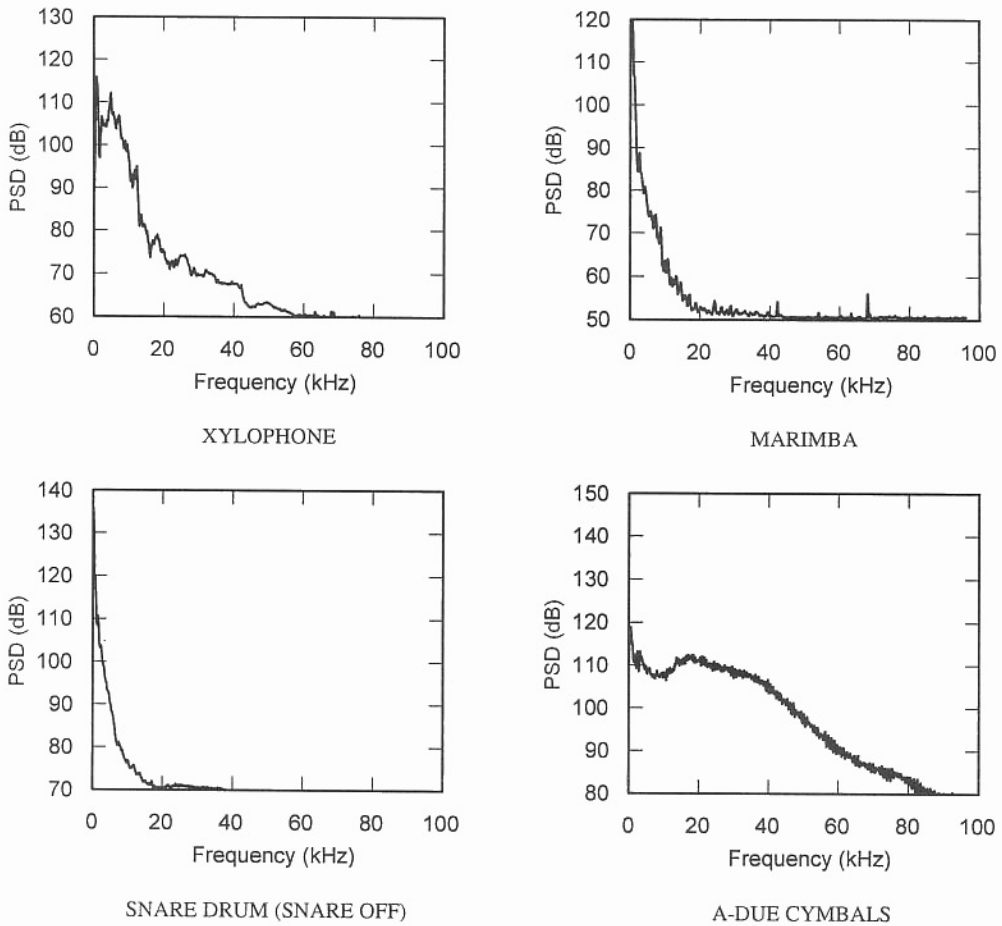

Fig. 1. Power spectral density spectra of the sound samples of four percussion instruments: xylophone, marimba, snare drum and A-Due cymbals.

Normalised functions of the effective frequency band for the four music instruments i.e. xylophone, marimba, snare drum and cymbals are represented in Fig. 3. Figure 4 presents initial phase of the sound G7 played on a xylophone with the use of plastic and

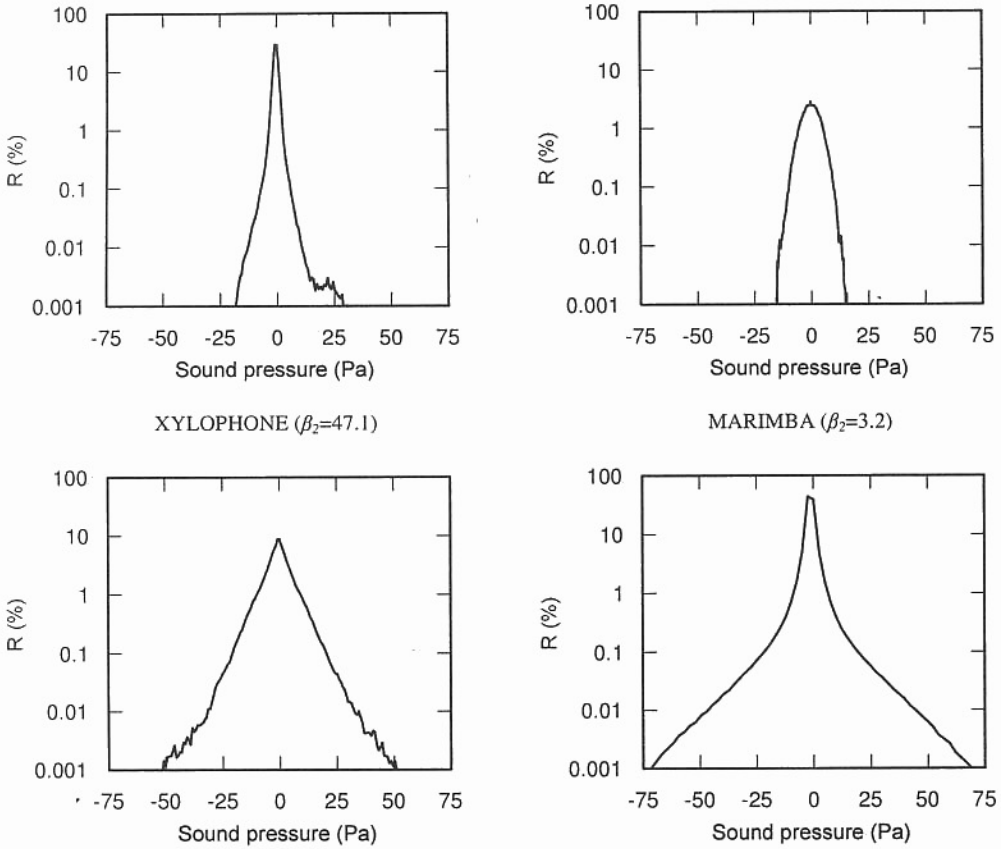

Fig. 2. The distribution of instantaneous pressure for sample sounds of four percussion instruments: xylophone, marimba, snare drum and A-Due cymbals; in parentheses the values of kurtosis.

Table 1. Statistical parameters of selected sample sounds of percussion instruments tested.

No.	Musical instrument	L_{peak} (dB)	L_1 (dB)	L_{eq} (dB)	I (dB)	CF (dB)	β_2
1	Orchestral bells	119.5	99.0	87.4	11.6	32.1	81.5
2	Tubular bells "Premier"	118.2	109.0	99.4	9.6	18.8	4.4
3	Kettledrum "Ludwig"	125.0	117.2	107.5	9.7	17.5	4.7
4	Xylophone "Musser Kelon 51"(*)	126.2	108.4	97.3	11.1	28.9	47.1
5	Xylophone "Musser Kelon 51"(**)	126.0	107.7	96.8	10.9	29.2	37.4
6	Marimba "One" Ron Samuels	117.8	113.9	105.6	8.3	12.2	3.2
7	Cymbals A-Due	136.7	119.5	106.3	13.2	30.4	67.1
8	Snare drum "Yamaha" (snare off)	130.8	120.8	110.2	10.6	20.6	8.2
9	Snare drum "Yamaha" (snare on)	127.5	117.9	106.5	11.4	21.0	9.3
10	Drums	132.8	124.3	114.8	9.5	18.0	4.4

(*) — plastic sticks; (**) — wooden sticks; CF — crest factor.

wooden drumsticks. Significant differences in the rise time for so produced sounds with practically constant peak values are evident.

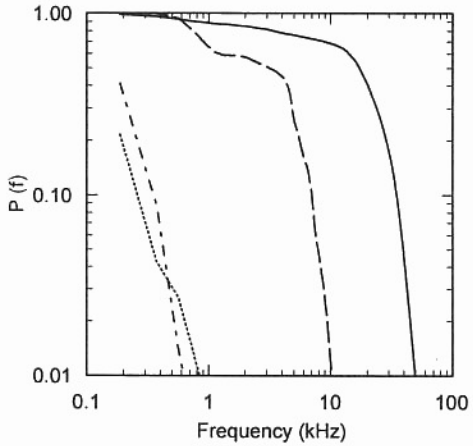

Fig. 3. Normalised effective frequency bands for sample sound of: xylophone — dashed line, marimba — dashed-dotted line, snare drum — dotted line and cymbals — solid line.

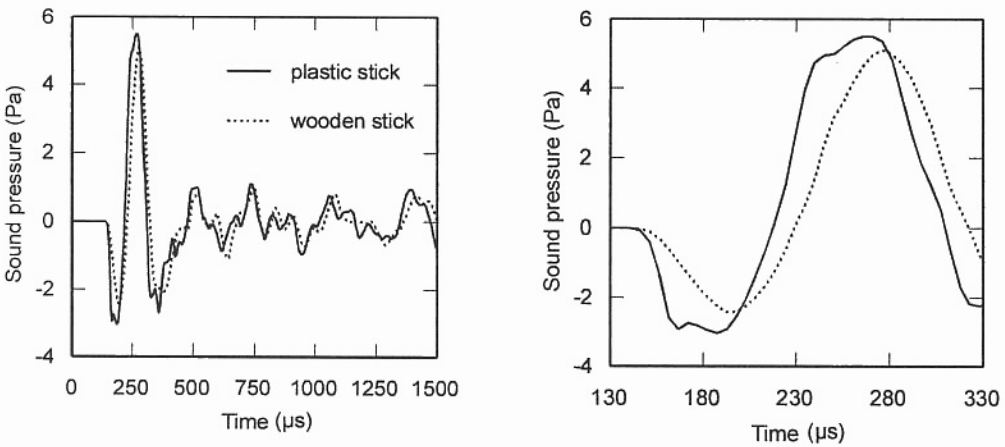

Fig. 4. Isolated G7 xylophone sound; temporal course of acoustic pressure for wooden and plastic drumsticks.

4. Discussion and conclusion

The analysis shows dangerously high sound pressure levels in sounds emitted by percussion instruments during individual practice sessions in classrooms of the Academy. Equivalent sound pressure levels for drums, snare drum, kettle-drums, marimba and cymbals reach 105 – 115 dB while peak sound pressure levels are in excess of 136 dB.

The characteristic of percussion sounds is significant impulsiveness which in terms of $I(L_1 - L_{eq})$ and $I(L_{peak} - L_{eq})$ amounts to 8.3–13.2 and 12.2–32.1 dB correspondingly. The values of kurtosis of the distribution of instantaneous sound pressure values differentiate the tested group of percussion instruments. Large kurtosis was found for xylophone, cymbals, and orchestral bells i.e. instruments without resonators.

The spectral analysis shows the presence of significant values of spectral power density in the range of supersonic frequencies for xylophone and for cymbals. In the case of cymbals the amount of energy emitted in the frequency range between 18 and 100 kHz equals the energy emitted in the auditory range.

In cymbals and particularly in xylophone sounds very small rise times were found amounting in some cases to only few microseconds. As it seems only kurtosis as a measure of impulsiveness is sensitive to this parameter. As mentioned, the xylophone with its rapid sound onset, is recognised by musicians as an instrument, which exerts a very heavy load on the hearing system.

According to the working hypothesis rapid sound onsets and relatively large sound pressure levels in xylophone may underlay the unpleasant effect of "blocked ears" in percussion players and may result in specific hearing loss in the frequency range between 8–16 kHz.

Acknowledgements

This work was supported by grant T 07B 051 15 from the State Committee for the Scientific Research. The authors are indebted to prof. St. SKOCZYŃSKI for his help and many helpful suggestions during many periods of the measurements. Parts of this paper were presented to the Open Seminar on Acoustics OSA'99 in Zakopane.

References

[1] A. AXELSSON and F. LINDGREN, *Hearing in classical musicians*, Acta-Otolaryngol. Suppl., 377, 261–284 (1981).

[2] R.F. DWEYER, *Use of kurtosis in the frequency domain as an aid in detecting random signals*, IEEE J. of Oceanic Engng., OE-**9**, 85–92 (1984).

[3] J. ERDREICH, *A distribution based definition of impulse noise*, J. Acoust. Soc. Amer., **79**, 990–998 (1986).

[4] S.A. FAUSTI, D.A. ERICKSON, R.H. FREY nad B.Z. RAPPAPORT, *The effects of impulsive noise upon human hearing sensitivity (8 to 20 kHz)*, Scand. Audiol., **10**, 21–29 (1981).

[5] R.W. FEARN, *Hearing loss in musicians*, J. Sound. Vib., **163**, 372–378 (1993).

[6] D. GRYCZYŃSKA and I. CZYŻEWSKI, *Damaging effects of music exposures on the hearing system in musicians* [in Polish], Otolaryngol. Pol., **31**, 527–531 (1977).

[7] R.G. HAMERNIK and K.D. HSUEH, *Impulse noise: Some definitions, physical acoustics and other considerations*, J. Acoust. Soc. Amer., **90**, 189–196 (1991).

[8] K. JAHTO and H. HELLMAN, *Zur Frage des Larm-und Klangtraumas des Orchestermusikers*, HNO 20, 21–29 (1972).

[9] D.W. JOHNSON, R.E. SHERMAN, J. ALDRIDGE and A. LORAINE, *Effects of instrument type and orchestral position on hearing sensitivity for 0.25 to 20 kHz in the orchestral musicians*, Scand. Audiol., **14**, 215–221 (1985).

[10] K. KARLSSON, P.G. LUNDQUIST and T. OLAUSSEN, *The hearing of symphony orchestra musicians*, Scand. Audiol., **12**, 257–264 (1983).

[11] B. OSTRI, N. ELLER, E. DAHLIN and G. SKYLV, *Hearing impairment in orchestral musicians*, Scand. Audiol., **18**, 243–249 (1989).

[12] P. ROGOWSKI, A. RAKOWSKI and A. JAROSZEWSKI, *High frequency hearing loss in percussion players*, 11th International Conference on Noise Control, "Noise Control'98", Krynica, 2–4 June 1998, ZB. ENGEL, D. AUGUSTYŃSKA [Eds.], vol. I, 163–170 (1998).

[13] J.D. ROYSTER, L.H. ROYSTER and M.C. KILLION, *Sound exposures and hearing thresholds in symphony orchestra musicians*, J. Acoust. Soc. Amer., **89**, 2793–2803 (1991).

[14] G. SCHACKE, *Sound pressure levels within an opera orchestra and its meaning for hearing*, Abstract of paper presented to the 22nd International Congress on Occupational Health. Sydney, Australia, 27.IX–2.X.1987.

[15] G.A. WESTMORE and I.D. EVERSDEN, *Noise-induced hearing loss and orchestral musicians*, Arch. Otolaryngol., **107**, 761–764 (1981).

ARCHIVES OF ACOUSTICS
25, 3, 291–316 (2000)

AUDITORY FILTERING AT LOW FREQUENCIES

A.P. SĘK

Institute of Acoustics
A. Mickiewicz University
(61-614 Poznań, ul. Umultowska 85, Poland)

This paper is concerned with the comparison of the critical bandwidth (CB) and the equivalent rectangular bandwidth (ERB) of the auditory filters at low frequencies. The method of critical bandwidth determination based on the critical modulation frequency (CMF) has been questioned, particularly for frequencies less than 500 Hz. The CMF, which is the modulation frequency at which amplitude modulation (AM) and frequency modulation (FM) detection thresholds become identical, is confounded as a proper measure of the auditory filter's width. It refers to the modulation rate for which one of the sidebands is most detectable. For low carrier frequencies the higher sideband is most detectable whereas for higher carrier frequencies the lower sideband becomes most detectable. Thus, at least for low carrier frequencies (i.e. less than 200 Hz), the CMF does not reflect the auditory system's sensitivity for detecting the phase differences of the spectral components of the signal. These findings can account for the fact that the critical bandwidth flattens off at low carrier frequencies, whereas the equivalent rectangular bandwidth of the auditory filters continues to decrease down to very low centre frequencies. Is was also shown that, at least for very low frequencies, critical bands do not reflect directly the auditory filtering that takes place in the peripheral auditory system.

1. Concepts of peripheral filtering

Since FLETCHER [4] described his band-widening experiment, the human peripheral auditory system has often been described as an array of linear bandpass filters with continuously overlapping centre frequencies. One of the first models of the auditory system (based on the Critical Band concept) assumed that the filters were rectangular in shape with bandwidth equal to the critical bandwidth, [4, 49, 50, 52]. Using this idea researchers tried to estimate a "breakpoint" in the data relating performance to bandwidth — a point at which subjective responses change "abruptly" (see below for details). PATTERSON and MOORE [26] used a different approach to modelling the auditory system's properties. They assumed a specific shape of the auditory filter described usually by means of a rounded exponential function (roex(f)) and based on the experimental data. They attempted to estimate parameters of the filter including its bandwidth.

Critical bandwidth and the equivalent rectangular bandwidth of the auditory filters are related by a constant factor in the frequency range above 1 kHz. However, for frequen-

cies lower than 500 Hz the critical bandwidth is constant while the equivalent rectangular bandwidth of the auditory filter decreases even for the lowest centre frequencies.

1.1. The critical band concept

FLETCHER [4] carried out an experiment, the results of which are the main basis of the Critical Band (CB) and the Auditory Filter (AF) concepts. He measured the detection thresholds of a sinusoidal signal as a function of the bandwidth of a bandpass noise masker (see Fig. 1, the left panel). The band of noise was characterised by a constant power density and its centre frequency was equal to the signal frequency. At first, the threshold of the signal increased with increasing masker width from very small values (see the right panel of Fig. 1). When the bandwidth reached a critical value (i.e. the critical bandwidth) the threshold flattened off and further increase in the noise bandwidth did not affect the signal threshold significantly.

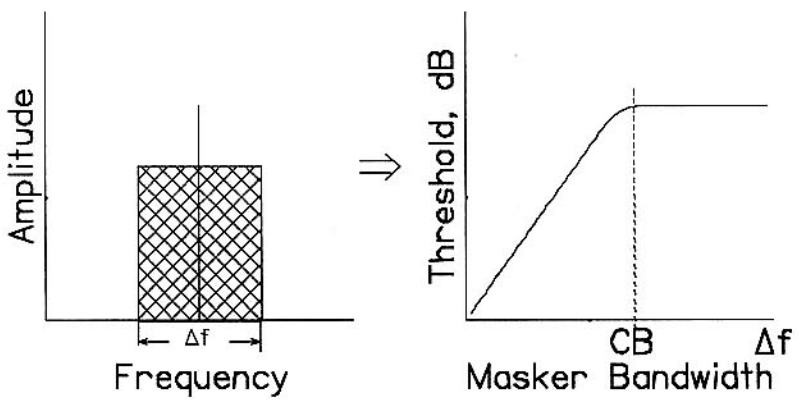

Fig. 1. A schematic illustrations of the signal spectrum and a pattern of results in FLETCHER's [4] band-widening experiment.

To account for these results Fletcher suggested that the auditory system behaved as if it contained an array of bandpass filters with overlapping passbands. The filters were assumed to be roughly rectangular in shape and their widths were equal to the CB. Based on physiological data [1] he also assumed that the basilar membrane provided the basis for these filters. Each point on the basilar membrane responds only to a very limited range of frequencies. Thus it may be considered as a filter with a specific centre frequency. Considering the detection of a signal in a background noise, it is assumed that a subject uses a filter with a centre frequency very close to the signal frequency. Only noise components passing through the filter affect the detection of the signal. At the detection threshold the power of the tone divided by the power of the noise inside the critical band (which is called the critical ratio) is constant.

Since FLETCHER [4] described the CB concept based on the band-widening experiment, results of different types of psychoacoustics experiments have confirmed this model. They gave very similar estimates of both the absolute widths of the CB and

of the way that the critical bandwidth varies as a function of frequency. The model was further developed by ZWICKER [44–48, 52, 53] who showed that the CB concept could summarise a great variety of psychoacoustical data. The concept also provides a valuable tool in the planning of experiments and the analysis of the data. ZWICKER [44–46, 48, 52] presented also some types of experiments in which the CB may by be demonstrated and/or measured.

• The loudness of a complex sound was approximately independent of its bandwidth, if the bandwidth was less than the width of the one critical band. Moreover, the complex sound was judged to be about as loud as pure tone of equal intensity lying at a centre frequency of the sound. However, if the bandwidth of the complex sound was increased beyond the critical bandwidth the loudness began to increase. The results of this experiment show that the loudness of a signal depends not only on its amplitude but also depends on its spectral structure. The increase in loudness with increasing signal bandwidth became one of the crucial proofs of the CB's existence and it was also used as a critical bandwidth determination/demonstration method.

• Masking. Thresholds for detecting a narrow band of noise in the presence of two tones symmetrically situated with respect to the centre frequency of the noise (see Fig. 2, the left panel) are approximately constant for small values of the frequency separation of the tones (Fig. 2, the right panel). But, when the frequency separation reached a critical value the threshold dropped very sharply. ZWICKER [46] assumed that the threshold remained constant as long as the frequency separation between masking tones did not exceed one critical band associated with the band of noise. However, when the frequency distance between masking tones became larger than the CB, the threshold decreased. The largest value of the frequency separation, for which the threshold was still constant, was used to estimate the critical bandwidth [46]. It was also shown that combination tones, resulting from a nonlinear process in the cochlea [15, 29], might affect the detection of the noise band. It is possible that the subject may detect the combination products even though the signal itself is inaudible. When the distortion products are masked by noise the threshold does not show an abrupt decrease [7].

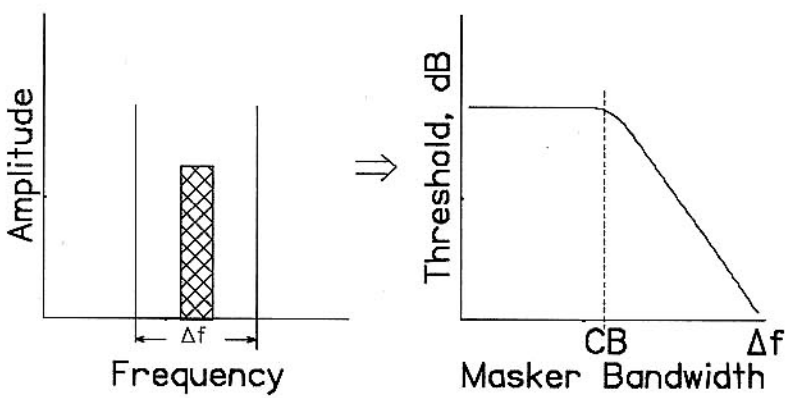

Fig. 2. A schematic illustrations of the signal spectrum and a pattern of results in ZWICKER's [51] masking experiment.

• Critical Modulation Frequency (CMF). Considering the detection of amplitude modulated (AM) and frequency modulated (FM) signals, ZWICKER [45] stated that the auditory system was capable of detecting the difference in the phase structure of the modulated signals spectra. Thresholds for detecting AM and FM, if expressed in terms of amplitude and frequency modulation indices (i.e. m and β), are markedly different for low modulation rates f_{mod}. The difference between these thresholds becomes much smaller when the modulation rate increases. When the modulation frequency reaches its critical value (called the Critical Modulation Frequency, CMF), AM and FM detection thresholds become identical and further increase in modulation rate does not affect the difference between them. ZWICKER [45] suggested, that the critical modulation frequency may be used as a CB estimator: $\text{CB} = 2 \cdot \text{CMF}$, (see Sec. 2 for further details).

Measures of the critical bandwidth obtained from a variety of experiments generally agree reasonably well for frequencies above 1 kHz. But for lower frequencies there are considerable discrepancies between the different measurements. SCHARF [34] summarised and averaged early measurements of the CB (based mainly on ZWICKER's [48] data) and since then his presentation has been widely used. Scharf's function relating the CB to the centre frequency, which is plotted in Fig. 3, flattens off for centre frequencies below 500 Hz at a value of 100 Hz. However for these centre frequencies this function is a simplified extrapolation because experimental data for this frequency region were rather sparse. The estimates were based mainly on the measurements of the critical modulation frequency and the critical ratio [34].

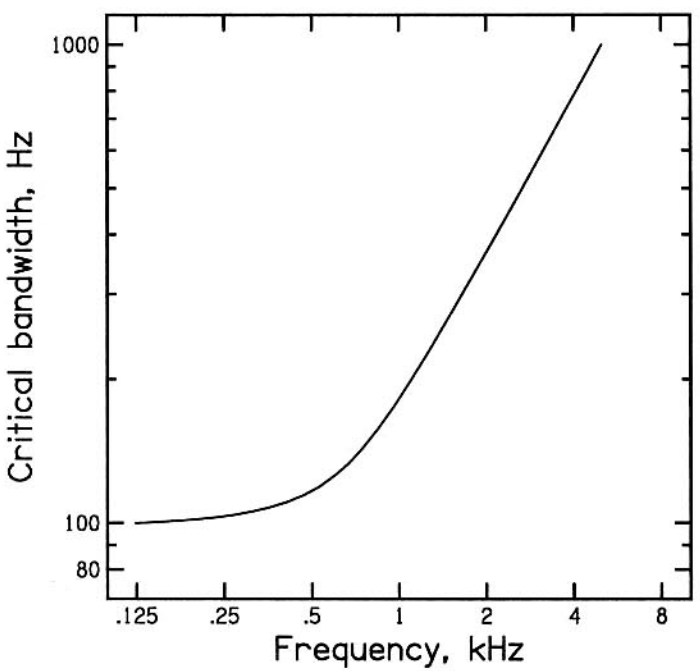

Fig. 3. Critical bandwidth as a function of centre frequency (adapted from SCHARF [34]).

There is no clear experimental evidence that the auditory filter's width is constant in the frequency range below 500 Hz. On the other hand, there is much evidence that the width of the auditory filter decreases with decreasing in frequency even at very low frequencies. The most important is the ability of the auditory system to resolve individual components in a multi-component complex sound. The frequency separation between two sinusoids at which these two sinusoids may be heard out as separate tones when presented simultaneously, depends on frequency. It gradually decreases even for the smallest values of frequency. A second piece of evidence is that frequency discrimination (i.e. the ability to detect changes in frequency over time) measured as the smallest detectable frequency difference between two successive tones, improves progressively with a decrease in frequency to very low values [42].

1.2. The auditory filter concept

An alternative approach to the modelling of the auditory filter is that proposed by PATTERSON and MOORE [26]. They assumed that the activity of the auditory system in response to acoustic stimuli (i.e. excitation pattern) may be considered as the output signal from a bank of linear bandpass filters (called the auditory filters AF) with the overlapping passbands. The activity of the peripheral auditory system may be understood as a displacement of the basilar membrane as a function of the distance from the oval window or as the number of the neural spikes per second as a function of the neurone's characteristic frequency. The filters have the general form suggested by PATTERSON *et al.* [28]:

$$W(g) = (1 + pg)e^{-pg}, \tag{1}$$

where g is the deviation from the centre frequency of the filter divided by the centre frequency, $W(g)$ is the intensity weighting function describing the shape of the filter, p is a parameter determining the sharpness of the passband of the filter, with p_l for the low- and p_u for the high-frequency skirts respectively. Assuming the power spectrum model [4, 26], PATTERSON and MOORE suggested that the activity of the peripheral auditory system and the auditory filter shape might be derived from masking experiments, (e.g. a notched-noise masking experiment). In this case the threshold at a given signal frequency corresponds to a constant signal-to-noise ratio at the output of an auditory filter centred close to the signal frequency.

• Psychophysical tuning curves. One of the methods of determining the auditory filter involves the measurement of psychophysical tuning curves (PTCs). To determine a PTC the threshold for detecting a sinusoidal signal with a low (fixed) level is measured. The masker is usually a narrow band of noise (a tonal masker would produce low frequency beats) with a different centre frequency. The level of the masker that just masks the signal is determined. It is assumed that the PTCs express the masker level required to produce a fixed output from the auditory filter as a function of the masker frequency. Examples of the PTCs are presented in Fig. 4. Psychophysical tuning curves are very similar in a general form to neural tuning curves [29] and they were obtained based on the same method, i.e. by determining the level of the tone required to produce a fixed output from a single point of the basilar membrane or single neurone. The similarities in both

the procedures and the results indicate that the shape of the PTCs reflects the activity of the auditory system and the auditory filter shape. PTCs reveal an "off frequency" listening phenomenon ([22, 27]). To detect the signal listeners use a filter whose output is characterised by the highest signal-to-noise ratio. In general case this means that subjects use a filter with a centre frequency very close to the signal frequency but not necessarily the filter with a centre frequency exactly equal to the signal frequency.

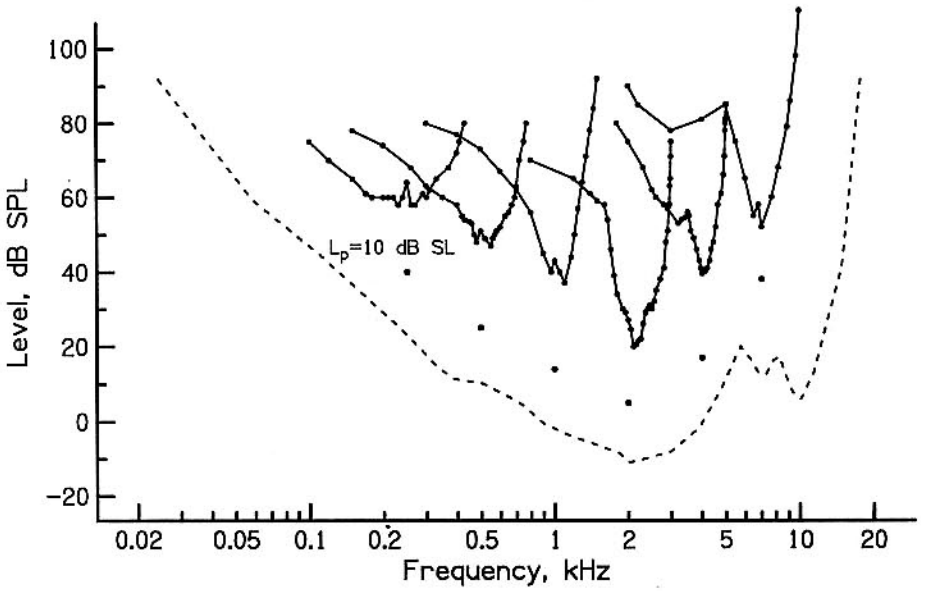

Fig. 4. Psychophysical tuning curves measured in simultaneous masking experiment (adapted from VOGTEN [41]).

• The notched noise method. PATTERSON [25] proposed a method of auditory filter shape determination based on the masking of a sinusoidal signal by means of two bands of noise symmetrically situated in the frequency domain (notched noise) with respect to the signal frequency, (see Fig. 5a). The method prevents off-frequency listening and decreases the influence of combination tones on the detection threshold. As the width of the spectral separation between the bands of noise is increased, less energy of the noise passes through the auditory filter (shaded areas in Fig. 5a) and the threshold for the signal drops. Based on the power spectrum model, the power of the signal P_s at the detection threshold may be expressed by means of the following equation:

$$P_s = K \int_0^\infty W(f)N(f)\,df, \tag{2}$$

where $W(f)$ is the intensity weighting function describing the auditory filter shape, $N(f)$ is the power spectrum of the noise and K is a constant that corresponds to the signal-to-noise ratio at the output of the auditory filter required for threshold.

Thus having the threshold values for different notch width ($2\Delta f$), and assuming the specific shape of the filter (Eq. (1)) it is possible to determine all parameters describing the shape of the auditory filter. An example of the auditory filter determined by means of this method is plotted in Fig. 5b.

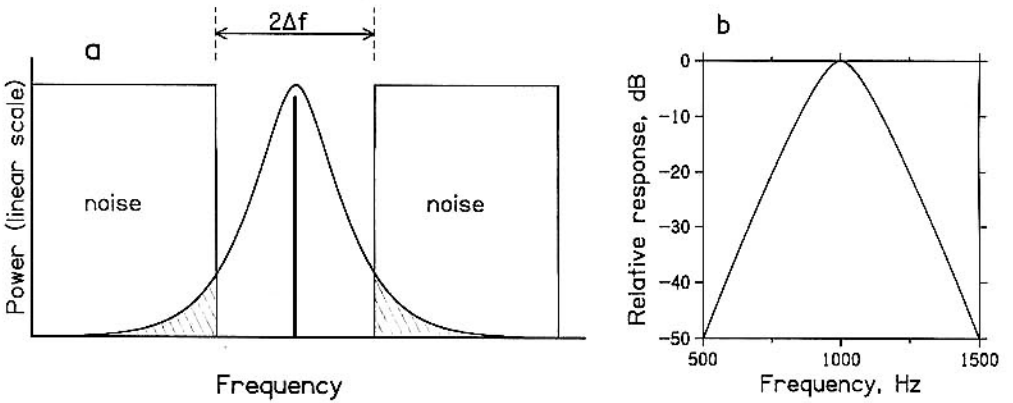

Fig. 5. PATTERSON's [25] method of auditory filter shape determination (a) and an example of the auditory filter shape at centre frequency of 1 kHz (b) determined using this method, (adapted from MOORE [15]).

Another measure of the auditory filter width is the Equivalent Rectangular Bandwidth (ERB). This expresses the bandwidth of the perfect rectangular filter whose transmission in its passband is equal to the transmission of the specified filter, and which transmits the same total power of white noise as the specified filter. The dependence of the equivalent rectangular bandwidth on its centre frequency is described by means of the equation [6, 15]:

$$\mathrm{ERB} = 24.7(4.37F + 1), \tag{3}$$

where F is a centre frequency of the filter in kHz. The dependence is well established over a wide frequency range including very low frequencies, [2, 3, 6, 14, 16, 17, 31, 32, 40, 43].

1.3. Comparison of the critical band and the ERB of the auditory filters

The comparison between the critical bandwidths CB suggested by SCHARF [34] and the equivalent rectangular bandwidth ERB [15] is presented in Fig. 6. Critical bandwidths have bigger values than the equivalent rectangular bandwidths of the auditory filters over the whole audible frequency range. In the frequency range 500 – 5000 Hz the ratio CB/ERB is approximately constant and equals about 1.22 – 1.5. The near-linear relationship between the CB and ERB in this frequency region suggests that any predictions of experimental results based on the critical band and the auditory filter concepts should be consistent. However, for frequencies less than 500 Hz, the discrepancy between the CB and the ERB gets much bigger with decreasing frequency; for a frequency of 100 Hz the ratio CB/ERB reaches a value close to 3. This discrepancy might indicate

that neither the ERB nor the CB are a proper measure of the auditory filter bandwidth. However the dependency of the ERB on centre frequency is well established over whole range of audible frequencies whereas Scharf's function relating the CBs to frequency may be in error for the lowest frequencies, since the data concerning the CB for this frequency region were very sparse. However the lack of critical bandwidth data for frequencies less than 500 Hz is not a proper argument in accepting the ERB estimates as the only measure of the auditory filter width. It is necessary to show that the critical band concept does not describe the auditory filtering in a proper way or to prove that the methods of the critical bandwidth determination are in error.

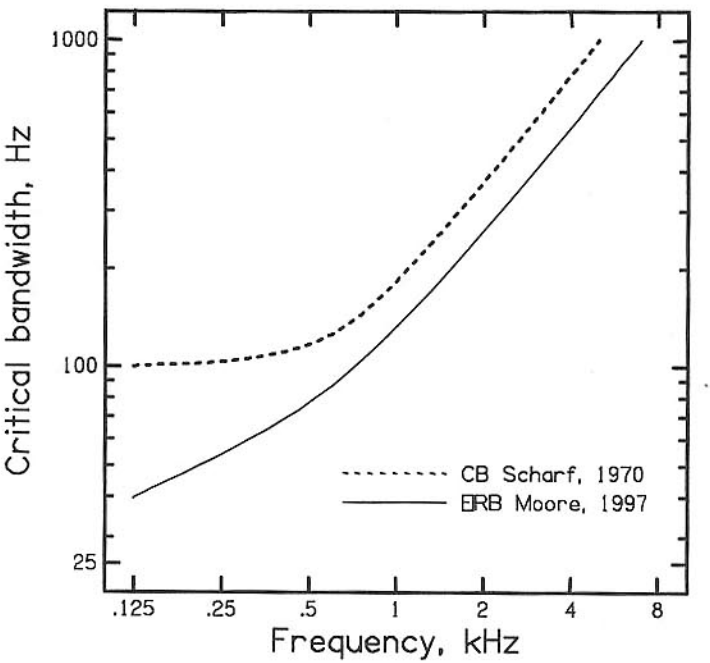

Fig. 6. Comparison between the critical bandwidth (CB) suggested by SCHARF [34] and the equivalent rectangular bandwidth (ERB) [15].

2. Critical modulation rate as a method of critical bandwidth measurement

2.1. Critical modulation rate concept

An amplitude modulated (AM) sinusoidal signal with modulation index m, and a frequency modulated (FM) sinusoidal signal with modulation index β, may each be considered as composed of three sinusoidal components, corresponding to the carrier frequency and two sidebands (the FM wave actually contains many sidebands but an approximation with two sidebands is correct for small modulation indices). A schematic structure of AM and FM signal spectra is presented over the top panel of Fig. 7. When the

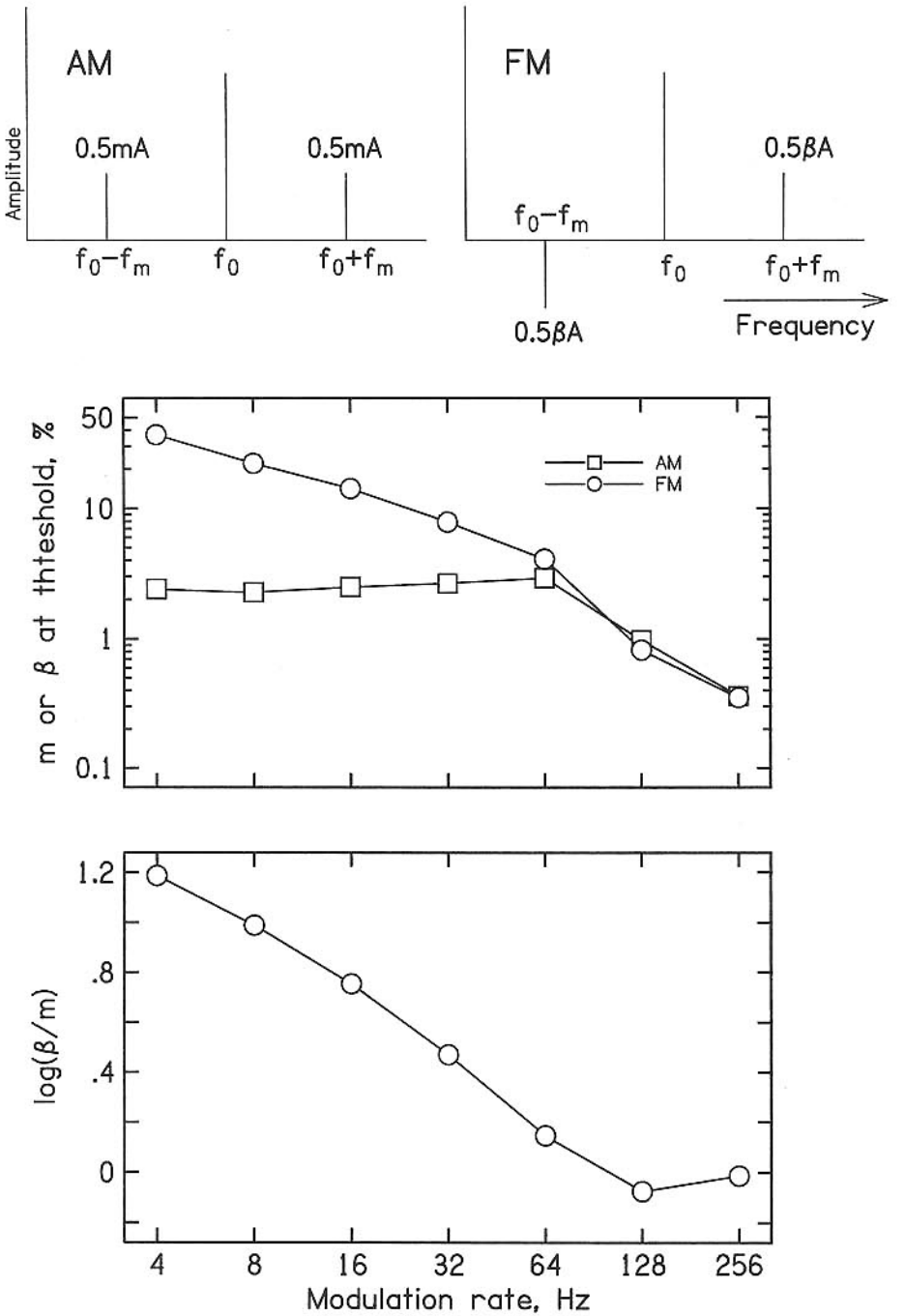

Fig. 7. The middle shows the thresholds for detecting AM or FM, expressed as the respective modulation indices, m or β, plotted as a function of modulation rate. The carrier frequency was 1000 Hz. The lower panel shows a dependence of $\log_{10}(\beta/m)$ on modulation rate which approaches zero at high modulation rates, indicating that the ratio β/m approaches unity. Data from Sᴇᴋ [38].

modulation indices are equal ($m = \beta$), and when the carrier frequencies and modulation frequencies are the same, the spectral components of AM wave and FM wave are identical in frequency and amplitude. The only difference between them being in the relative phase of the components, in particular, the lower one. If, then, the two types of wave are perceived differently, the difference is likely to arise from a sensitivity to the relative phase of the components (so-called monaural phase effect [12]), which affects the temporal structure of the sound.

ZWICKER [45, 51], SCHORER [35] and SĘK [38] measured the just-detectable amounts of amplitude or frequency modulation, for various rates of modulation. They found that for high rates of modulation, where the frequency components were widely spaced, the detectability of FM and AM was equal when the components in each type of wave were of equal amplitude ($m = \beta$). However, for low rates of modulation, when all three components fell within a narrow frequency range, AM could be detected when the relative levels of the sidebands were lower than for a wave with a just-detectable amount of FM ($m_{th} < \beta_{th}$). This is illustrated in the middle panel of Fig. 7 (based on data from [38]). Thus for small frequency separations of the components, subjects appear to be sensitive to the relative phases of the components (which is also known as a monaural phase effect [12]), while for wide frequency separations they are not.

If the threshold for detecting of modulation is expressed in terms of the modulation index, m or β, the ratio β/m decreases as the modulation frequency increases, and approaches value of unity (or zero if the value of $\log(\beta/m)$ is used). This is illustrated in the lower panel of Fig. 7. The modulation frequency at which the ratio first becomes unity is the CMF. ZWICKER [45, 51] suggested that the CMF is reached when the spectral sidebands in the stimulus first become detectable. Once the modulation is detected in this way, the relative phases of the components do not play a role. ZWICKER [45, 51] suggested further that the CMF corresponded to half the value of the CB; essentially the CMF was assumed to be reached when the overall stimulus bandwidth reached the CB. If this is correct, then the CMF may be regarded as providing an estimate of the CB at the carrier frequency.

SCHORER [35] and SĘK [38] argued that the CMF was one of the best ways of estimating the CB, especially at low centre frequencies. They gave several reasons supporting this argument:

1. The whole stimulus falls within a very restricted spectral region. At the CMF only one critical band is excited.

2. Variations in the absolute threshold with frequency have only a small influence on the results, due to small stimulus bandwidth.

3. There is no "off-frequency" listening ([22, 27]).

4. Combination tones do not appear to influence the threshold. Thus the method can be used over a wide range of sound pressure levels.

2.2. Measurements of the critical modulation frequency

. Figure 8 presents data obtained by SĘK [38] and SCHORER [35] who measured the critical modulation rate for the whole frequency range and then converted it into the critical

bandwidth. This figure shows also the critical bandwidth data collected by SCHARF [34] and the equivalent rectangular bandwidths [15] to make a comparison between these two sets of data slightly easier. As can be seen from this picture Sęk's and Schorer's data are very similar since they used the same experimental methods. For frequencies above 1 kHz the dependence of the critical bandwidth determined based on CMF on frequency is very similar to that of Scharf. However, the values of the critical bandwidth obtained for frequencies lower than 1 kHz are slightly lower and the difference between them and those of Sharf appears to be statistically significant [36, 38]. The critical bandwidth determined by Sęk and Schorer tends to decrease gradually as frequency decreases even below 500 Hz. This is a very important result since it shows a qualitative difference between the most recent measurements and traditionally accepted data that suggest that below 500 Hz the critical bandwidth is constant and independent of frequency.

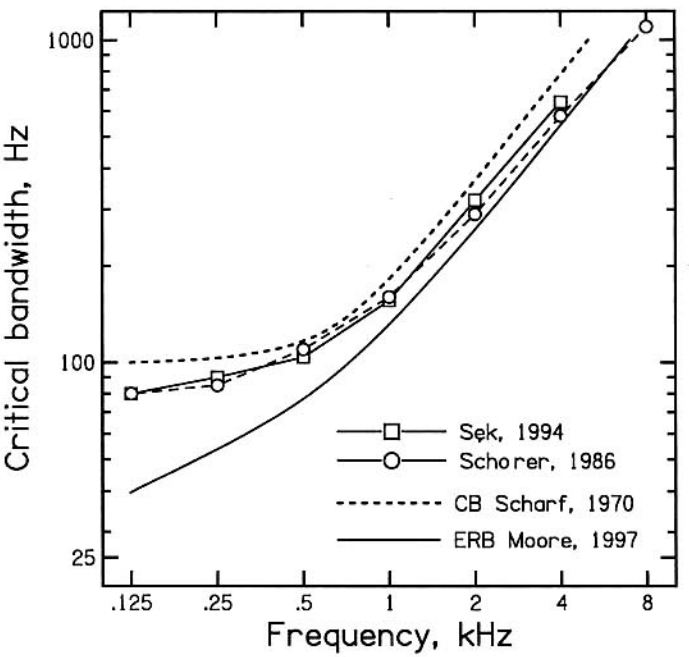

Fig. 8. Critical bandwidth as a function of frequency obtained by SCHORER [35] and SĘK [36, 38] based on measurements of the critical modulation frequency. The critical bandwidth (CB) suggested by SCHARF [34] and the equivalent rectangular bandwidth (ERB) [15] are also presented in the figure.

The data presented in Fig. 8 are not fully compatible with the equivalent rectangular bandwidth of the auditory filter. For frequency above 1 kHz, however, the relation between ERB and CB determined by Sęk and Schorer is approximately linear and it may be assumed that differences observed in this frequency area are not important and may be ignored. Quite a different situation is observed in the low-frequency region i.e. below 500 Hz. As frequency decreases, the difference between critical bandwidth measured be SĘK [36, 38] and SCHORER [35] on one side and ERBs measured

by Moore on the other becomes statistically significant and gets progressively larger; for frequency of 125 Hz the difference reaches about 25 – 30 Hz. Thus even though the estimates based on the critical modulation rate showed that the auditory filter bandwidth decreases as frequency decreases below 500 Hz there is no agreement between CB and ERB. The difference observed between them is not just quantitative but also qualitative.

The above presented comparison rises some questions. For example, is the critical band model correct or does the critical modulation frequency properly describe the auditory filtering that takes place in the peripheral auditory system? Does the critical modulation frequency properly describe a phase sensitivity of the auditory system for very low frequencies?

To check on this, some predictions based on the excitation pattern model have been made as well as results of two experiments have been compared. This is described in the following sections.

3. Further analysis of the critical modulation frequency concept

A more detailed analysis of Schorer and Sęk's arguments that the critical modulation rate is a proper estimator of the critical bandwidth was elaborated theoretically and experimentally and is presented below. It suggests that all Schorer and Sęk's arguments may not be entirely valid. Furthermore, the interpretation of the CMF proposed by ZWICKER [45] and SCHORER [35] may not be completely correct. HARTMANN and HNATH [10] suggested that the CMF corresponded to the point where the lower sideband in the spectrum first becames detectable. The threshold for detecting the lower sideband depends more on the selectivity of auditory filters centred close to the frequency of the sideband than on the selectivity of the auditory filter centred on the carrier frequency. Furthermore, the level of the sideband relative to that of the carrier may be altered by transmission through the middle ear, especially at low frequencies, where the efficiency of transmission may change markedly with frequency [33, 54].

Perhaps a more serious problem comes from the possibility that, at the CMF, detection is not always based on the lower sideband. The results of several experiments support the idea that, at medium to high centre frequencies, the lower sideband is more detectable than the upper sideband [10, 19, 24]: the lower sideband is entirely responsible for modulation detection since the upper sideband is totally masked by the carrier. However, this may not be the case at low centre frequencies i.e. below 500 Hz because the absolute threshold strongly increases as the frequency decreases. For a modulated signal with carrier frequency less than 500 Hz, the lower sideband ($f_c - f_{\mathrm{mod}}$) may by attenuated by the middle ear much more than the upper one and modulation detection may be based on the upper sideband ($f_c + f_{\mathrm{mod}}$) of the modulated signal. If the detection were based on the upper sideband at low carrier frequencies, then the monaural phase effect would not occur and the CMF would not provide a good estimate of the CB, or the ERB of the auditory filter, since the sideband on which detection is based would change as the centre frequency was changed.

The main purpose of the theoretical consideration, as well as the experimental studies reported below, was to explore the mechanism of modulation detection for low carrier frequencies and for modulation frequencies around the CMF. More specifically, the main aim was to determine whether the detection of AM and FM for modulation frequencies at and above the CMF depends on detection of the lower sideband, the upper sideband or both, and whether this changes with carrier frequency. To establish this the results of theoretical and experimental results were considered.

3.1. Theoretical consideration

In the first part of the theoretical considerations an excitation pattern model was used to evaluate the differences between the excitation patterns produced by modulated and unmodulated signals. It was done in order to show a simple subtraction between those two excitations and to check on which frequency side of the excitation pattern a bigger difference can be observed.

The excitation pattern that were used in these considerations were calculated using a program suggested by GLASBERG and MOORE [6]. The excitation is defined there as the output from each auditory filter as a function of center frequency. Each auditory filter is assumed to have the form of a rounded exponential, as in Eq. (1). This program enables to use two independent slopes for low and high frequency sides of the filter using B_u and B_l parameters [6, 13]. It also enables to control a nonlinearity on both sides of the filter independently by means of NL_l and NL_u parameters. However in this considerations the simplest case of the excitation pattern model was used. Thus the values of described above parameters were set to be equal 1, i.e. $B_u = B_l = NL_l = NL_u = 1$. The ERB spacing was assumed to be equal 0.1. Evaluations of any differences between excitation patterns produced by modulated and unmodulated signals were calculated based on those ERBs for which the excitation pattern was bigger than 10 dB, as in MOORE and SĘK [20]. They are referred to as the active channels.

GLASBERG and MOORE's program [6] also requires a correction file connected with the intensity weighing function. Thus the threshold correction file describing the ASA standard absolute threshold was used in all the theoretical considerations.

Evaluations of the differences between the excitations pattern produced by a modulated and unmodulated signal were calculated for carrier frequencies of 125 and 200 Hz. The modulating frequency was assumed to be equal to $1.1 \cdot \mathrm{CMF}$ based on SĘK's [38] results. Thus the unmodulated signal consisted of one component (f_c) whereas the modulated one consisted of three components with frequencies: $f_c - 1.1 \cdot \mathrm{CMF}$, f_c and $f_c + 1.1 \cdot \mathrm{CMF}$. The sound pressure level of the carrier was assumed to be equal to 70 dB SPL. Thresholds for detecting amplitude and frequency modulation for low carrier frequencies and for modulating frequency $1.1 \cdot \mathrm{CMF}$, expressed in appropriate modulation indices are equal to $\beta_{th} = m_{th} = 0.06$, [38, 45]. The thresholds for detecting both AM and FM do not depend significantly on carrier frequency below 1 kHz. Thus the sidebands of modulated signals were assumed to be equal to 40 dB SPL each ($m = \beta = 0.06$).

Results of these calculations were presented in Fig. 9 for carrier frequencies of 125 and 200 Hz. The upper panels present two excitation patterns. A solid line in each

panel identifies the excitation pattern of unmodulated (pure sinusoid) signal whereas dotted line presents the excitation pattern of modulated signals. Those two curves are almost identical in these panels and it is difficult to see any difference between them. However, the differences of those two patterns are presented in the lower panels. The spectral structure of modulated signals was schematically presented in each panel of Fig. 9. Sidebands were marked as small arrows and the carrier was marked as a slightly bigger arrow.

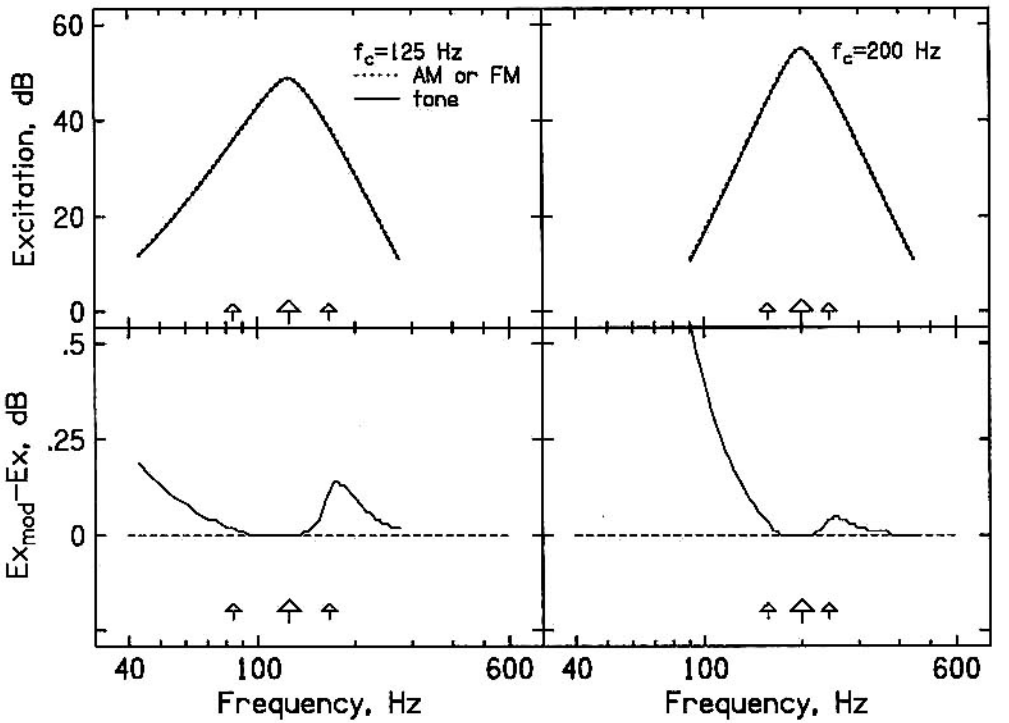

Fig. 9. Excitation patterns produced by unmodulated (solid lines) and modulated (dotted lines) carriers at frequencies of 125 Hz (left upper panel) and 200 Hz (right upper panel). Modulation rates were equal to $f_{mod} = 1.1 \cdot \mathrm{CMF}$ and modulation index (m or β) was equal to 0.06. Lower row shows differences in the excitation patterns presented in the upper row.

The left column of Fig. 9 shows the excitation patterns (the upper panel) and their difference (the lower panel) for modulated and unmodulated signals with carrier frequency of 125 Hz. Similar differences can be observed on the low and high frequency sides of the excitation pattern. However, the difference observed on the high-frequency side can be characterized by a local maximum for frequency corresponding to the higher sideband of a modulated signal. Moreover, an exact value of this difference of excitation patterns for frequency corresponding to the higher sideband is slightly bigger than the difference corresponding to the lower sideband. Taking into account a single band model [11, 51] which assumes that detection of modulation takes place when the difference of

excitation patterns of modulated and unmodulated sounds exceeds a certain amount in the single band (in this case in one active channel), it may be stated that the upper sideband of the modulated signal is decisive for modulation detection in this case.

The right column of Fig. 9 presents the results for $f_c = 200$ Hz. The difference in the excitation patterns observed on the low-frequency side is bigger than the difference on the high-frequency side. Thus, based on a single band model, it seems that the lower sideband of the modulated signal might be decisive for modulation detection in this case. Similar results were also obtained for frequencies higher than 200 Hz. A single-band model predicts that the lower component of the modulated signal is decisive for modulation detection for frequency range higher than about 200 Hz. This is consistent with experimental data obtained for carrier frequencies of 1 kHz [10, 18].

In the next step of this analysis evaluation of the differences between excitation patterns produced by modulated and unmodulated signals, based on a non-optimal multi-band excitation pattern model were carried out. Like Zwicker's model the model assumes that the detection of modulation is based in this case on a single form of information, namely changes in excitation level. However, this model assumes that information from different parts of the excitation pattern can be combined in a non-optimal way (see [20, 37] for details). The model is similar in its general form to the model proposed by FLORENTINE and BUUS [5] and is based on the integration model [8].

This model is based on the assumption that changes in amplitude or frequency of signal are detected by virtue of the changes in the excitation level that are produced in the peripheral auditory system. If the changes in excitation level in the i-th critical band or auditory filter gives rise to a value d'_i then overall value of d' is given by:

$$d' = \sqrt{\sum (d'_i)^2}\,. \tag{4}$$

As the first approximation it might be assumed that d'_i is proportional to the difference in the excitation level observed in this channel [37] thus the overall value of d' was assumed to be:

$$d' = K \sum_{i=1}^{n} \frac{\Delta L_i^2}{\sqrt{n}}\,, \tag{5}$$

where n is the number of active channels and K is a constant.

Using the above described excitation pattern program the values of $\sum \frac{\Delta L_i^2}{\sqrt{n}}$ were calculated for both the low- and the high-frequency side of the excitation pattern. Similarly to earlier considerations only those auditory filters, that gave the excitation level greater than 10 dB, were taken into account.

Results of these calculations are presented in Fig. 10 and 11. Figure 10 presents differences (expressed as $\sum \frac{\Delta L_i^2}{\sqrt{n}}$) of the excitation patterns of modulated and unmodulated signals as a function of a carrier frequency. In this case modulation frequency was equal to $f_{\mathrm{mod}} = 1.1 \cdot \mathrm{CMF}$, sound pressure level of the carrier signal 70 dB SPL and sound pressure level of the sidebands was equal to 40 dB SPL each. A continuous line in this figure presents a difference between excitation levels of modulated and unmodulated sig-

nals on the high-frequency side whereas the dotted line presents this difference observed on the low-frequency side of the excitation pattern.

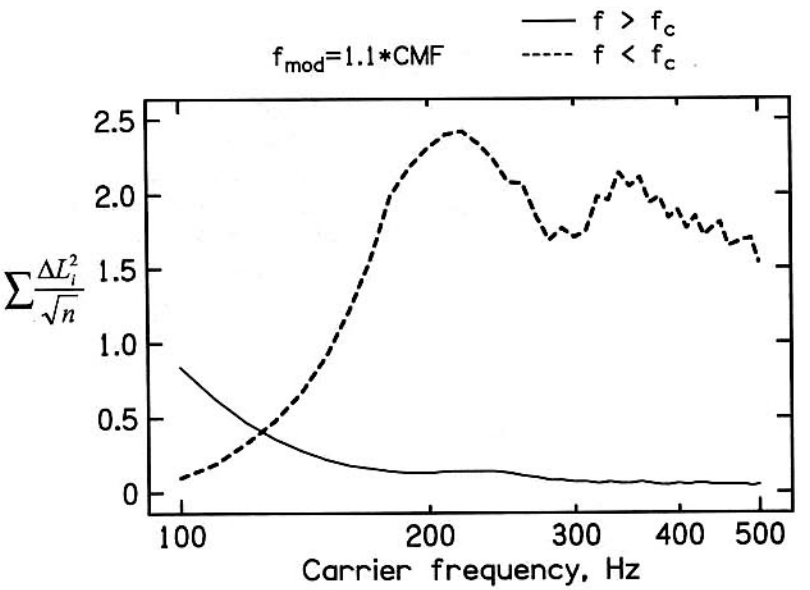

Fig. 10. Differences in the excitation pattern (expressed as $\sum \frac{\Delta L_i^2}{\sqrt{n}}$) produced by modulated and unmodulated signals as a function of carrier frequency. Modulation frequency was equal to $f_{\mathrm{mod}} = 1.1 \cdot \mathrm{CMF}$, sound pressure level of the carrier signal 70 dB SPL and sound pressure level of the sidebands 40 dB SPL each. Continuous line in this figure presents difference between excitation levels of modulated and unmodulated signals on the high-frequency side whereas the dashed line presents this difference on the low-frequency side of the excitation pattern.

The difference obtained for the high-frequency side of the excitation pattern is bigger than the difference observed on the low-frequency side only in a very restricted region of carrier frequencies i.e. up to 140 Hz only. Therefore it may be assumed that for this carrier frequency range the upper sideband is decisive for modulation detection which is not consistent with the HARTMANN and HNATH [10] model. However, for carrier frequencies greater than 140 Hz the difference obtained for the low-frequency side of the excitation pattern is much bigger than the difference on the high-frequency side. It means that above 140 Hz and for modulation rates above the critical modulation frequency, the lower sideband of the modulated signal might be responsible for modulation detection. So the predictions of the single-band and multi-band models are similar.

Figure 11 presents differences in the excitation patterns (expressed as $\sum \frac{\Delta L_i^2}{\sqrt{n}}$) observed on the low- and high-frequency sides of the excitation pattern obtained for modulated and unmodulated signals as a function of modulation rate for carrier frequencies of 125 Hz, and 250 Hz. Dashed lines in this figures denote the differences observed on the low-frequency side and continuous lines denote differences observed on the high-frequency side of the excitation pattern.

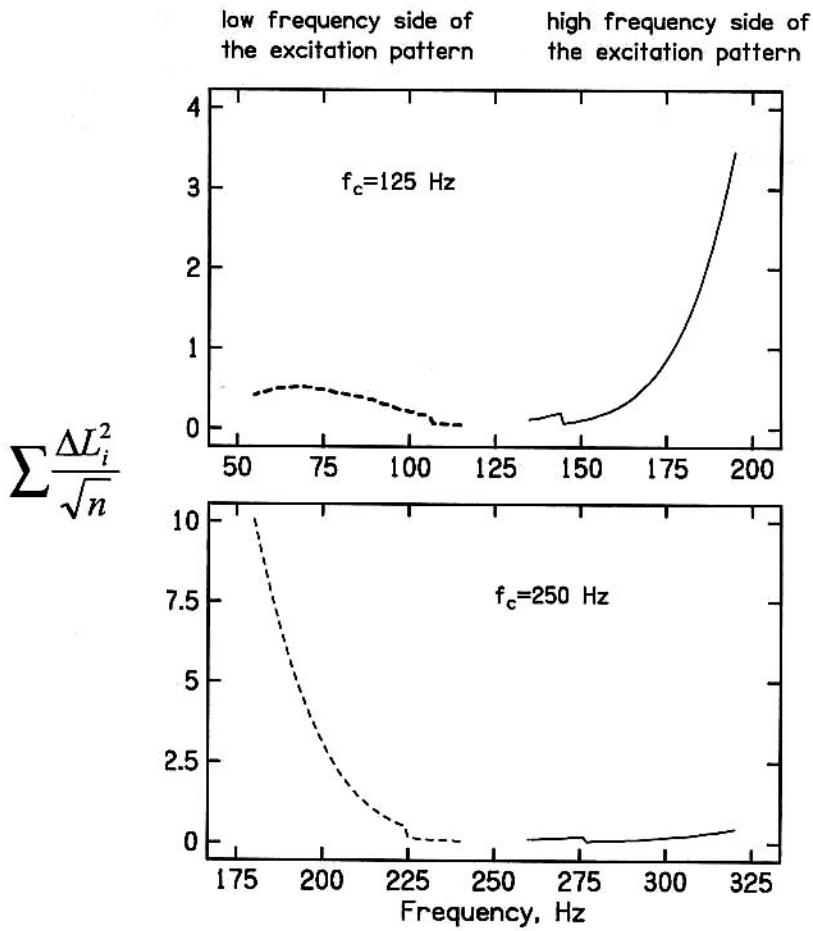

Fig. 11. Differences in the excitation patterns (expressed as $\sum \frac{\Delta L_i^2}{\sqrt{n}}$) observed on the low- and high-frequency side of the excitation pattern (for modulated and unmodulated signals) as a function of modulation rate, for carrier frequencies equal to 125 Hz and 250 Hz. Dashed lines denote the differences observed on the low-frequency side and continuous lines — on high-frequency side of the excitation pattern respectively.

As can be seen from the top panel of Fig. 11 the difference observed on the high-frequency side of the excitation pattern is much bigger than the difference on the low-frequency side when a carrier frequency was equal to 125 Hz. It can be stated that for modulation frequencies greater than the CMF the detection of modulation for this particular carrier frequency might be based on changes in the high-frequency side of the excitation pattern. These changes were evoked by the higher sideband of the modulated signal. So this sideband might be decisive for modulation detection in this case.

A quite oppsite situation can be observed for carrier frequencz 250 Hz (see Fig. 11 the bottom panel). The difference of excitation patterns evoked bz modulated and unmodulated signals is bigger on the low-frequencz side than on the high-freqencz side of

the excitation pattern. The lower sideband of the modulated signal might be responsible for modulation detection in this case.

Based on the above considerations it can be stated that modulation, either AM or FM, might be detected not only by means of the lower frequency sideband of modulated signal's spectrum, as HARTMANN and HNATH's [10] model predicts. In the case when carrier frequency is equal to 125 Hz and modulation frequency is slightly bigger than the CMF modulation detection might be based on the higher sideband. It might be also expected that for carrier frequencies from the range of 125 – 160 and for modulation frequencies bigger than the CMF, a contribution of the upper sidebands of the modulated signal's spectrum in the detection of modulation might be bigger than a contribution of the lower one. In this frequency range, modulation might be detected based on the upper sideband.

3.2. Results of some experimental studies

SĘK [36] has presented evidence that the interpretation of the CMF proposed by ZWICKER [45], and generally accepted in the literature, is not quite correct. For medium to high frequencies the critical modulation frequency appears to correspond to the point where the lower sideband in the spectrum of the modulated signal first becomes detectable. This is often referred to as the HARTMANN and HNATH [10] model. However, SĘK and MOORE [39] showed, that for very low carrier frequencies the upper sideband becomes first detectable before the lower sidebands. So it seems that the lower sideband is not always decisive for modulation detection.

To determine which sideband is decisive for modulation detection SĘK and MOORE [39] compared the results of two separate experiments. In the first one thresholds were determined for the detection of amplitude modulation and frequency modulation using several low carrier frequencies, namely f_c = 125, 160, 200 and 250 Hz. The following modulation rates were used: f_{mod} = 20, 30, 40, 50, 60 and 70 Hz. They expressed measured thresholds for detection either AM or FM in terms of the sound pressure levels of the sidebands i.e. L_{AM} and L_{FM} for amplitude and frequency modulation. In the second experiment thresholds were measured for detecting a single sinusoid, corresponding to either the lower (L_l) or the upper (L_u) sidebands of the modulated signal used in the first experiment, in the presence of a sinusoidal masker corresponding to the carrier frequency of the modulated signal. A schematic structure of the signal spectra they used is presented in Fig. 12. If a component corresponding to a given sideband, say the lower one, has a lower threshold than a component corresponding to the other sideband, i.e. $L_l < L_u$ at the threshold, then the given sideband should be more detectable in a situation where both sidebands are present, as for example, in the modulation detection task. Moreover, if modulation detection thresholds are determined by the threshold for the most detectable sideband, then the thresholds measured for that sideband in the second experiment should correspond with those determined in the first experiment.

The results of these experiments are presented in Fig. 13. Each panel shows the data averaged across three subjects for one carrier frequency. The value of the carrier fre-

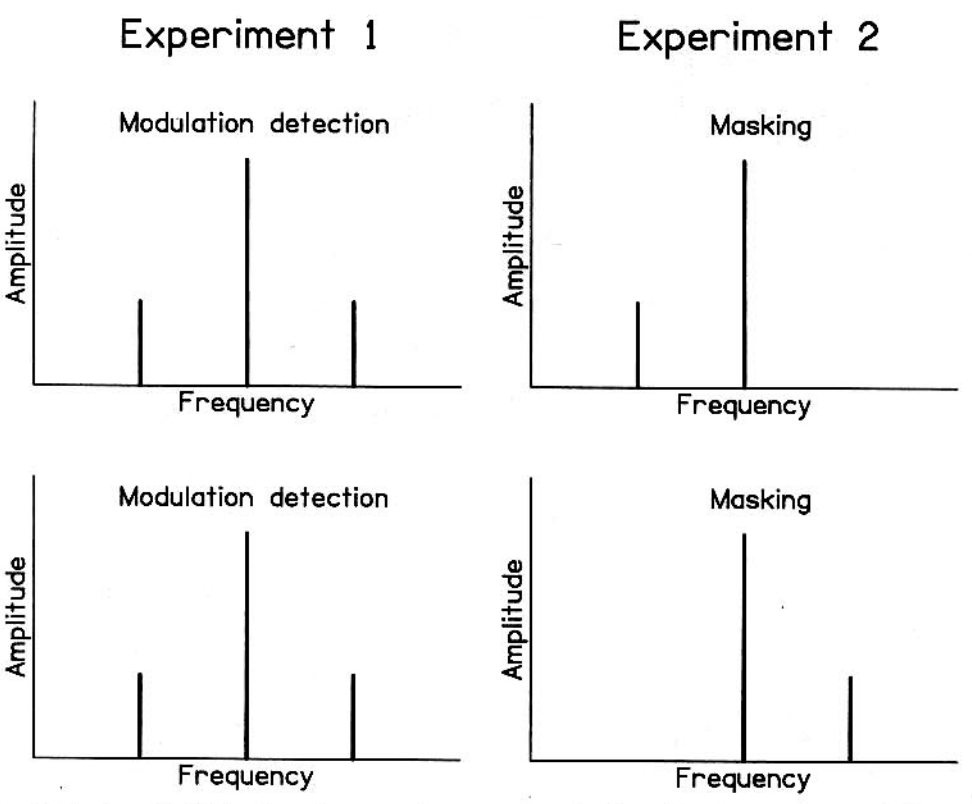

Fig. 12. A schematic illustration of a spectral structure of stimuli used by SĘK and MOORE [39] in two separate experiments.

quency is marked in each panel by an arrow. Dashed lines show absolute thresholds (standard threshold and the subject's threshold measured directly in the experiment). Squares and circles in each panel show the results of the first experiment 1. The level of each sideband at the modulation detection threshold, i.e. the values of L_{AM} and L_{FM}, is plotted as a function of its frequency. Since the lower and upper sidebands for both type of modulation were always equal in level, each measured threshold is presented twice giving a pattern symmetrical about carrier frequency. For the higher modulation frequencies used, the AM and FM thresholds coincide ($L_{\mathrm{AM}} = L_{\mathrm{FM}}$), whereas for the lower values used, i.e. when sideband were closer to the carrier, the thresholds for detecting FM are higher than the thresholds for detecting AM, ($L_{\mathrm{FM}} > L_{\mathrm{AM}}$). This is consistent with previous findings, see for example ZWICKER [45], SCHORER [35] or SĘK [36] and Fig. 8, showing that the CMF for low carriers is typically is about 40 Hz. This also reflects the fact that the modulation frequencies were chosen properly to span the critical modulation frequency.

The stars and diamonds in Fig. 13 show the results of the second experiment (i.e. the values of L_u and L_l, for the lower and the upper sideband respectively) where the thresholds were measures for a single sinusoid corresponding to the lower or the upper

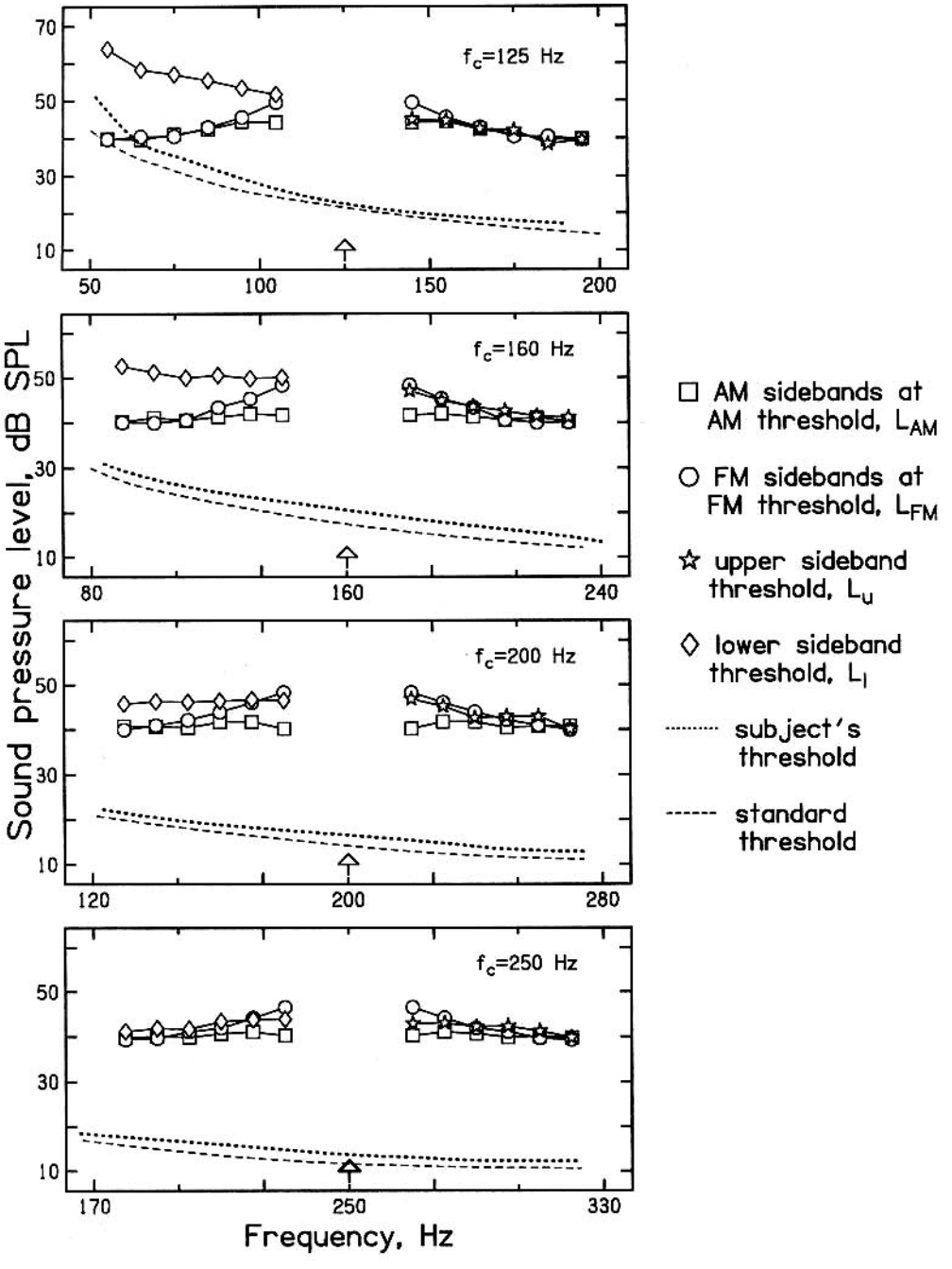

Fig. 13. Each panel shows data averaged across three normal hearing subjects for one carrier frequency. Modulation detection thresholds are expressed in terms of the levels of the sidebands.

sidebands in the spectrum of the modulated signal. The thresholds obtained for the signals with frequencies below the frequency of the carrier (diamonds) were generally higher than those for signals with frequencies above the carrier ($L_u > L_l$). This suggests that when both sidebands were present simultaneously, as in the experiment concerned with the detection of modulation, detection was based on the upper sideband rather than on the lower sideband. This is consistent with the above presented consideration based on the excitation pattern model.

Comparing the results of these two experiments it is clear that, at least for the two lowest carrier frequencies used (125 and 160 Hz), the thresholds for the lower sideband alone (diamonds) are markedly higher than the levels of the lower sideband at the modulation detection threshold (circles and squares). This indicates that, at the modulation detection threshold, the lower sideband would have been undetectable. Indeed, for the highest modulation frequency used the lower sideband would have been below absolute threshold. In contrast, for the modulation frequencies above the critical modulation frequency the levels of the upper sideband at the modulation detection threshold (circles and squares) are almost identical with the detection thresholds for the upper sideband when presented alone i.e. $L_{AM/FM} = L_u$ (stars). This is true for all carrier frequencies used. Taken together, these results indicate, that modulation detection thresholds for modulation frequencies above the critical modulation frequency and carrier frequencies of 125 and 160 Hz were determined by the threshold for detecting the upper sideband. This is also consistent with the above presented theoretical predictions based on the excitation pattern model.

The results of SĘK [36] suggest that for carrier frequencies from 200 to 250 Hz there is a certain transition region. For modulation rates above the critical modulation frequency and for carrier below that region modulation detection threshold were determined by the threshold for detecting the upper sideband. This is clearly seen in the two upper panels of Fig. 13 that present the results for carrier frequencies of 125 and 160 Hz. However, for carriers above that region detection is probably based mainly on the threshold for detecting the lower sideband. This is consistent with the above presented theoretical consideration (see Sec. 3.1 and Figs. 9–11) and with previous data of HARTMANN and HNATH [10], OZIMEK and SĘK [23] and MOORE and SĘK [18]. However, in that region both sidebands may contribute to detection of the modulation. It may be assumed that modulation is detected by means of the auditory filter at a centre frequency close to the frequency of the decisive (the most detectable) sideband.

The fact that the most detectable sideband switches from the lower one to the upper one as the carrier frequency decreases means clearly that the critical modulation frequency is not a satisfactory measure of the auditory filter bandwidth or the frequency selectivity of the auditory system, since the auditory filter centred on the upper sideband has a broader bandwidth than the auditory filter centred on the lower sideband.

4. Conclusions

The auditory system is usually considered an array of bandpass overlapping linear filters, called auditory filters. This basic point of view has been confirmed in a variety of

experiments and at present is well established. One of the most important factors describing the properties of the auditory filter is its bandwidth. So far two measures have been proposed: the Critical Bandwidth CB and the Equivalent Rectangular Bandwidth ERB. These two measures are consistent in a high-frequency region, i.e. for frequencies higher than 1 kHz where the ratio of CB to ERB is approximately constant. However these two measures are considerably different in a low-frequency region, i.e. for frequencies lower than 1 kHz.

Estimates of the critical bandwidth, as collected by SCHARF [34], were based on the results of band-widening and two-tone masking experiments while the equivalent rectangular bandwidth were based on the data collected in notched noise masking or psychophysical tuning curves experiments. ZWICKER [45] and SCHORER [35] have suggested that the critical band reflects also a sensitivity of the auditory system to phase differences of spectral components of stimulus, as observed in so-called monaural phase effect [12]. If a bandwidth of a given stimulus with a centre frequency f is less than the critical bandwidth for this frequency, then its phase structure is very important and influences a sensation evoked by the stimulus. However, when a bandwidth of a stimulus is greater than one critical band then its phase structure is less important: a change in the relative phase of components in the stimulus may have not influenced the sensation evoked by the stimuli. Such a situation has been observed in a case of modulation detection. The phase of the lower component of amplitude and frequency modulated signal is different. Due to this difference a marked discrepancy in AM and FM thresholds are observed, particularly for low modulation frequencies. However, when modulation rate reaches so-called critical modulation frequency (CMF) the threshold for detecting AM and FM becomes identical. It has been suggested that the CMF determines that point at which one of the sidebands of the modulated signal's spectrum first becomes detectable. As long as the lower sideband (i.e. that one whose phase is different in AM and FM case) first becomes detectable and responsible for modulation detection the critical modulation frequency may be considered as a measure of the phase sensitivity of the auditory system or a proper measure of the auditory filter bandwidth.

However, as shown in this paper, for very low carrier frequencies the thresholds for detecting both AM or FM were not determined by the detection of the lower sideband in the modulated signal's spectrum.

The CMF is defined as the modulation frequency at which AM and FM thresholds first become identical. However, the results considered in this paper show that for very low values of the carrier frequency the threshold for detection of either AM or FM was not determined by the detection of the lower sideband in the modulated signal's spectrum. Thus the CMF does not reflect the ability of the auditory system to detect the phase difference between the spectral component of the complex sound, since upper components have the same phases. The CMF, then, is confounded as a proper estimate of the critical bandwidth since, at least for low frequencies, it does not say anything about phase sensitivity of the auditory system.

The above considerations also give an explanation of the discrepancy observed between the critical bandwidth and the equivalent rectangular bandwidth for very low carrier frequencies. For carrier frequencies less than 200 Hz modulation detection was

entirely based on detection of the upper sideband in the modulated signal's spectrum, (i.e. at frequency $f_c + f_{mod}$). Excitation evoked by this frequency component was associated with the activity of an auditory filter with a centre frequency higher than the frequency of the carrier signal i.e. with a frequency close to this component. Thus modulation detection in this carrier frequency region was based exclusively on the auditory filter with centre frequency higher than the carrier frequency.

For frequencies 200 – 250 Hz both sidebands, the upper one and the lower one, contribute to the detection of modulation. Excitation changes associated with these components have approximately the same value. It is difficult to state which auditory filter (i.e. either with lower or with higher centre frequency than the carrier) is responsible for modulation detection in this case. This carrier frequency area is probably a transition area in which the activity of the auditory filters with centre frequencies lower and higher than the carrier are nearly the same. These filters are equally responsible for modulation detection.

For the frequency range above 250 Hz modulation detection was entirely based on the detection of the lower spectral component ($f_c - f_{mod}$) of the modulated signal. Excitation evoked by this sideband was associated with the activity of the auditory filter with a centre frequency close to the frequency of this component. Thus modulation detection in this case was exclusively based on an auditory filter with a centre frequency lower than the carrier frequency.

If the modulation detection had always been based on the auditory filter with centre frequency lower than the carrier, then the critical bandwidth would have decreased even for very low carrier frequencies. However, when the carrier frequency decreases, in the transition area (i.e. 200 – 250 Hz), the auditory filter that is responsible for modulation detection switches from a filter at a centre frequency lower than the carrier to a filter at a centre frequency higher than the carrier. The equivalent rectangular bandwidth of the filter at a centre frequency higher than the carrier is bigger than the ERB of the filter at a centre frequency lower than the carrier. Thus the change of the filter is the reason that dependence of the CBs on the frequency flattens off while ERBs decrease even for very low carrier frequencies.

There are several factors that might cause the lower sideband to be less detectable for low carrier frequencies. These include the effect of the transfer function of the middle ear [54], the possibility that the cochlea is characterised by a relatively high level of internal noise, particularly at low frequencies [21] and the possibility, that the signal-to-masker ratio required for the threshold increases at low frequencies. Is seems likely that the main detection cue used for signal detection in the case when a single sideband was presented were beats produced by the interaction of a signal (imitating one of the sidebands) and masker. HARRIS [9] showed that a "depth of modulation" produced by beats required for threshold increased mainly at low frequencies. In addition, the detectability of beats decreases with an increasing beats rate above 3 – 4 Hz and with decreasing in level, [30].

These factors provide further justification for a claim that the critical modulation frequency is confounded as a measure of the auditory filter bandwidth or frequency selectivity of the auditory system. None of these factors is directly connected with frequency selectivity, yet may influence the value of the critical modulation frequency for

low carrier frequencies. The above presented results show that, taking these factors into account, the values of the critical modulation frequencies for low carrier frequencies can be reconciled, at least to a first approximation, with the estimates of auditory filter bandwidth and shape summarised by MOORE [15].

The critical bands determined based on the critical modulation rate are confounded as a measure of auditory filter's bandwidth for very low frequencies. They do not reflect directly the frequency selectivity of the auditory system. The assumption that the auditory filter has a constant width, as used in the critical band concept presented by SCHARF [34] and used up to the present for this frequency region, is in error.

Acknowledgments

This work was supported by the Committee for Scientific Research, project no. T07B 052 16 and 8T11E 01717.

I would like to thank an anonymous reviewer for very helpful comments on an earlier version of this paper.

References

[1] G. BEKESY, VON, *Zur Theorie des Hornes; die Schwingungsform Der Basilar Membran*, Phys. Z., **29**, 793–810 (1928).

[2] J.R. DUBNO and D.D. DIRKS, *Auditory filter characteristics and consonant recognition for hearing-impaired listeners*, J. Acoust. Soc. Am., **85**, 1666–1675 (1989).

[3] J.R. DUBNO and D.D. DIRKS, *Filter characteristics and consonant recognition for hearing- impaired listeners*, J. Acoust. Soc. Am., **85**, 1666–1675 (1989).

[4] H. FLETCHER, *Auditory patterns*, Rev. Mod. Phys., **12**, 47–65 (1940).

[5] M. FLORENTINE and S. BUUS, *An excitation-pattern model for intensity discrimination*, J. Acoust. Soc. Am., **70**, 1646–1654 (1981).

[6] B.R. GLASBERG and B.C.J. MOORE, *Derivation of auditory filter shapes from notched-noise data*, Hear. Res., **47**, 103–138 (1990).

[7] B.R. GLASBERG, B.C.J. MOORE and I. NIMMO-SMITH, *Comparison of auditory filter shapes derived with three different maskers*, J. Acoust. Soc. Am., **75**, 536–544 (1984).

[8] D.M. GREEN and J.A. SWETS, *Signal detection theory and psychophysics*, Krieger, New York 1974.

[9] J.D. HARRIS, *Loudness discrimination*, J. Speech. Hear. Disord., Monographs, Supplement **11**, 1–63 (1963).

[10] W.M. HARTMANN and G.M. HNATH, *Detection of mixed modulation*, Acustica, **50**, 297–312 (1982).

[11] D. MAIWALD, *Ein Funktionsschema des Gehörs zur Beschreibung der Erkennbarkeit kleiner Frequenz- und Amplitudenänderungen*, Acustica, **18**, 81–92 (1967).

[12] R.C. MATHES and R.L. MILLER, *Phase effects in monaural perception*, J. Acoust. Soc. Am., **19**, 780–797 (1947).

[13] B.C.J. MOORE, *Characterization of simultaneous, forward and backward masking*, [in:] Perception of Reproduced Sound, S. BECH [Ed.], Audio Engineering Society, New York 1993.

[14] B.C.J. MOORE, *Frequency analysis and masking*, [in:] Hearing, B.C.J. MOORE [Ed.], Academic Press, Orlando, Florida 1995.

[15] B.C.J. MOORE, *An introduction to the psychology of hearing*, 4th Ed., Academic Press, London 1997.

[16] B.C.J. MOORE and B.R. GLASBERG, *Suggested formuale for calculating auditory-filter bandwidth and excitation patterns*, J. Acoust. Soc. Am., **74**, 750–753 (1983).

[17] B.C.J. MOORE, R.W. PETERS and B.R. GLASBERG, *Auditory filter shapes at low center frequencies*, J. Acoust. Soc. Am., **88**, 132–140 (1990).

[18] B.C.J. MOORE and A. SĘK, *Detection of combined frequency and amplitude modulation*, ASA Meeting, Salt Lake City, USA 1992.

[19] B.C.J. MOORE and A. SĘK, *Detection of combined frequency and amplitude modulation*, J. Acoust. Soc. Am., **92**, 3119–3131 (1992).

[20] B.C.J. MOORE and A. SĘK, *Effects of carrier frequency and background noise on the detection of mixed modulation*, J. Acoust. Soc. Am., **96**, 741–751 (1994).

[21] V. NEDZELNITSKY, *Sound pressures in the basal turn of the cat cochlea*, J. Acoust. Soc. Am., **68**, 1676–1689 (1980).

[22] B.J. O'LOUGHLIN and B.C.J. MOORE, *Off-frequency listening: effects on psychoacoustical tuning curves obtained in simultaneous and forward masking*, J. Acoust. Soc. Am., **69**, 1119–1125 (1981).

[23] E. OZIMEK and A. SĘK, *Perception of amplitude and frequency modulated signals (mixed modulation)*, J. Acoust. Soc. Am., **82**, 1598–1603 (1987).

[24] E. OZIMEK and A. SĘK, *Perception of mixed modulation signals*, Archives of Acoustics, **21**, 413–426 (1986).

[25] R.D. PATTERSON, *Auditory filter shapes derived with noise stimuli*, J. Acoust. Soc. Am., **59**, 640–654 (1976).

[26] R.D. PATTERSON and B.C.J. MOORE, *Auditory filters and excitation patterns as representations of frequency resolution*, [in:] Frequency Selectivity in Hearing, B.C.J. MOORE [Ed.], Academic, London 1986.

[27] R.D. PATTERSON and I. NIMMO-SMITH, *Off-frequency listening and auditory filter asymmetry*, J. Acoust. Soc. Am., **67**, 229–245 (1980).

[28] R.D. PATTERSON, I. NIMMO-SMITH, D.L. WEBER and R. MILROY, *The deterioration of hearing with age: frequency selectivity, the critical ratio, the audiogram, and speech threshold*, J. Acoust. Soc. Am., **72**, 1788–1803 (1982).

[29] J.O. PICKLES, *An introduction to the physiology of hearing*, 2nd Ed., Academic Press, London 1988.

[30] R.R. RIESZ, *Differential intensity sensitivity of the ear for pure tones*, Physical Reviews, **31**, 867–875 (1928).

[31] S. ROSEN, R.J. BAKER and S. KRAMER, *Characterizing changes in auditory filter bandwidth as a function of level*, [in:] Auditory Physiology and Perception, Y. CAZALS, K. HORNER and L. DEMANY [Eds.], Pergamon Press, Oxford 1992.

[32] S. ROSEN and D. STOCK, *Auditory filter bandwidths as a function of level at low frequencies* (125 Hz–1 kHz), J. Acoust. Soc. Am., **92**, 773–781 (1992).

[33] J.J. ROSOWSKI, *The effects of external- and middle-ear filtering on auditory threshold and noise-induced hearing loss*, J. Acoust. Soc. Am., **90**, 124–135 (1991).

[34] B. SCHARF, *Critical bands*, [in:] Foundations of Modern Auditory Theory, J.V. TOBIAS [Ed.], Academic Press, New York 1970.

[35] E. SCHORER, *Critical modulation frequency based on detection of AM versus FM tones*, J. Acoust. Soc. Am., **79**, 1054–1057 (1986).

[36] A. SĘK, *Critical modulation frequency and critical band based on random amplitude and frequency changes*, Archives of Acoustics, **19**, 59–74 (1994).

[37] A. SĘK, *Detection and discrimination of modulation at a low modulation rate*, Archives of Acoustics, accepted (1998).

[38] A. SĘK, *Modulation thresholds and critical modulation frequency based on random amplitude and frequency changes*, J. Acoust. Soc. Jpn. (E), **15**, 67–75 (1994).

[39] A. SĘK and B.C.J. MOORE, *The critical modulation frequency and its relationship to auditory filtering at low frequencies*, J. Acoust. Soc. Am., **95**, 2606–2615 (1994).

[40] M.J. SHAILER, B.C.J. MOORE, B.R. GLASBERG, N. WATSON and S. HARRIS, *Auditory filter shapes at 8 and 10 kHz*, J. Acoust. Soc. Am., **88**, 141–148 (1990).

[41] L.L.M. VOGTEN, *Pure-tone masking: A new result from a new method*, [in:] Facts and Models in Hearing, E. ZWICKER and E. TERHARDT [Eds.], Springer-Verlag, Berlin 1974.

[42] C.C. WIER, W. JESTEADT and D.M. GREEN, *Frequency discrimination as a function of frequency and sensation level*, J. Acoust. Soc. Am., **61**, 178–184 (1977).

[43] B. ZHOU, *Auditory filter shapes at high frequencies*, J. Acoust. Soc. Am., **98**, 1935–1942 (1995).

[44] E. ZWICKER, *Die elementaren Grundlagen zur Bestimmung der Informationskapazität des Gehörs*, Acustica, **6**, 356–381 (1956).

[45] E. ZWICKER, *Die Grenzen der Hörbarkeit der Amplitudenmodulation und der Frequenzmodulation eines Tones*, Acustica, **2**, 125–133 (1952).

[46] E. ZWICKER, *Die Verdeckung von Schmalbandgeräuschen durch Sinustöne*, Acustica, **4**, 415–420 (1954).

[47] E. ZWICKER, *Direct comparison between the sensations produced by frequency modulation and amplitude modulation*, J. Acoust. Soc. Am., **34**, 1425–1430 (1962).

[48] E. ZWICKER, *Subdivision of the audible frequency range into critical bands (Frequenzgruppen)*, J. Acoust. Soc. Am., **33**, 248 (1961).

[49] E. ZWICKER and H. FASTL, *On the development of the critical band*, J. Acoust. Soc. Am., **52**, 699–702 (1972).

[50] E. ZWICKER and H. FASTL, *Psychoacoustics — facts and models*, Springer-Verlag, Berlin 1990.

[51] E. ZWICKER and R. FELDTKELLER, *Das Ohr als Nachtrichtenempfänger*, Hirzel-Verlag, Stuttgart 1967.

[52] E. ZWICKER, G. FLOTTORP and S.S. STEVENS, *Critical bandwidth in loudness summation*, J. Acoust. Soc. Am., **29**, 548–557 (1957).

[53] E. ZWICKER and B. SCHARF, *A model of loudness summation*, Psychol. Rev., **72**, 3–26 (1965).

[54] J.J. ZWISLOCKI, *The role of the external and middle ear in sound transmission*, [in:] The Nervous System, Vol. 3. Human Communication and its Disorders, D.B. TOWER and E.L. EAGLES [Eds.], Raven Press, New York 1975.

ARCHIVES OF ACOUSTICS
25, 3, 317–329 (2000)

FACTORS THAT INFLUENCE THE CALCULATION OF ACOUSTIC SCATTERING BY THE METHOD OF SOURCE SIMULATION

P.H.T. ZANNIN

Universidade Federal do Paraná
Depet° de Engenharia Mecânica
(CEP 81531-990 Curitiba, Brasil — Caixa Postal 19011)
e-mail: zannin@demec.ufpr.br

In this work the source simulation technique was used to calculate the scattering of a plane wave by a cylinder with radial or elliptical transverse section. The basic idea of the source simulation technique is to replace the scattering (or radiating) body with a system of simple sources located within the envelope of the scatterer (or radiator). The extent to which the simulated field reproduces the original one depends on the degree of correspondence between the simulated and the given boundary conditions. Numerical simulations have shown that: 1) the shape of the auxiliary surface, 2) the number of sources, and 3) the way the sources are distributed are the most relevant parameters to ensure an accurate solution of the problem. In the case of the single-layer method, the sources should not be positioned close to the surface or to the center of the body, because the problem becomes ill-conditioned. The auxiliary surface and the scatterer should be as similar as possible in order to minimize the boundary error. With respect to the number of sources (N), there are two opposite effects: 1) if (N) is too small, the sound field is not reproduced accurately; 2) if (N) is too large, the computing time increases and the solution accuracy decreases. The method breaks down when the excitation frequency coincides with the eigenfrequencies — a narrow range of frequencies — of the space formed by the auxiliary surface. As the auxiliary surface is frequently represented by simple surfaces (cylinder, sphere), one can easily calculate the eigenfrequencies and therefore avoid them.

1. Introduction

The mathematical treatment of radiation and acoustic scattering represents a very old and much studied problem by mathematical physics (see [1] and [2]). Radiation and scattering are present in all ondulatory phenomena (elastic waves in rigid bodies, electromagnetic waves, surface waves on the water, etc). The present study, however, deals only with "pure" acoustical waves, that is, acoustical waves in gases or liquids. Another important limitation is that all steps of the solution of the problem are considered linear. Consequently, the Superposition Principle is valid. As radiation and scattering represent classical problems of mathematical physics, there is a vast literature on the subject. The solution methods can be classified into three different groups:

a) Analytical methods, which make possible an exact solution for the problem. However, these methods are limited to a few very simple geometric figures (sphere, cylinder).

The classical works of LORD RAYLEIGH [1], P. MORSE [2] and many other authors present the analytical solution for the radiation and acoustic scattering problems in bodies with spherical and cylindrical shapes.

b) Semi-analytical and semi-empirical methods for the calculation of radiation and acoustic scattering. The utilization of the radiation coefficient, for example, belongs to this category (e.g. GÖSELE [3] and CREMER and HECKL [4]).

c) Numerical methods in which the problem is approached by a set of differential or integral equations. In this case the equations model a linear system, which is in general very large. It is meant here the use of the finite elements method (FEM) or the boundary elements method (BEM). The relatively new method of simulation by elementary sources also belongs to this group.

The method of simulation by elementary sources leads, similarly to FEM and BEM, to the solution of large systems of equations. It comes into question what are the differences between those methods. From the literature [4, 7], one can say:

— In FEM, the number of equations to be solved depends on the volume of the space considered in the solution of the problem. As this number (for problems of radiation and acoustic scattering) increases with the third power of the relationship D/λ (D is a dimension typical of the space of the solution of the problem and λ is the sound wave length), one can expect for high frequencies a system of equations with extremely large matrices.

— In BEM, the number of elements to be calculated depends on the size of the surface of the body considered. The number of equations to be solved increases with the second power of the relationship D/λ, where D is a dimension typical of the body and not of the total solution space of the problem. One can have, in consequence, with BEM a significantly smaller number of equations than with FEM. However, the matrix elements are practically all non-zero numbers, and as a result one has full matrices. The great problem in the use of BEM is that there are no solutions for the problem close to the characteristic frequencies, which correspond to the resonance frequencies of the internal space delimited by the surface of the body. Several methods were developed in order to solve this problem.

— In the method of simulation by elementary sources there is in principle no minimal number of elements to be utilized. However, the number of elements has a crucial role in the accuracy attained by the solution of the problem. BOBROVNITSKII [7] states that the source method is the only one among those here cited that allows for a quantitative evaluation of the the precision of the calculations. This statement is however only valid for the precision with which the velocity of the surface of the body is approached by the elementary sources. A statement about the accuracy of the calculation of intensity and potency has not been shown possible until now. Likewise, in BEM the critical frequencies exist. These frequencies correspond to the resonance frequencies of the internal surface over which the sources are positioned (e.g., monopoles). Choosing an adequate internal surface, as will be demonstrated later in this work, this problem can be easily overcome. Using an open internal surface or a multipole positioned only in one point in the interior of the body, the resonance frequencies do not appear.

2. Description of the scattering problem and the source simulation technique

Considering a harmonic wave with sound pressure amplitude p_e in an infinite and homogeneous space E which encounters in its displacement the body K, internal space is defined by I, the scattered wave by p_s and the surface of the body by S. Over the surface of the body the unitary vector $\mathbf{n}$ is defined:

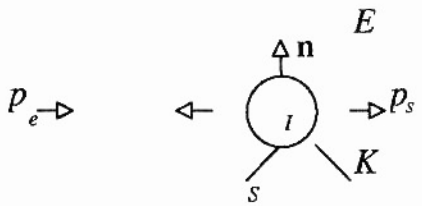

Fig. 1. Geometry of the acoustic scattering problem.

Pressure and velocity of the particle can be determined as the result of the sum of the components p_e and p_s. Respectively,

$$p_t = p_e + p_s \qquad \text{and} \quad v_t = v_e + v_s\,. \tag{2.1}$$

The complex sound pressure p_t has to satisfy the Helmholtz equation:

$$\Delta p_t + k^2 p_t = 0 \tag{2.2}$$

in E, where $k = \omega/c$ is the wave number, ω is the circular frequency, c the speed of sound, and Δ is the Laplace operator. Since sound scattering into the free three-dimensional space is considered, the pressure p_t has to satisfy the Sommerfeld radiation condition:

$$\lim_{r\to\infty}\left[\frac{\partial p_t}{\partial n} + jkp_t\right]\cdot r = 0 \tag{2.3}$$

which can be interpreted as a boundary condition at infinity. Here,

$$r = \|x\| = \sqrt{x_1^2 + x_2^2 + x_3^2}$$

denotes the distance from x to the origin, where we represent points in space by simple letters like $x = (x_1, x_2, x_3)$. Solutions of the Helmholtz equation in E which also satisfy the radiation equation condition are called radiating wave functions. To get a complete description of the problem, boundary conditions on the surface are needed. For simplicity, we only consider the Neumann boundary value problem where the normal velocity and therefore the gradient of pressure

$$\partial p/\partial n = -j\omega\rho v \tag{2.4}$$

is prescribed [8]. Here ρ is the fluid density and ∂/∂_n is the derivative in the direction of the outward normal.

The principle of the method here presented is based on a treatment of the scattering problem through a system of radiating sources, which should be chosen so that they

reproduce as well as possible the sound field generated by the body of Fig. 1. The sources are taken as point sources, and therefore do not represent an obstacle to the sound field. As a consequence the field generated by each one can be summed without taking into consideration interference effects. As the sources are known, i.e., their amplitudes, the sound field can then be easily calculated through the sum of the fields generated by each source individually. The true problem consists then in finding the sources that can best replace the original body. As a consequence, two important questions arise:

a) Which is the type of source to be used and how should they be placed inside the body?

b) Which optimization method should be employed for the results?

Mathematically the problem is based on representing the sound field by summing up the contributions of the individuals sources

$$p = \sum_{q=1}^{N_q} \sum_{m=-\infty}^{\infty} A_{q,m} \Phi_{q,m} \,, \tag{2.5}$$

where p represents the scattered pressure or the radiated pressure in the field; $A_{q,m}$ is the complex source strength of the q-th source at a point x_q in the field; m is the order of each source and $\Phi_{q,m}$ is the sound field generated by the sources. In Eq. (2.5) $\Phi_{q,m}$ could also be called the source function [8]. Equation (2.5) intrinsically has the condition that each field can be represented by a sum of functions of the type $\Phi_{q,m}$. This is naturally the case, only if all functions $\Phi_{q,m}$ satisfy the wave equation and if they form a complete function system. The first condition is certainly satisfied if $\Phi_{q,m}$, represents for example the field generated by a monopole, dipole or quadrupole. The second condition, i.e., if it is possible to represent any acoustic field as a sum in the form of Eq. (2.5), seems to be as yet unproven with all mathematical rigor [8]. As no difficulty has been noted by other authors (CREMER [9]; HECKL [10], OCHMANN [11]) when miltipole sources were used for the reconstruction of the acoustic field, the same procedure will be used in the present work. In other words, the multipole sources will be used to represent the radiation or scattering problem of the original body.

We have then two distinct situations:

a) one can use a variable order multipole localized in a single point inside the body, that is, in Eq. (2.5) $N_q = 1$ and M is very large,

or

b) one can use only monopole sources positioned in several points inside the body, which renders N_q very large and $M = 1$ in Eq. (2.5).

One can also have a combination of both extreme cases presented in a) and b), that is, to use a multipole (for example, monopole + dipole) positioned in several points. Together with the choice of the type and the positioning of the sources, the choice of the optimization criterium also imposes a fundamental question for the use of the source simulation technique. Basically the idea is to try to approximate the field generated by the sources, determining its source strength (which are ultimately the solution of the problem), to the real field generated by the original body. The error derived from this approximation should be minimized. Several methods can be used to that end, such as

the null field method, the collocation method, the Cremer's method [8]. In this work we have used the least squares minimization.

3. Influence parameters

The parameters that influence the performance of the method, that is, the capacity of the method to reproduce boundary conditions are the following: the type and number of sources, their positioning in the interior of the body, the shape of the source surface, and the existence of critical frequencies. For that purpose a surface error will be defined, which will aid in the evaluation of the performance of the above mentioned parameters:

$$E(\%) = \sum_{i=1}^{N_\varphi} \frac{|Z_m - Z_\varphi|^2}{|Z_m|^2}, \tag{2.6}$$

where Z_m is the measured impedance and Z_φ is the calculated impedance with the source simulation technique for each angle φ around the geometry of the studied body.

3.1. Type of sources

By definition the sources must be radiating wave functions. It is convenient to work with available analytical functions. Only solutions of the Helmholtz equation in separable coordinate systems can be constructed explicitly [8]. In practice, spherical radiators (for three-dimensional problems) or cylindrical radiators (for two-dimensional problems). In the usual systems of coordinates, the wave functions or sources will be represented by:

— generalized spherical coordinates

$$\phi = P_{m_1}^{m_2} \cos(\vartheta) h_{m_1}^{(2)}(kr) e^{jm_2\varphi};$$

— spherical coordinates independent from φ

$$\phi = P_m \cos(\vartheta) h_m^{(2)}(kr);$$

— cylindrical coordinates

$$\phi = H_m^{(2)}(kr) e^{jm\varphi},$$

where P are the Legendre polynomials; $h_m^{(2)}$ the spherical Hankel function of the second order and $H_m^{(2)}$ the cylindrical Hankel function of the second order.

3.2. Location of the sources

A general assumption of the source simulation technique is that the sources must be located in the interior of the closed surface S. It is also possible to put sources on the boundary itself. But this leads to boundary integral equations and to the corresponding BEM, which are not topics of this paper. For the choice of the source location, essentially two alternatives are possible [8]: 1) only a few source locations are chosen, but at these locations a source with increasing order is used; or 2) a continuous source distribution

of simple sources on an inner auxiliary surface is employed. The contrast between both methods is the greatest if a closed auxiliary surface with a layer of monopoles is chosen as one extreme and a infinite series of multipoles at only one source location as the other extreme [8]. The first method is called "the single-layer method" and the second one "the one-point multipole method" [8]. If the geometry of the body is spherical or cylindrical (or not far from those), the use of the one-point multipole method is recommended with the multipole located in the center of the body. This procedure facilitates the convergence of the wave functions and reduces computing time. On the other hand, sources positioned very close to the center when using the single-layer method tend to cause the matrix of linear equations to became more ill-conditioned, leading to an increased surface error (see Fig. 2 and Fig. 3). If the sources are positioned very close to the boundary, the accuracy will deteriorate due to the inadequate integration of the source singularity.

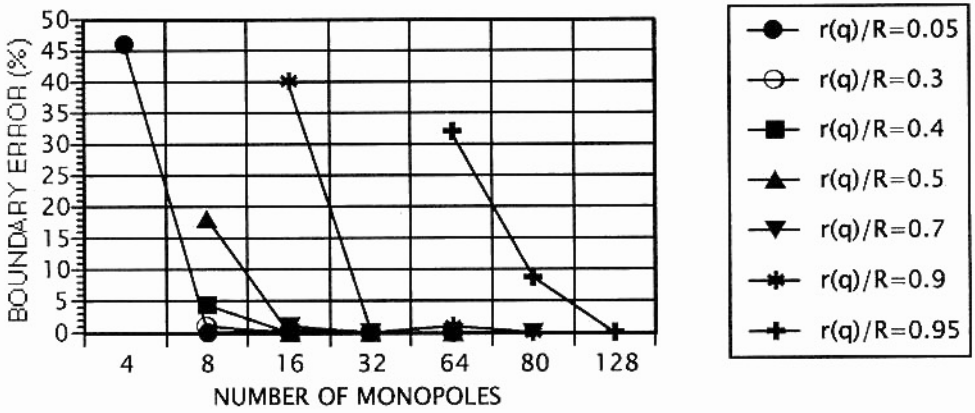

Fig. 2. Error when satisfying the boundary error as a function of the position of the source surface with radius $r(q)$ and a circular cylinder with radius R, $kR = 0.73$.

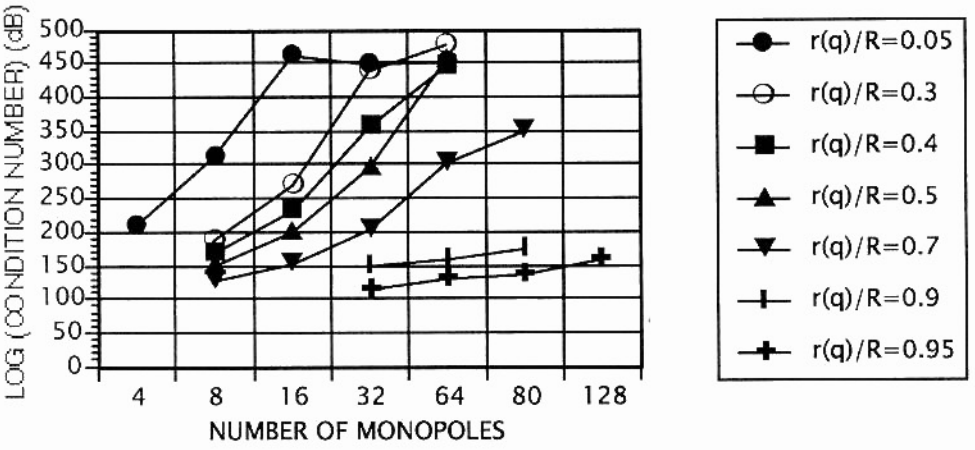

Fig. 3. Condition number in dB as a function of the position of the source surface with radius $r(q)$ and a circular cylinder of radius R, $kR = 0.73$.

There is again substantial increase in computing time due to the increase in the number of sources necessary in order to minimize the surface error. Our findings are not in agreement with TOMILINA [12] and BOBROVNITSKII and TOMILINA [13], who say that the source surface should be close to the body surface in order to improve the accuracy of the problem of reducing the boundary error. This is only correct when kR is very large.

3.3. Number of sources

The number of sources is influenced by several parameters, but mainly by the geometry of the body and the type of the source. In the determination of the number of sources, with respect to the single-layer method considering a circular cylinder, an expression was intended which would give the smallest number of monopoles necessary to satisfy the boundary conditions. Additionally, the position $r(q)/R$ (see Figs. 2 and 3) of the source surface should also comply with the assumption of a minimal number of monopoles.

The simulation leads us to the following:

$$N = \beta \cdot kR, \tag{2.7}$$

where β is an unknown factor, and R is the cylinder radius. This expression establishes a relationship between the wave number, the size of the body, and the number of monopoles. With the simulation the following values have been found for:

a) for $0.73 \leq kR \leq 1.46$ and $r(q)/R = 0.4 \rightarrow \beta = 16$,
b) for $1.83 \leq kR \leq 3.66$ and $r(q)/R = 0.5 \rightarrow \beta = 8$,
c) for $4.58 \leq kR \leq 7.33$ and $r(q)/R = 0.6 \rightarrow \beta = 6$,
d) for $9.16 \leq kR \leq 23.10$ and $0.7 \leq r(q)/R \leq 0.8 \rightarrow \beta = 4$.

3.4. Shape of the source surface

One aspect rarely considered in the utilization of the source simulation technique is the shape of the source, that is, the shape of the auxiliary surface over which the sources are positioned (see ZANNIN [5] and see Subsec. 3.2). The object of study here is a circular cylinder, and for the source surface the following shapes have been used: a) cylindrical, b) elliptical, c) non-elliptical (see Fig. 4). Surface error could be minimized and boundary condition satisfied in all tested cases. The number of monopole sources needed grew in direct proportion to the deviation of the source surface from a circular cylindrical shape (case "a"). This can be observed in Table 1 below:

Table 1. Influence of the shape of the source surface in minimizing boundary error.

Shape	Error (%)	Sources — N
(a)	0.01	8
(b)	0.0005	40
(c)	0.5	20

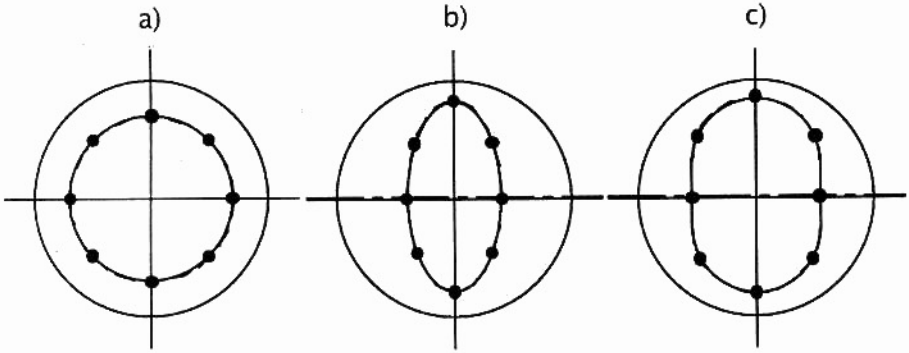

Fig. 4. Shape of the source surface.

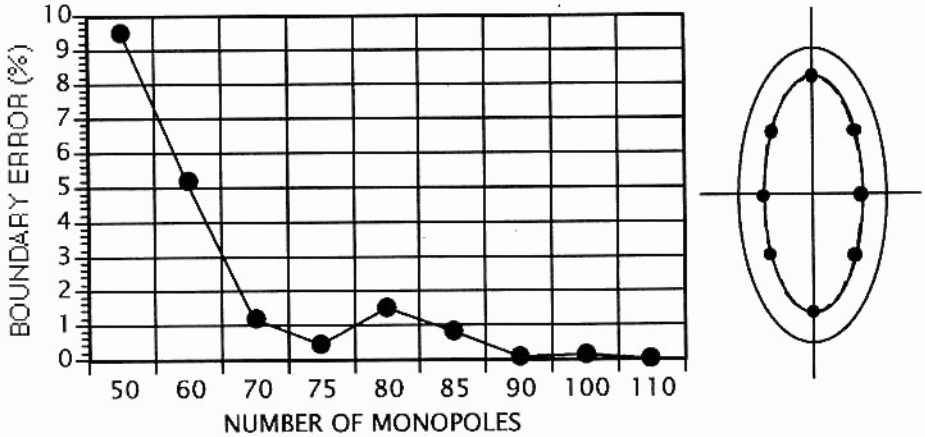

Fig. 5. Elliptical cylinder with elliptical source surface.

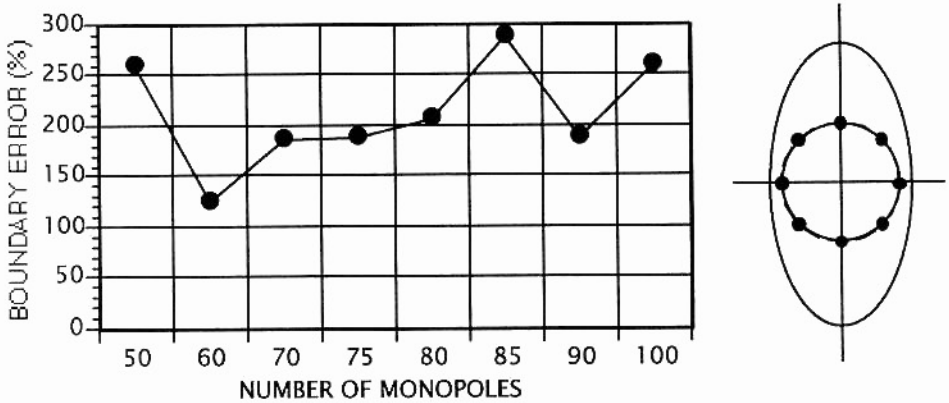

Fig. 6. Elliptical cylinder with cylindrical source surface.

A cylinder with elliptical transverse section was also used as a second object of study. The results obtained were very consistent as long as the source surface was identical with the external surface (see Fig. 5). For the case of a cylindrical source surface located within the elliptical body, the boundary condition could not be satisfied (see Fig. 6). The elliptical body required a significantly larger number of monopole sources in order to get the boundary error minimized.

3.5. Critical frequencies

There are frequencies, sometimes called fictitious eigenfrequencies, at which, or close to which, the solution of the Helmohltz integral equation is non-unique. It is well known that the boundary element method breaks down at these frequencies [14, 15].

JEANS and MATHEWS [16] have demonstrated that in the use of the source simulation technique the critical frequencies correspond to the eigenfrequencies of the internal space formed by the closed source surface, when over this surface the boundary condition of Dirichlet is considered. The eigenfrequencies of a circular space with the Dirichlet condition over its surface are represented by the roots of the Bessel function (see [17]):

$$J_n(kr) = 0, \quad n = 0, 1, 2, 3, \ldots, \tag{2.8}$$

where r is the radius of the source surface.

Nevertheless, other authors report that they have not observed the presence of inner eingenfrequencies when utilizing the source simulation technique, in the calculation of both the acoustic radiation and of the acoustic scattering. Part of the conclusions of these studies are cited in what follows: "*The SUP solution does not appear to be affected by spurious internal resonances which have plagued the integral formulations in the past [18]*"; "*Numerical experiments suggest that this nonuniqueness problem does not exist in the MFS... The reciprocal of the condition number at the eigenfrequencies and* $ka = 4.4934094$ *is not worse than at the other frequencies and it does not seem to deteriorate at any of the frequencies. Our findings agree with those of Koopman et al., who reported the absence of fictitious eigenfrequency difficulty with this method for acoustic radiation problems [19]*"; "*The results for* $R = 1$ *and* $k = 2.40483$ *which is the smallest zero of the Dirichlet eigenvalue for the circle, illustrate that there is no unique problem at the critical wave number [20]*".

In this work we tried to identify the presence or absence of the eigenfrequencies. Figure 7 shows the error when satisfying the boundary conditions close to and at the first frequency of resonance of a circle: $kr = 2.4048255577$. It is fairly obvious that there is a huge error at this frequency and that the problem formulation breaks down. In Fig. 8 we have the logarithm of the condition number.

One important conclusion that can be drawn from Figs. 7 and 8 is that resonance belongs to a very narrow range of frequencies. For source surfaces like a cylinder or a sphere resonance can be easily calculated and therefore avoided. This is one of the advantages of the source simulation technique with respect to the boundary element method.

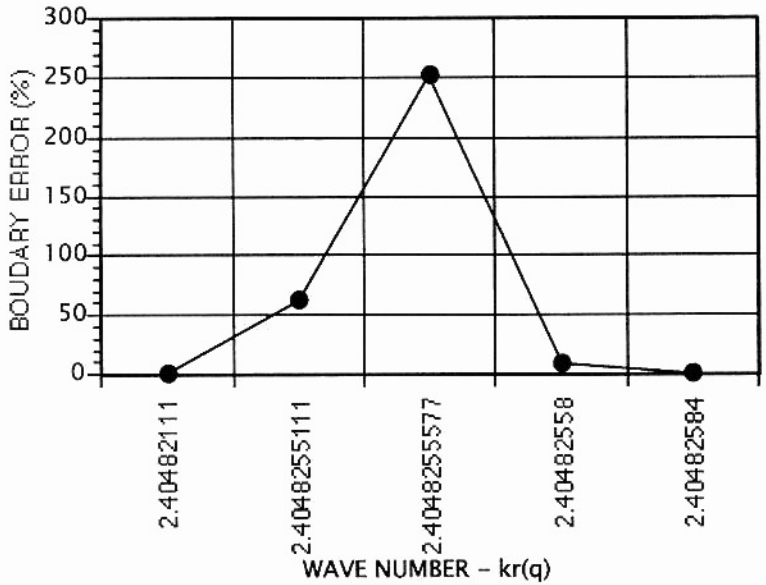

Fig. 7. Boundary error close to and at the resonance frequency of a circle — $kr(q) = 2.4048255577$.

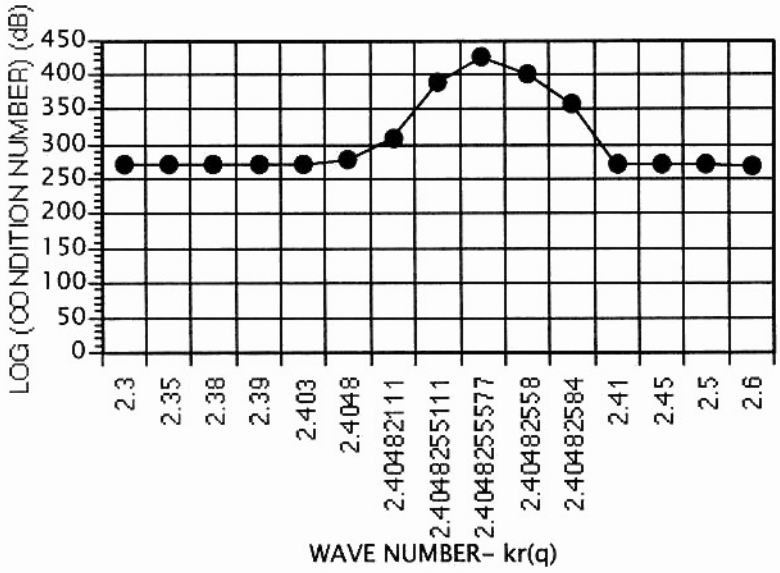

Fig. 8. Logarithm of the condition number at the proximities of the first resonance frequency of a circle — $kr(q) = 2.4048255577$.

One question always present with respect to the source simulation technique is whether the ill-conditioning of the problem (see Figs. 2 and 3) is due to the eigenfrequencies of the inner closed source surface. In Fig. 9 the boundary error can be seen, calculated for the first resonance of a circle — ($kr = 2.4048255577$) — as a function of

the number of sources. It can be observed that the error is extremely large (see Fig. 7), though remaining constant despite a substantial increase in the number of sources: 20 to 150 monopoles. In ill-conditioned problems the trend is toward an increase in the error and in the condition number (see Figs. 2 and 3 and [21]) when the number of sources increases [22]. Therefore, one can conclude that the ill-conditioning of the problem is a characteristic of the source simulation technique and is not caused by the eigenfrequencies of the internal space formed by the source surface.

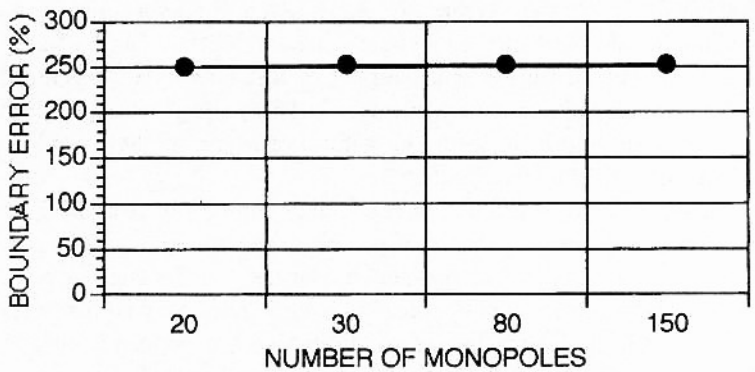

Fig. 9. Influence of the number of monopoles on the boundary error for $kr = 2.4048255577$.

4. Concluding remarks

The quality of the results obtained by the source simulation technique depends on the relationship between some parameters. The most relevant of them are: the shape of the inner source surface, the location of the sources at the source surface, and the number of sources. If one of these parameters is inadequately chosen, this will negatively influence the development of the whole numerical calculation.

In the case of the single-layer method, sources should not be positioned very close to the center of the body, as in this case the condition number of the matrix grows rapidly meaning that it is becoming ill-conditioned. If the wave number is small, one can position the sources close to the center of the body. The advantage of doing so is in the use of a small number of sources in order to minimize the boundary error, which is also translated into less computing time. On the other hand, as the wave number grows, the sources are located closer to the surface. However, the positioning of the sources should obey a relationship between the smallest dimension of the source surface and the largest dimension of the body under study. For the case of a cylinder of radius R and a source surface of radius $r(q)$, the relationship is given by $r(q)/R = 0.9$. Above this value the method becomes very unstable due to the occurence of singularities.

With respect to the shape of the source surface, numerical results have shown that the shape of the studied body and the shape of the source surface should be as similar as possible to each other. Proceeding this way it is possible to minimize the boundary error and to satisfy the boundary conditions, which was not possible when the body considered was an elliptical cylinder and the source surface a circular cylinder.

With respect to the number of sources used there are two opposing effects. If the number of sources is too small the acoustical field cannot be reproduced with precision. If the number of sources is too large, both computing time and computational errors end up increasing. Numerical experiments led us to the conclusion that the ill-conditioning of the problem is not caused by the eigenfrequencies of the source surface, but is a characteristic of the method itself. The method breaks down when the excitation frequency coincides with the eigenfrequencies of the inner space formed by the source surface. The numerical experiments have shown that the eigenfrequencies belong to a very narrow band. In this way, for non-complex surfaces such as a sphere or a circle, they can be easily calculated and avoided. This is one advantage with respect to BEM, as in the last method there is not the possibility of choosing a source surface. In BEM the sources are positioned over the surface of the body and as a result the help of other methods is needed in order to overcome the problem of the eigenfrequencies.

The great disadvantage in the use of the source simulation technique is in the fact that rules for the positioning of the source surface are not known *a priori*. The positioning of the source surface and in consequence of the sources themselves, is based on the experience of the programmer. Further research is necessary to investigate how the method performs with complex surfaces. In that case the main question is about the shape of the source surface.

References

[1] LORD RAYLEIGH, *The theory of sound*, Dover Publications, New York 1945.

[2] P.M. MORSE, *Vibration and sound*, MacGrawHill Book Company, New York 1948.

[3] K. GÖSELE, Acustica, **3**, 243–253 (1953).

[4] L. CREMER and M. HECKL, Kap. 6, *Körperschall Phisikalische Grundlagen und technische Anwendungen*, Springer-Verlag, Berlin 1995.

[5] P.H. ZANNIN, Kap. 5, *Berechnung der Schallstreuung nach der Quellsimulationstechnik und Vergleich mit den Meßergebnissen*, Technische Universität Berlin, Berlin 1996.

[6] A.F. SEYBERT *et al.*, *The solution of coupled interiour acoustic problems using the boundary element method*, J. Acoust. Soc., **90**, 1612–1618 (1990).

[7] YU.I. BOBROVNITSKII and T.M. TOMILINA, *General properties and fundamental errors of the method of equivalent sources*, Sov. Phys. Acoust., **41** (1995).

[8] M. OCHMANN, *The source simulation technique for acoustic radiation problems*, Acustica, **81**, 512–527 (1995).

[9] L. CREMER, *Die Synthese de Schallfeldes eines beliebigen festen Körper in Luft mit beliebieger Schnelleverteilung aus Kugel schallfelder*, Acustica, **55**, 44–46 (1984).

[10] M. HECKL, *Bemerkung zur Berechnung der Schallabstrahlung nach der Methode der Kugelfeldsynthese*, Acustica, **68**, 251–257 (1989).

[11] M. OCHMANN, *Die Multipolstrahlersynthese — ein effektives Verfahren zur Berechnung der Schallabstrahlung von schwingenden Strukturen beliebiger Oberflächengestalt*, Acustica, **72**, 233–246 (1990).

[12] T.M. TOMILINA, *Equivalent sources method for noise prediction problem: Analysis of errors*, Inter-Noise-95, Newport Beach, CA, USA 1995.

[13] Yu.I. Bobrovnitskii and T.M. Tomilina, *Calculation of radiation from finite elastic bodies by the method of auxiliary sources*, Sov. Phys. Acoust., **36** (1990).

[14] H.A. Schenk, *Improved integral formulation for acoustic radiation problems*, J. Acoust. Soc. Amer., **44**, 41–58 (1968).

[15] K.A. Cunefare, G. Koopmann and K. Brod, *A boundary element method for acoustic radiation valid for all wave numbers*, J. Acoust. Soc. Am., **85**, 39–48 (1989).

[16] R. Jeans and I.C. Mathews, *The wave superposition method as a robust technique for computing acoustic fields*, J. Acoust. Soc. Amer., **92**, 1156–1165 (1992).

[17] E. Skudrzyk, *The foundation of acoustics*, Springer, Vienna 1971.

[18] D.M. Russel *et al.*, *A comparision between the boundary element method and the wave superposition approach for the analysis of the scattered fields from rigid bodies and elastics shelles*, J. Acoust. Soc. Amer, **89**, 5, 2185–2196 (1991).

[19] P.S. Kondapalli, D.J. Shippy and G. Fairweather, *Analysis of acoustic scattering in fluids and solids by the method of fundamental solutions*, J. Acoust. Soc. Amer., **91**, 1844–1854 (1992).

[20] R. Kress and A. Mohsen, *On the simulation source technique for exterior problems in acoustics*, Math. Meth in the Appl. Sci., **8**, 585–597 (1986).

[21] R.J. Hanson, *A numerical method for solving Fredholm integral equations of the frist kind using singular values*, SIAM J. Numer. Anal., **8**, 3 (1971).

[22] A. Bogomolny, *Fundamental solutions methods for elliptic boundary value problems*, SIAM J. Numer. Anal., **22**, 4, 644–669 (1985).

ARCHIVES OF ACOUSTICS
25, 3, 331–358 (2000)

SOLITON MODELS OF DISLOCATION AND ACOUSTIC EMISSION IN METALLIC MATERIALS

A. PAWEŁEK

Polish Academy of Sciences
Aleksander Krupkowski Institute of Metallurgy and Materials Science
(30-059 Kraków, ul. Reymonta 25, Poland)

S. PILECKI

Polish Academy of Sciences
Institute of Fundamental Technological Research
(00-049 Warszawa, Świętokrzyska 21, Poland)

In this paper the analysis of the dislocation models and the possibilities of their application to the description of the acoustic emission (AE) sources, which are acting during plastic deformation of metallic materials are presented. Especially the one-dimensional atomic Frenkel–Kontorova model of dislocation (model FK) has been discussed with particular reference to its nonlinear properties which determine the movement of the dislocation kink along the dislocation line as a solitary wave process. At the same time the equivalence of the FK model with the string model of dislocation (S model) has been demonstrated. In consequence, the FK model has been generalized by the consideration of new terms of higher order responsible for the anharmonic (nonlinear) interaction between the atoms (including also the second coordination zone). A new class of nonlinear partial differential equations (NLPD equations), which may play a role in the theory of lattice vibration of the crystal with dislocation as well as in the theory of dislocations, has been obtained. The results are discussed in the context of rich experimental data (obtained at IMIM) which establish the correlations between the measured AE parameters and the plastic deformation mechanisms as well as microstructure evolution occurring in fcc single and polycrystals subjected to channel-die compression, especially at the liquid nitrogen temperature.

1. Introduction

The phenomenon of acoustic emission (AE), occurring particularly at a moderate degree of plastic strain, is generally explained on the basis of various forms of the dislocation movements [1–4]. However, there exists no model, which would be commonly accepted. On the other hand, the experimental data obtained so far at the IMIM, suggest that there exist strong correlations between the AE behaviour and the dislocation mechanisms of plastic deformation [5–9]. In particular, it was suggested in the quoted papers

that the AE phenomenon during channel-die compression of both fcc monocrystalline (Cu, Ag, Cu–2% Al) and polycrystalline (Cu, Cu–30% Zn) metals may be interpreted on the basis of two main dislocation processes. The first one is the acceleration (or deceleration) of the dislocation motion and the other one is the annihilation of dislocations occurring especially during the escape of dislocations to the free surface of a sample.

For these reasons the main aim of this paper is to search for such a model of dislocation which could serve simultaneously as a model of the AE source. To attain this, the existing dislocation models have been briefly reviewed. Especially, the atomic Frenkel–Kontorova dislocation model (FK model) and its equivalent of the model of dislocation as a string (S model) has been reconsidered. As a consequence, the FK model has been generalized by the consideration (including the second coordination zone) of the anharmonic interaction between the atoms.

2. Survey of dislocation models

Generally, there are two kinds of dislocation models: the discrete models and continuous ones. The more important models among the discrete ones are: the Peierls–Nabarro model (PN model), the Maradudin static and dynamic models, the Tewary dynamic model and the FK model. These models are discussed in greater detail in [10]. Here we want to note that thanks to the PN model, we are familiar with the concepts of both energetic barriers (PN barriers) and sinusoidal periodic force, f, commonly called the PN force, which is given by

$$f = b\tau_p \sin(2\pi x/a), \tag{1}$$

where $\tau_p = U_p/ab$ is called the Peierls stress, and U_p defines just the energy of the PN barriers; a is the lattice parameter and b is the magnitude of the Burgers vector of dislocation.

Other dislocation models are based on the static and/or dynamic properties of the crystal lattice. The simplest of them, at least from the point of view of lattice vibrations, is the atomic FK model of dislocation in a one-dimensional crystal (Fig. 1). In the FK model the PN force is also taken into account, and it is very interesting to note that the FK model is mathematically equivalent to the continuous model of dislocation as an infinite string (S model, Fig. 2), vibrating within two adjacent valleys of the Peierls potential, $U(x)$, defined as follows

$$U(x) = -\int f(x)\,dx = (U_p/2)[1 - \cos(2\pi x/a)]. \tag{2}$$

The movement of the dislocation in a real crystal is the consequence of the dislocation kink motion along the dislocation line. The basic solutions of the governing equation in the FK model, as presented further in Sec. 3, describe clearly the properties of the moving dislocation kinks and particularly also their behaviour as the solitary (nonlinear) wave processes. Moreover, the FK model is, at the same time, a quite good analytical model of the dislocation core, the elastic properties of which are highly nonlinear, and thus their description in terms of the linear theory of elasticity is completely insufficient.

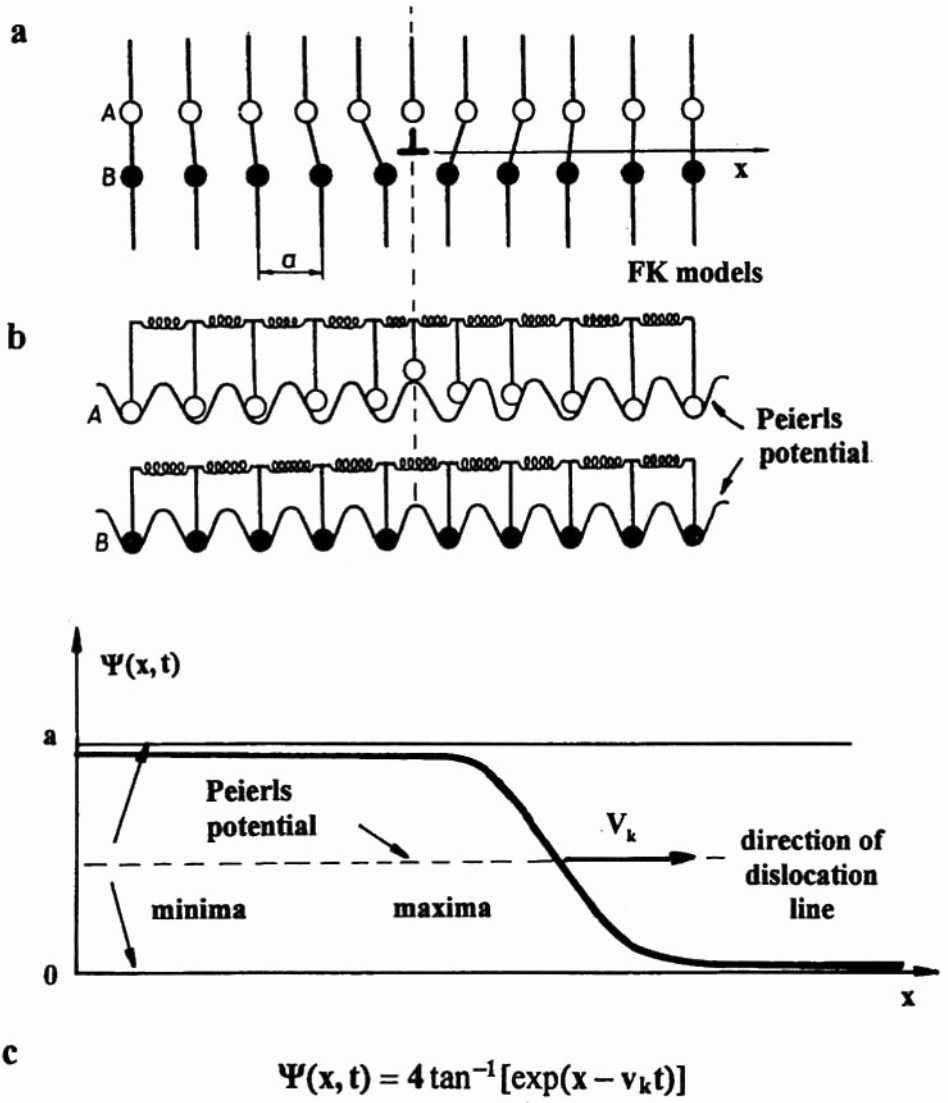

Fig. 1. One-dimensional Frenkel–Kontorova model (FK model) of edge dislocation (a), the corresponding atom configuration in the Peierls potential (b), and the kink motion as a solitary wave process (c).

This strong nonlinearity of the dislocation core determines the solitary wave behaviour of the moving dislocation kink. Since the vibrating motion of the dislocation core as well as the mutual annihilation of the dislocation kinks of opposite signs may be, in our oppinion, the real causes of the acoustic waves in plastically deformed crystals, both the FK and the S models will be reconsidered below in greater detail as they now constitute the basis of the dislocation models of AE sources.

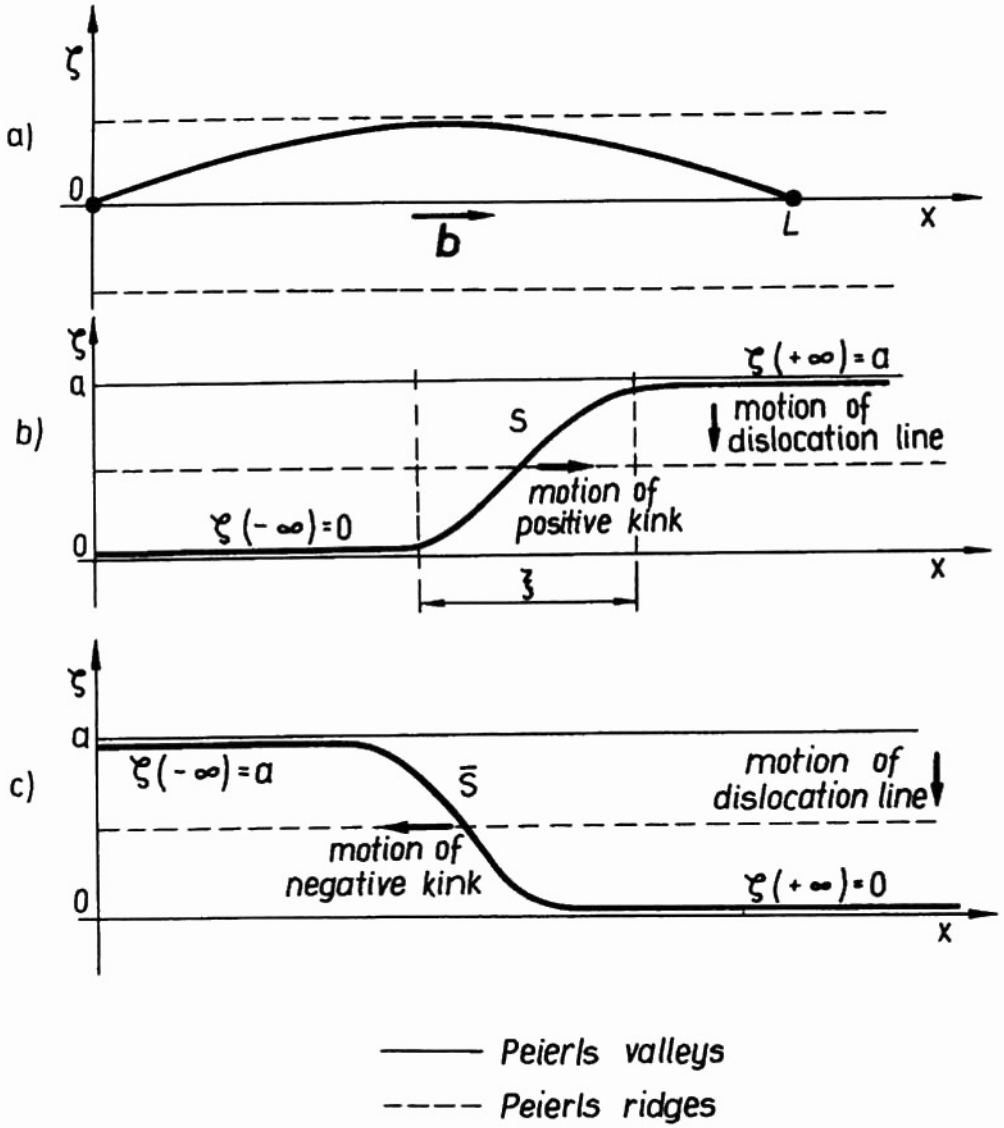

Fig. 2. String model (S model) of dislocation (a) and the kink motion (b), (c) along an infinite dislocation line.

2.1. The Frenkel–Kontorova dislocation model (FK model)

In the one-dimensional FK model two series of atoms are considered (Fig. 1, at the top). The lower series (B) is immobile and contains n atoms which are treated as perfectly rigid and elastic balls lying in the potential valleys and connected by the springs (Fig. 1, at the middle). On the other hand, the higher series (A) contains $(n + 1)$ atoms which

may vibrate along the x-axis. In this way a system of two such series of atoms forms an object like the nonius of the effective length ξ in which to $(n+1)$ marks (atoms) in the higher part there correspond only n marks (atoms) in the lower one.

Let assume that u_k is the displacement of the k-th atom in the higher row in relation to the equilibrium position occupied by its counterpart in the lower row of atoms. In further considerations it will be assumed that the lower row of atoms constitutes a perfect, one-dimensional crystal in which the atom at the position x_k determines simultaneously the position of the k-th node of an ideal one-dimensional crystal lattice of the parameter a. For simplicity it is also assumed that the magnitude of the Burgers vector is $b \cong a$. Then the position of the k-th atom in the higher row can be written as follows

$$x_k = k\,a + u_k\,, \tag{3}$$

and the total potential energy, Φ, of the atoms in the higher row in relation to those in the lower one may be written in the following form

$$\Phi = A_0 \sum_{k=-\infty}^{\infty} [1 - \cos(2\pi u_k/a)] + (\alpha_0/2) \sum_{k=-\infty}^{\infty} (u_{k+1} - u_k)^2, \tag{4}$$

where A_0 and α_0 are the interaction constants characteristic of the FK model. The first term in Eq. (4) describes the part of potential energy related to the changes in positions of the atoms in the dislocated crystal. On the other hand, the second term describes the energy of the mutual interactions between the vibrating atoms in the higher row. Moreover, this term is derived by using the so-called approximation of the first nearest neighbours (e.g. for the k-th atom there are atoms in the nodes with the numbers $(k-1)$ and $(k+1)$ only). With these assumptions, the equation of motion for the k-th atom of mass m has the following form

$$m\partial^2 u_k/\partial t^2 = -\partial\Phi/\partial u_k\,, \tag{5}$$

or, after differentiation of Eq. (4), the form

$$m\partial^2 u_k/\partial t^2 = -(2\pi \cdot A_0/a)\sin(2\pi u_k/a) + \alpha_0(u_{k+1} + u_{k-1} - 2u_k). \tag{6}$$

Furthermore, in the FK model it is also assumed that the quantities u_k are continuous functions of the position x and the time t, and that the displacements of any two neighbouring atoms from the equilibrium position are not drastically different, i.e. the following relations are satisfied

$$u_{k+1}(x) \cong u_k(x+a) \qquad \text{and} \qquad u_{k-1}(x) \cong u_k(x-a). \tag{7}$$

Using Eq. (7) and the second order Taylor expansion the next relation can be obtained

$$u_{k+1} + u_{k-1} - 2u_k \cong a^2\partial^2 u_k/\partial x^2. \tag{8}$$

Finally, putting Eq. (8) into Eq. (7) and denoting for simplicity, $u_k(x,t) \equiv u(x,t) \equiv u$, one can obtain the equation which is a governing one in the FK model. This is the nonlinear partial differential equation (NLPD equation) which is very well known in the theory of solitons and is called the sine-Gordon equation (SG equation)

$$m\partial^2 u/\partial t^2 - \alpha_0 a^2 \partial^2 u/\partial x^2 + (2\pi A_0/a)\sin(2\pi u/a) = 0. \tag{9}$$

In physical contexts the SG equation is often written in the form

$$\partial^2\Psi/\partial t^2 - c_0^2\partial^2\Psi/\partial x^2 + \omega_0^2 \sin\Psi = 0, \tag{10}$$

where it is assumed that $\Psi = 2\pi u/a$ and both the velocity c_0 and the frequency ω_0 constants, characteristic of the FK model, are given by

$$c_0^2 = \alpha_0 a^2/m \qquad \text{and} \qquad \omega_0^2 = 4\pi^2 A_0/ma^2. \tag{11}$$

In further considerations other notations will be used for the derivatives, e.g. $\partial^2\Psi/\partial x^2 \equiv \Psi_{xx}$. Then the SG equation (10) may be written in a more simple form

$$\Psi_{tt} - c_0^2\Psi_{xx} + \omega_0^2 \sin\Psi = 0. \tag{12}$$

The basic solutions of the SG equation, reflecting the essence of the FK model, and describing the soliton nature of the movement of dislocations, will be discussed further, in Sec. 3, where the generalization of the FK model is proposed. Below, the reconsideration of the string model of dislocation (S model) and its equivalent of the FK model will be also presented briefly in the new aspect of the dislocation models for AE sources (see also [10]).

2.2. The string model of dislocation (S model)

The S model is only one of the continuous models which is reconsidered here in the context of the dislocation models of AE sources. Other types of continuous dislocation models are based on the Somigliano model which was constructed within the theory of continuous media and they will not be considered here.

The dislocation segment in a real crystal, lying in a slip plane (Fig. 2) between two point obstacles (e.g. of the type of forest dislocations), and, at the same time, being potentially the dislocation source of the Frank-Read type (FR source, Fig. 3), can be treated as a string vibrating in a single Peierls potential valley (Figs. 2a and 3a, b). The general equation of the motion of a dislocation as a vibrating string was derived by Koehler and later this equation was considered also by Granato and Lücke in the context of the theory of internal friction (see also [10]).

It appears that in the particular case, when the infinite string is considered and both damping and external forces are neglected, the shape, $\zeta(x,t)$, of a freely vibrating dislocation string is described by the following NLPD equation

$$M\partial^2\zeta/\partial t^2 - T\partial^2\zeta/\partial x^2 + b\tau_p \sin(2\pi\zeta/a) = 0, \tag{13}$$

where M is the effective mass of the dislocation unit length, T is the line tension of the dislocation, and the Peierls stress τ_p is defined by Eq. (1). One can see that Eq. (13) is the same as the SG Eq. (12), and that the characteristic constants are now given by

$$c_0^2 = T/M, \qquad \omega_0^2 = 2\pi b\tau_p/Ma. \tag{14a}$$

The expressions (14a) mean that the FK and S models are mathematically equivalent. There are two kinds of the consequences of this equivalence (see also [10, 11]). First,

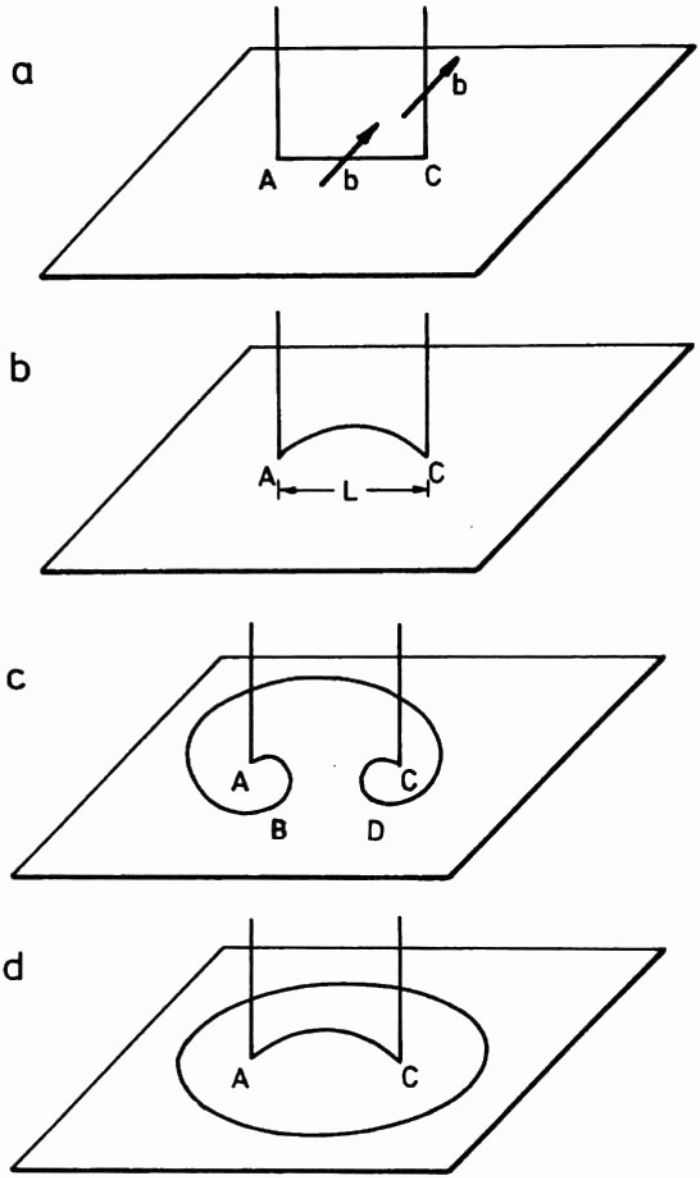

Fig. 3. The model of the Frank-Read dislocation source operation (FR model).

the parameters α_0 and A_0 in the FK model can be expressed by the corresponding parameters M and T in the S model because the characteristic constants c_0 and ω_0, appearing in the common SG equation (12), are given by

$$c_0^2 = T/M = \alpha_0 a^2/m, \qquad \omega_0^2 = 4\pi^2 A_0/ma^2 = 2\pi b\tau_p/Ma. \tag{14b}$$

More detailed considerations [10, 11] show that the effective mass of the dislocation of a length equal to the lattice parameter a, is, as a good approximation, equal to the mass of the atom, i.e. $Ma \cong m$. Thus, the interaction constants α_0 and A_0 in the FK model may be expressed as

$$\alpha_0 = T/a, \qquad A_0 = \tau_p ab/2\pi = U_p/2, \tag{15}$$

i.e. the microscopic parameters α_0 and A_0 may be expressed by the macroscopic parameters of line tension T and the Peierls stress τ_p, which are often estimated as $T \cong \mu b^2$ and $\tau_p \cong 10^{-4}\mu$ for fcc and $\tau_p \cong 10^{-2}\mu$ for bcc crystals; μ is the shear modulus for a given crystal.

Secondly, the equivalence of the FK and S models means also that their common Eq. (12), and particularly its solutions, can be, in a sufficiently satisfying way, referred to a three-dimensional real crystal in which the movement of dislocation is, after all, a very complex process perturbed by various internal interactions, and in general, it proceeds also under the perturbations of external forces. In this way, the SG equation and its solutions, when related to an idealized case, describe the basic unperturbed forms of the dislocation motion which have been extracted from the real more or less perturbed and chaotic movement. The simplest cases of such solutions will be further discussed in detail in Sec. 3.

3. Generalization of the FK model

The generalization of the FK model, proposed in this paper, consists in taking into account new assumptions. The first one is the interaction between atoms in the second coordination zone and the second one is the nonlinear (anharmonic) interaction between the atoms in both the coordination zones.

The starting point is the expression for the potential energy of a simple ideal crystal of regular structure. This expression contains the terms of the Taylor expansion including those of fourth order [12]. Thus, instead of Eq. (4), the following formula will be considered now

$$\begin{aligned}\Phi \;=\; & \Phi_{p.} + (1/2)\sum_{k}\Bigg\{(1/2!)\sum_{mn}\Phi^{(2)}_{\alpha\beta}(\mathbf{m},\mathbf{n})u_\alpha(\mathbf{m})u_\beta(\mathbf{n}) \\ & + (1/3!)\sum_{mnp}\Phi^{(3)}_{\alpha\beta\mu}(\mathbf{m},\mathbf{n},\mathbf{p})u_\alpha(\mathbf{m})u_\beta(\mathbf{n})u_\mu(\mathbf{p}) \\ & + (1/4!)\sum_{mnpq}\Phi^{(4)}_{\alpha\beta\mu\nu}(\mathbf{m},\mathbf{n},\mathbf{p},\mathbf{q})u_\alpha(\mathbf{m})u_\beta(\mathbf{n})u_\mu(\mathbf{p})u_\nu(\mathbf{q})\Bigg\},\end{aligned} \tag{16}$$

where the vectors

$$\mathbf{m} = \mathbf{l} - \mathbf{k}, \qquad \mathbf{n} = \mathbf{l}' - \mathbf{k}, \qquad \mathbf{p} = \mathbf{l}'' - \mathbf{k}, \qquad \mathbf{q} = \mathbf{l}''' - \mathbf{k}, \tag{17}$$

are lattice vectors related to the corresponding components, u_α, of the vectors of relative displacements of the atoms in the positions defined by the respective vectors $\mathbf{k}$ and $\mathbf{k}+\mathbf{m}$,

etc. These components are determined by

$$u_\alpha(\mathbf{m}) \equiv u_\alpha(\mathbf{l}) - u_\alpha(\mathbf{k}) = u_\alpha(\mathbf{k}+\mathbf{m}) - u_\alpha(\mathbf{k}). \tag{18}$$

Instead, the quantities, $\Phi^{(i)}_{\alpha\beta\ldots}$, where $i = 2,3,4$, are the force constants of the second, third and fourth order, respectively. They are defined as the values of the respective second, third and fourth order derivatives calculated with respect to the corresponding components $u_\alpha(\mathbf{m})$. For most crystals, the values of the force constants are known and are not given here.

In the one-dimensional case, considered here, we have $\alpha = \beta = \mu = \nu \equiv x$, $u_\alpha(\mathbf{m}) = u(\mathbf{l}) - u(\mathbf{k}) \equiv u_{k+m} - u_k$, $\Phi^{(i)}_{\alpha\beta\ldots}(\mathbf{m},\mathbf{n}) \equiv \Phi_{mn}$, and $\Phi_p = (U_p/2)[1 - \cos(2\pi u_k/a)]$. Then all the expressions become simpler and one can obtain the following formula for the potential energy of a one-dimensional crystal with a dislocation

$$\begin{aligned}\Phi \;=\; & (U_p/2)[1-\cos(2\pi u_p/a)] + (1/2)\left\{\sum_{k=-\infty}^{\infty}(1/2!)\sum_{mn}\Phi_{mn}(u_{m+k}-u_k)(u_{n+k}-u_k)\right.\\ & + (1/3!)\sum_{mnp}\Phi_{mnp}(u_{m+k}-u_k)(u_{n+k}-u_k)(u_{p+k}-u_k)\\ & \left.+ (1/4!)\sum_{mnpq}\Phi_{mnpq}(u_{m+k}-u_k)(u_{n+k}-u_k)(u_{p+k}-u_k)(u_{q+k}-u_k)\right\},\end{aligned} \tag{19}$$

where the summation proceeds over m, n, p and q, as including the second coordination zone, and should be taken from -2 up to $+2$. In this way the final form of the equation of motion for the k-th atom may be written as follows

$$\begin{aligned}m\partial^2 u_k/\partial t^2 \;=\; & -\partial\Phi/\partial u_k = -b\tau_p \sin(2\pi u_k/a)\\ & + A_1\left[(u_{k+1}-u_k)-(u_k-u_{k+1})\right] + A_2\left[(u_{k+2}-u_k)-(u_k-u_{k+2})\right]\\ & + B_1\left[(u_{k+1}-u_k)^2-(u_k-u_{k+1})^2\right] + B_2\left[(u_{k+2}-u_k)^2-(u_k-u_{k+2})^2\right]\\ & + C_1\left[(u_{k+1}-u_k)^3-(u_k-u_{k+1})^3\right] + C_2\left[(u_{k+2}-u_k)^3-(u_k-u_{k+2})^3\right],\end{aligned} \tag{20}$$

where the constants A_i, B_i and C_i, $(i = 1,2)$ may be expressed by the force constants Φ_{mn}, and by the force constants of higher orders, i.e. the third Φ_{mnp} and fourth Φ_{mnpq} ones. Consequently, like in the case of the FK model, we use the continuous approximation and the fourth order Taylor expansion, i.e. it is assumed that

$$u_{k+n}(x) \cong u_k(x + an), \tag{21}$$

and

$$\begin{aligned}u_{k+n} - u_k \;=\; & (an)\partial u_k/\partial x + (1/2!)(an)^2\partial^2 u_k/\partial x^2\\ & + (1/3!)(an)^3\partial^3 u_k/\partial x^3 + (1/4!)(an)^4\partial^4 u_k/\partial x^4,\end{aligned} \tag{22}$$

where the index n proceeds over ±1, ±2. In this way a new NLPD equation is obtained governing in the generalized FK model. Namely, after the replacements, $\Psi = 2\pi u/a$ and $u \equiv u_k$, and using a simple notation of the derivatives, it has the following form

$$\Psi_{tt} - c_0^2\Psi_{xx} + \omega_0^2 \sin\Psi = c_1^3\Psi_x\Psi_{xx} + c_2^4\Psi_x^2\Psi_{xx} + c_3^4\Psi_{xxxx}\,, \tag{23}$$

where the constants c_i $(i = 0, 1, 2, 3)$ and the ω_0 are expressed by the formulae

$$c_0^2 = \alpha a^2/m, \qquad c_1^3 = \beta a^3/m, \qquad c_2^4 = \gamma a^4/m,$$
$$c_3^4 = \delta a^4/m, \qquad \omega_0^2 = 2\pi^2 U_p/ma^2, \tag{24}$$

in which the α, β, γ and δ constants depend only on the force constants $\Phi_{mn\ldots}$. Below the most important cases of the general Eq. (23) will be briefly considered.

3.1. A non-dislocated crystal ($\omega_0 = 0$)

This case is mostly discussed in the theory of crystal lattice vibrations. FLYTZANIS *et al.* [13] have shown that it leads to the type of the NLPD equation well known in the theory of solitons as the Boussinesq equation. Namely, after the substitution $\Theta = \Psi_x$ Eq. (23) with $\omega_0 = 0$ becomes the so-called generalized Boussinesq equation in which both kinds of anharmonicity (cubic and quartic) are taken into account

$$\Theta_{tt} - c_0^2\Theta_{xx} = (c_1^3/2)(\Theta^2)_{xx} + (c_2^4/3)(\Theta^3)_{xx} + c_3^4\Theta_{xxxx}\,. \tag{25}$$

On the other hand, considering only the cubic anharmonicity (in Eq. (25) $c_2 = 0$) we obtain the NLPD equation which is known simply as the Boussinesq equation, whereas the consideration of the quartic anharmonicity only, i.e. the nonlinearity of the fourth order (in Eq. (25) $c_1 = 0$), leads to the NLPD equation which is called the modified Boussinesq equation. The explicit forms of these NLPD equations are not given here, though it is worth of notice that all the NLPD equations of Boussinesq type are of very great importance in the theory of crystal lattice vibrations.

3.2. A dislocated crystal with cubic ($c_2 = 0$) *and quartic* ($c_1 = 0$) *anharmonicities*

The consideration of the cubic anharmonicity only in the generalized FK model is described by Eq. (23) with the constant $c_2 = 0$, i.e. by a new type of the NLPD equation

$$\Psi_{tt} - c_0^2\Psi_{xx} + \omega_0^2 \sin\Psi = c_1^3\Psi_x\Psi_{xx} + c_3^4\Psi_{xxxx}\,. \tag{26}$$

Instead, the consideration of the anharmonicity of the fourth order only (Eq. (23) with the constant $c_1 = 0$) also leads to a new type of the NLPD equation

$$\Psi_{tt} - c_0^2\Psi_{xx} + \omega_0^2 \sin\Psi = +c_2^4\Psi_x^2\Psi_{xx} + c_3^4\Psi_{xxxx}\,. \tag{27}$$

In this way, we have obtained a new class of NLPD equations not discussed so far in the theory of solitons. It is very probable that they have solitary wave solutions which also (like in the case of the Boussinesq equations) may play a role not only in the theory of dislocated lattice crystal vibrations, but also in the very theory of dislocations. To our knowledge, any solutions of these equations are not known and some efforts to solve them are undertaken now by using both the analytical and numerical methods. These attempts are limited rather to literature studies, though the computer simulation of numerical solutions is sufficiently advanced now.

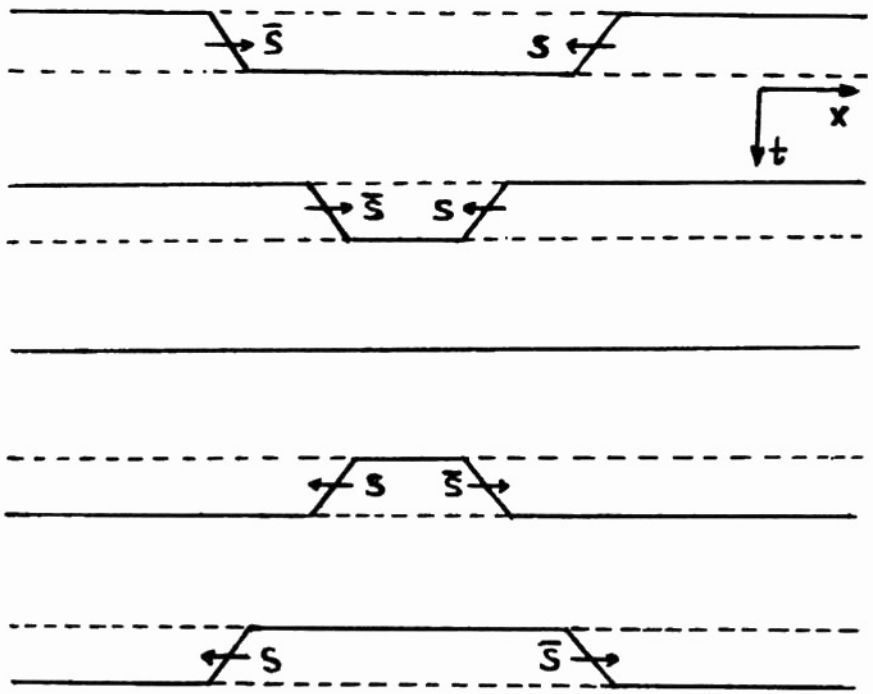

Fig. 4. A schematic illustration of the annihilation and creation of dislocation kinks described by the two-soliton solution of the SG equation in the FK model.

3.3. A harmonic crystal with dislocation ($c_1 = c_2 = c_3 = 0$)

It appears that the harmonic vibrations of atoms within the first coordination zone in a one-dimensional crystal with a dislocation is still the case best recognized. It is described by Eq. (23) with $c_1 = c_2 = c_3 = 0$, i.e. just by the well known SG equation (12)

$$\Psi_{tt} - c_0^2 \Psi_{xx} + \omega_0^2 \sin \Psi = 0, \tag{28}$$

which is the fundamental equation in the FK model. The SG equation was discussed sufficiently in Sec. 2.1, and here we present its simplest solutions which was found for the first time by SEEGER *et al.* [14] (see also [10]). These solutions can serve as the basic dislocation models for the elementary acoustic emission events.

The fundamental one-soliton solution of the SG equation (28) may be written in the form

$$\Psi(x,t) = 4 \tan^{-1} \{\exp[\pm(x - vt)/\xi]\}, \tag{29}$$

where $\xi = \xi_0(1 - v^2/c_0^2)^{1/2}$ is the width of the dislocation kink and v is its velocity; ξ_0 is the kink rest width. The solution (29) describes the movement of the dislocation kinks, i.e. both the positive (sign "+" in expression (29)) and the negative (sign "-" in (29)) kinks as a solitary wave process (or simply as the soliton, s, and the antisoliton, $\bar{s}$, respectively; Fig. 2b, c; $\xi = \Psi$).

The simplest two-soliton solution of SG equation, given by the formula

$$\Psi(x,t) = \tan^{-1}[c_0 \sinh(vt/x)/v\cosh(x/\xi)], \tag{30}$$

describes, in turn, the movement of a system of two dislocation kinks of opposite signs which are approaching each other from infinity, and, at first, they are annihilated and next created in subsequent Peierls potential valley, and in the further evolution they run away again in opposite directions to infinity. Thus, this solution describes the elementary dislocation annihilation process inside the crystal as a solitary wave process. There exists another two-soliton solution of the SG equation, i.e. the so-called pulson

$$\Psi(x,t) = 4\tan^{-1}\left\{(\omega_0^2 - \omega_p^2)^{1/2}\sin(\omega_p t)/\omega_p.\cosh\left[x(1-\omega_p^2/\omega_0^2)^{1/2}/\xi_0\right]\right\}, \tag{31}$$

which is a stable system of two dislocation kinks of opposite signs vibrating at the frequency ω_p. Similarly, the kinks here are also approaching each other, and after anni-

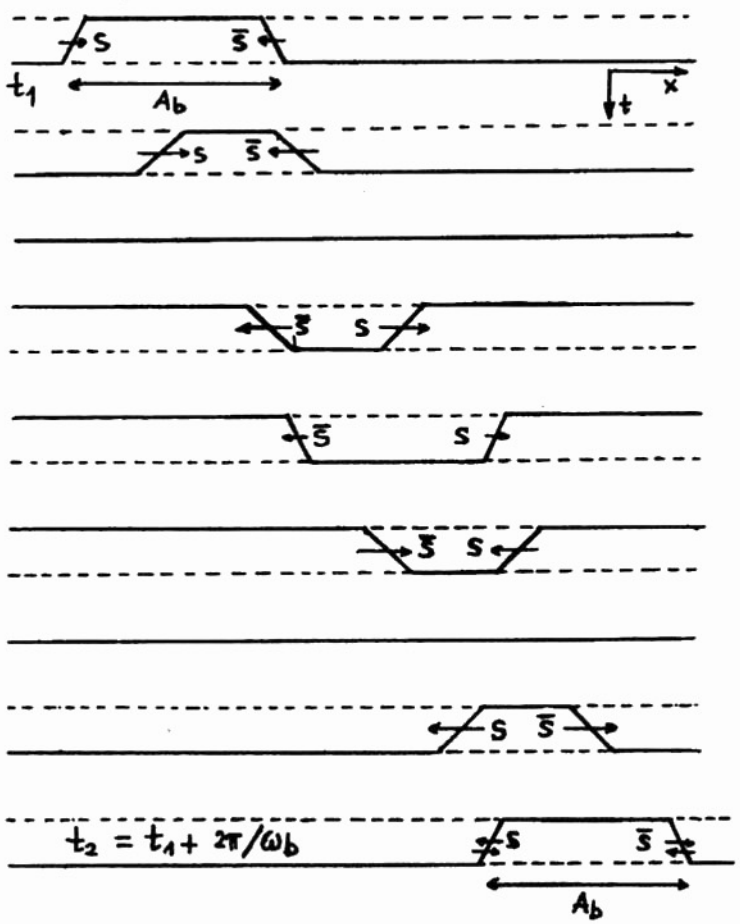

Fig. 5. A schematic illustration of the stable vibrating system of a pair of dislocation kinks (the so-called pulson) as described also by a two-soliton solution of the SG equation in the FK model.

hilation and creation they are again running away in opposite directions, but now only by a finite distance A_b (Fig. 5). Then the process is repeated in the same way.

4. Dislocation models of the acoustic emission sources (AE models)

A concept is proposed below saying that the basis of the acoustic emission phenomenon, observed during the plastic deformation of regular crystals, are elementary dislocation processes, the description of which is given in the three above mentioned simplest soliton solutions of the SG equation as the one governing both the FK and S dislocation models.

4.1. AE models based on changes in the dislocation velocity

The starting point is here the theory in which ESHELBY [15], considered the vibrations of a dislocation kink (Fig. 6a) and derived, as the first, the formula shows that the rate, P, of the acoustic energy emitted by the vibrating kink is proportional to the mean value of the square of the time derivative of its velocity

$$P = m_k \gamma_k \langle \dot{v}^2 \rangle, \tag{32}$$

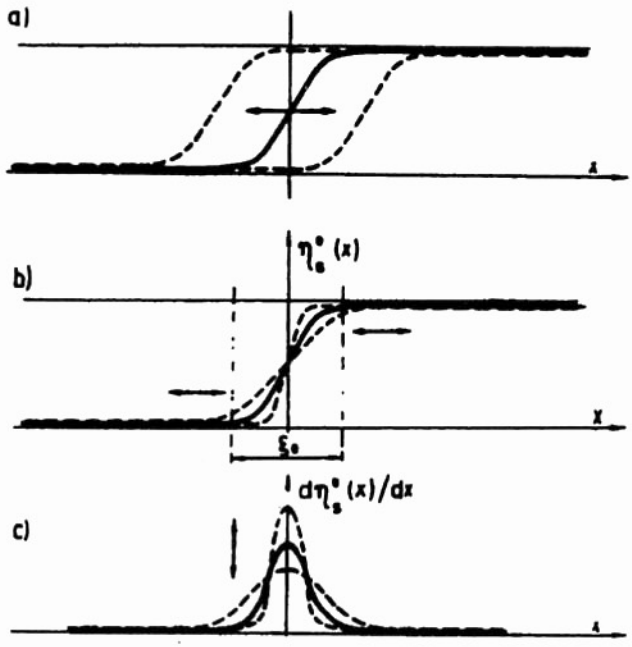

Fig. 6. Scheme illustrating the dislocation kink vibrations: (a) the rigid kink vibrating as a whole along the dislocation line, (b) the kink vibration as related to the changes in its width, and (c) the changes in the derivative of the kink shape.

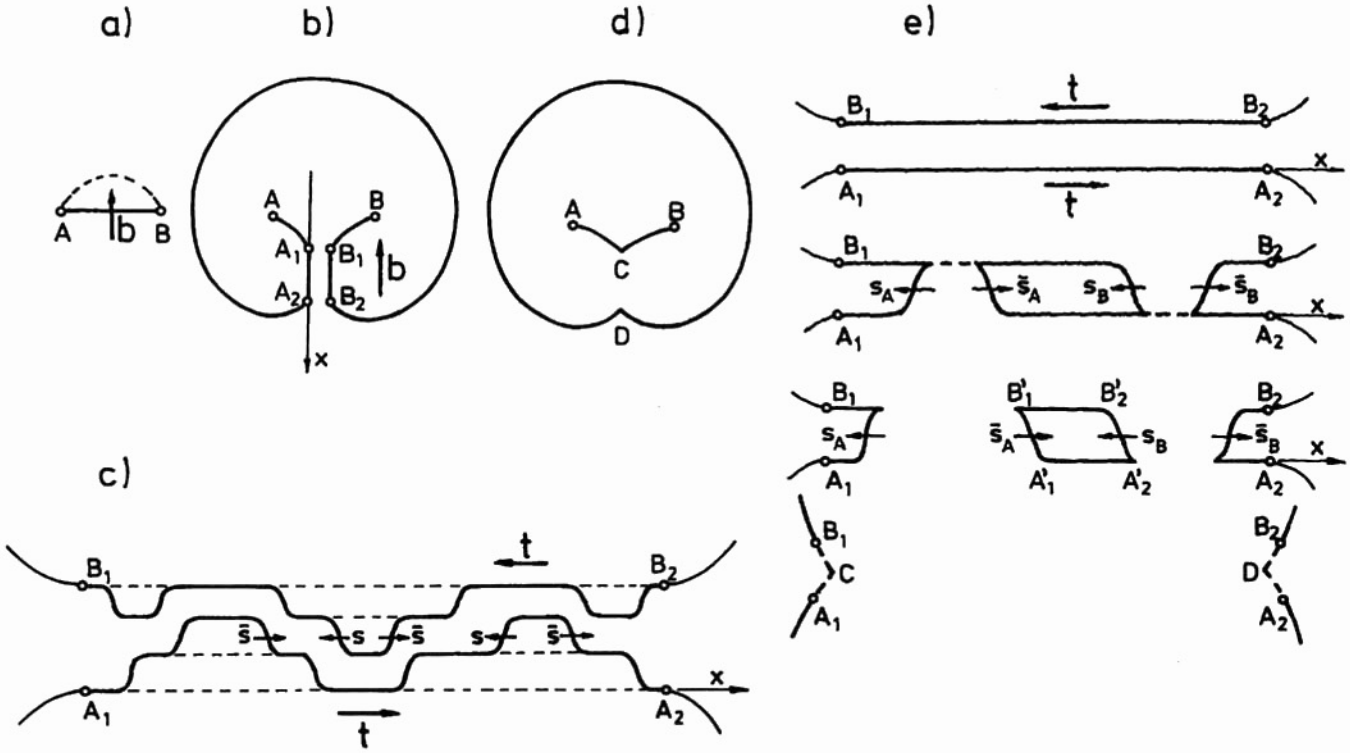

Fig. 7. The mechanism of the Frank–Read dislocation source operation (FR model) as the dislocation model of the source of elementary AE events.

where m_k is the kink effective mass, $\gamma_k = \mu a^2/10\pi m_k c^3$ with $c^{-3} = c_t^{-3}(1 + c_t^5/3c_l^5)$, where c_t and c_l are the transverse and longitudinal velocities of the sound, respectively. It should be noted, on the other hand, that the expression (29) says also that the changes in the kink velocity, v, result in corresponding changes of its width ξ. Namely, the shape of the accelerating kink becomes more sharp, whereas the shape of the decelerating one is more soft, thus the kink vibrations can occur also in a way illustrated schematically in Fig. 6b. In terms of the derivative of the function of the kink shape it means that the "hump" is more sharp or more broadened, respectively (Fig. 6c). In consequence, the solution (29) and the formula (32) constitute a dislocation model for the source of elementary acoustic emission events, related generally to the changes in the dislocation kink velocities (or simply in the dislocation velocities) including also those changes of various kinds of their vibrating movement.

It should be also stressed here that the result, similar to Eq. (32), but describing the dislocation mechanism of AE sources in a macroscopic scale, was obtained later by KOSEVICH [16]. In general, he used the methods of the continuous theory of dislocations in reference to the dynamics of any system of moving dislocation loops, and particularly to the system of dislocation loops emitted by sources of the Frank–Read type (Figs. 3 and 7). In a general way, KOSEVICH [16] stated that the density of the elastic energy flux, I, is proportional to the mean value of the square of the second time derivative of the so-called dislocation moment, $\mathbf{D}$, for the system of moving dislocation loops

$$I \approx \langle \ddot{\mathbf{D}}^2 \rangle, \tag{33}$$

where $\mathbf{D}$ is the dislocation moment tensor which, e.g. for a single dislocation loop, is defined as $\mathbf{D} = \mathbf{A}\,\mathbf{b}$, i.e. as the diadic product of the vector $\mathbf{A}$ of the area of the expanding loop by the Burgers vector $\mathbf{b}$ of the dislocation. Though in the case of a system of dislocation loops, the soliton behaviour is not completely recognized as yet (some suggestions given in Figs. 12 and 13 are discussed also in [17, 18]), the formula (32), and similarly, the expression (33) describe the same large class of dislocation models of AE sources related to the dislocation acceleration.

4.2. AE models based on the dislocation annihilation

The starting point is the basic two-soliton solution of the SG equation, given by (30), which describes the annihilation of dislocations in a completely analytical way. This solution is referred to the unperturbed case when after an annihilation event there occurs a creation, and next the dislocation kinks move in opposite directions (Fig. 4). However, in fact, such perturbations as lattice friction and/or various obstacles to the dislocation motion (e.g. forest dislocations, solute atoms, etc.) do not favour the repeated creation of kinks and the whole elastic energy revealed in the annihilation process can be transferred into the energy, E, of the acoustic wave.

The energy, E, was estimated for the first time by NATSIK and CHISHKO [19] by the methods of the linear theory of elasticity of continuous media. Their result says that the energy, E, is proportional to the square of the relative velocity V of the annihilating

dislocations of unit length. For screw dislocations, it is given by the expression

$$E = (\rho b^2/8\pi)V^2 \ln(L/b), \tag{34a}$$

whereas for edge dislocations by the formula

$$E = (\rho b^2/8\pi)V^2(1+\gamma_c^4)\ln(L/b), \tag{34b}$$

where L is the linear dimension of the crystal, $\gamma_c = c_t/c_l$, and ρ is the medium density. It is often assumed that $\ln(L/b) \cong 4\pi$, $\gamma_c \ll 1$, and $\rho b^2 \cong M$, i.e. the quantity ρb^2 is equal in the order of magnitude to the effective mass of a dislocation unit length. From the above estimations and from the formula (34) it follows that the energy, E, at the approximation of the linear theory of elasticity, has the form

$$E = MV^2/2, \tag{35}$$

which implies a simple physical interpretation, saying that during the annihilation, only the kinetic energy of the relative motion of dislocations is transferred into acoustic energy.

On the other hand, a similar expression, though only in the sense of an additive term, can be derived on the basis of two-soliton solution (30) of the SG equation: the energy, E_k, of a single dislocation kink of the effective mass m_k may be written as a "non-relativistic" approximation (when the kink velocity is $v \ll c_0$; see also [10]) in the following form

$$E_k = E_0 + m_k v^2/2, \tag{36}$$

where the kink rest energy, E_0, (energy of the dislocation core) as well as the kink effective mass, m_k, can be expressed by the characteristic constants c_0 and ω_0 in the SG equation, or by the parameters α_0 and A_0 in the FK model, or by the parameters τ_p and T in the S model (such an expressions has been derived and analysed in more details in [10]). In consequence, for the energy, E, revealed during the annihilation of two dislocation kinks, the following expression was obtained

$$E = 2E_k = 2E_0 + m_k V^2/2, \tag{37}$$

where $V = 2v$ is the relative velocity of the annihilating kinks; for the unit length of dislocation it was assumed that it is equal to the kink width ξ. The formulae (35) and (37) differ only by the term $2E_0$ (the quantities M and m_k are of the same order of magnitude). The explanation for this difference is quite simple. In the linear theory of elasticity, the very strong nonlinear effects appearing due to the existence of the dislocation core cannot be taken into acount. On the contrary, in the FK model, which, at the same time, is a dislocation core model, these effects are considered. They are reflected in the solitary wave properties of the dislocation kinks. Thus, the quantity E_0, given by the formula

$$E_0 = 2a(2U_p T)^{1/2}/\pi, \tag{38}$$

as an additive term in Eq. (37), does not change the quantitative physical interpretation: the AE caused by the dislocation annihilation is proportional to the square of their relative velocity. Perhaps, the term E_0 can play a role in the qualitative estimations of the number of AE events.

As a result of the above considerations, one can say that the formulae (30) and (37) constitute the basic dislocation model of the source of elementary AE events which, in general, are related to the dislocation annihilation processes. It should be emphasized that this model can also serve as a model of AE sources related to the dislocation annihilation processes occurring at the free surface of the sample due to the escape of dislocations from the crystal because, from the mathematical point of view, the problem is in this case equivalent to the annihilation of a dislocation with its virtual image of opposite sign in respect to this surface. However, it should be strongly emphasized that the models (29), (30) and (31) describe the soliton behaviour of dislocation kinks in a conservative, closed system in that the energy and velocity remain unchanged, thus they cannot be related immediately to a deformed sample which is an open system. Nevertheless, these models are useful for the qualitative understanding of the operation of AE sources in deformed metals where the perfect soliton behaviour is perturbed by external and local stresses.

4.3. Other AE models

First of all, the mixed models based, in an inseparable way, on both the dislocation velocity changes and the dislocation annihilation processes should be mentioned here. The two-soliton solution of the SG equation, given by Eq. (31), i.e. the so-called pulson illustrated schematically in Fig. 5, may serve as an example of such a model on a microscopic level. According to the formula (29), the stably vibrating pulson generates acoustic waves due to the continuous changes in the linear velocity of its kinks. On the other hand, the total destruction of the pulson results also in the generation of acoustic waves related, in turn, to the annihilation of its kinks according to formula (37). Such a situation is very probable because repeated creations of the kinks may be often impossible, for example due to strong local perturbations.

Another example of the mixed AE models is the Frank–Read mechanism of the dislocation source operation (FR model, Figs. 3 and 7). In this case the annihilation of many dislocation kinks takes place in each time interval when the closing of the dislocation loop occurs (along the sections C and D of the dislocation line in Fig. 3c; see for more details Fig. 7b and c). This leads, according to formula (36), to the generation of elementary AE events. On the other hand, each of the just closed dislocation loops which is still expanding, e.g. under external stresses, is undergoing the acceleration and thus it generates an acoustic wave according to Eq. (29); see also [4, 10, 18].

Also the dislocation pole mechanism of the twin formation (Fig. 8, T model) is another example of mixed models of the AE source. The increase of the velocity of twinning dislocations, which is especially high just in the twinning processes, is the main cause of the acoustic wave generation according to the formula (29). Similarly, during the escape of the twins from a crystal to its free surface, i.e. the annihilation of twinning dislocations, elastic energy is released and transformed into the acoustic wave energy according to Eq. (37).

All the AE models discussed have their more or less immediate origin in the corresponding (governing) type of the equation of the dislocation motion. In most of the

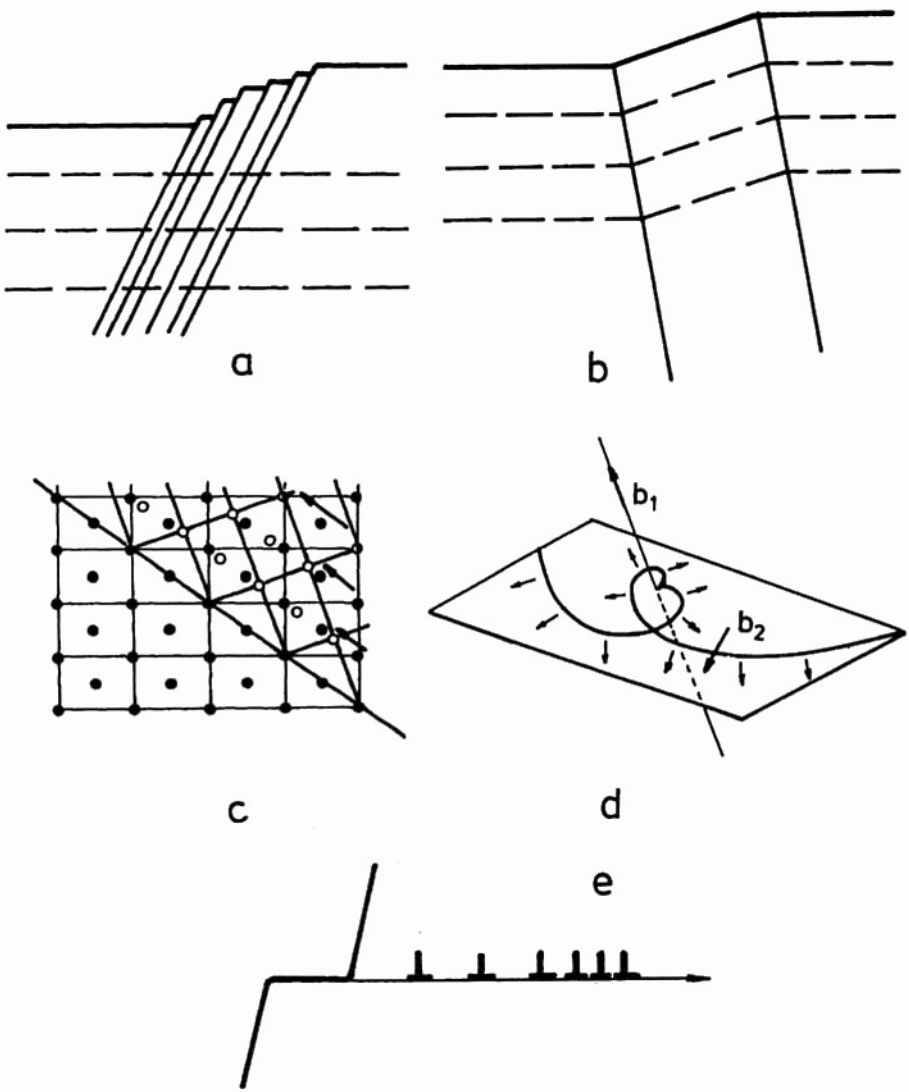

Fig. 8. A schematic illustration of the twinning process: the dislocation pole mechanism (d) leads to the mirror positions of atoms (c), and the final deformation of the crystal (b) differs from the step formed only due to the slip (a); both cases, at a one-dimensional approximation, are equivalent to the dislocation pile-up (e).

cases considered here, it is the SG equation that can be qualified as the equation of *string* type. Thus it is worthy of pointing out that also equations of the *diffusion* (or *heat transfer*) type may have solutions of the solitary wave type (see e.g. [18]), and they can serve too as possible dislocation models of AE sources. Such a suggestion, just in a new context of AE, is briefly reconsidered below.

4.4. AE models based on a "diffusion" equation of the dislocation motion

Starting from the equation of continuity for a coplanar array of moving dislocations (e.g. generated by the FR source and distributed continuously), we consider the dynamics of dislocations in terms of a concept of the dislocation flux which would obey the equation formally similar to those describing the diffusion or heat transfer processes. In a one-dimensional space, we may define the dislocation flux in the form

$$J(x,t) = \rho(x,t)v(x,t), \tag{39}$$

which satisfies the equation of continuity

$$\partial\rho(x,t)/\partial t = -\partial J(x,t)/\partial x, \tag{40}$$

where $\rho(x,t)$ is the linear density, and $v(x,t)$ is the mean velocity of dislocations (see e.g. [21, 22]). For simplicity, we restrict our treatment to the one-dimensional case, i.e. we consider a dislocation flux in only one direction corresponding to the single active slip system. Using the results of our earlier papers [18, 23] on the thermally activated motion of dislocations, the following expression, analogous to that for heat conduction or diffusion processes, may be obtained

$$J(x,t) = -D\partial\rho(x,t)/\partial x, \tag{41}$$

and finally, using Eq. (40) we get the evolution equation for the density of activated dislocations which is analogous to the Fourier law of heat transfer or to the second Fick law of diffusion

$$\partial\rho(x,t)/\partial t = D\partial^2\rho(x,t)/\partial x^2. \tag{42}$$

This equation is the simplest version of that one discussed earlier [24, 25] in the form

$$\partial\rho/\partial n = D\Delta\rho + k_1\rho - k_2\rho^2, \tag{43}$$

where, additionally, n is the number of the imposed load cycles in the fatigue process considered there, and the constants k_1 and k_2 are the multiplication and annihilation coefficients, respectively; Δ is the laplacian. In this way, Eq. (42) is related to the ideal extracted case of the dislocation motion, where the terms responsible for both the multiplication and annihilation of dislocations are neglected (i.e. in Eq. (43) k_1=0 and $k_2 = 0$).

In order to determine the flux, $J(x,t) = \rho(x,t)v(x,t)$, of activated dislocations, it is necessary to find the evolution equation for the dislocation velocity $v(x,t)$. Assuming that the mean value of the dislocation flux is, $J = \rho v/2$, Eq. (41) may be written in the following form (see also in [18, 23])

$$\rho(x,t)v(x,t)/2 = -D\partial\rho(x,t)/\partial x. \tag{44}$$

It is, perhaps, very interesting to note that this equation has the form of the Cole–Hopf transformation which is known in the mathematical theory of solitons, and is usually given by

$$v(x,t) = -2D\rho_x/\rho. \tag{45}$$

This transformation maps solutions of the diffusion type equation (42) onto solutions of the NLPD Burgers type equation, the form of which may be written as follows

$$\partial v(x,t)/\partial t + v(x,t)\partial v(x,t)/\partial x - D\partial^2 v(x,t)/\partial x^2 = 0, \tag{46}$$

or simply in the form

$$v_t + vv_x - Dv_{xx} = 0. \tag{47}$$

One of the analytical well-known solutions of the Burgers equation is of the solitary wave character, the form of which is the Taylor shock profile given by [26] (see also in [18, 23])

$$v(x,t) = \alpha D\{1 - \tanh[(x - \alpha Dt)/2]\}, \tag{48}$$

where $2\alpha D = v$ is the velocity at $x \to -\infty$, and $\alpha v_\infty/2 \equiv w$ is the rate of changes in the dislocation velocity during their propagation. These changes are of the step-like front character and they are localized within a narrow region of the space [26].

In agreement with the above considerations we can now treat the motion of a group of dislocations as a nonlinear wave process, i.e. during each local movement of the dislocation group inside the crystal (related e.g. to the FR mechanism of the dislocation source operation in the simplest case, or in a more general case to the slip and/or shear band propagation), the mean velocity of the group changes in space and time like a solitary wave impulse. Thus, in the sense of changes in the dislocation velocities with time, the movement of a dislocation group can be considered as the AE source of the type described by the formula (32) or (33). Finally, it is worthy of pointing out that there exist also the periodic solutions of the SG equation. Such solutions, for example, were discussed elsewhere [27] in the context of the behaviour of the moving dislocation kink as the soliton on the background of a quasi-periodic process.

5. Discussion and conclusions

Firstly, we present some chosen most representative experimental data which illustrate the existence of strong correlations between the behaviour of the acoustic emission (AE) and the mechanisms of plastic deformation in mono- and polycrystalline metals of a fcc lattice that undergos a channel-die compression at both the ambient and liquid nitrogen temperatures [5–9].

In Figs. 9–11 the behaviours of AE, i.e. the rate of the AE events, $\Delta N_z/\Delta t$, as well as functions of the external compressing force (diagrams at the top) together with the corresponding microstructure (photos at the bottom) are presented. These figures reflect the more significant deformation mechanisms during the channel-die compression which are connected, first of all, with the processes of twinning (Figs. 9 and 10) and with the formation of the primary family of shear bands (Fig. 11). For example, in Fig. 9 it is shown that the formation of exactly three thin plates of twins (in the direction marked on the photo) is accompanied also by exactly three very pronounced peaks of the rate of the AE events (in this case the compression test has been especially stopped at the moment in that the twinning process begins). In Fig. 10 the characteristic steps (see also

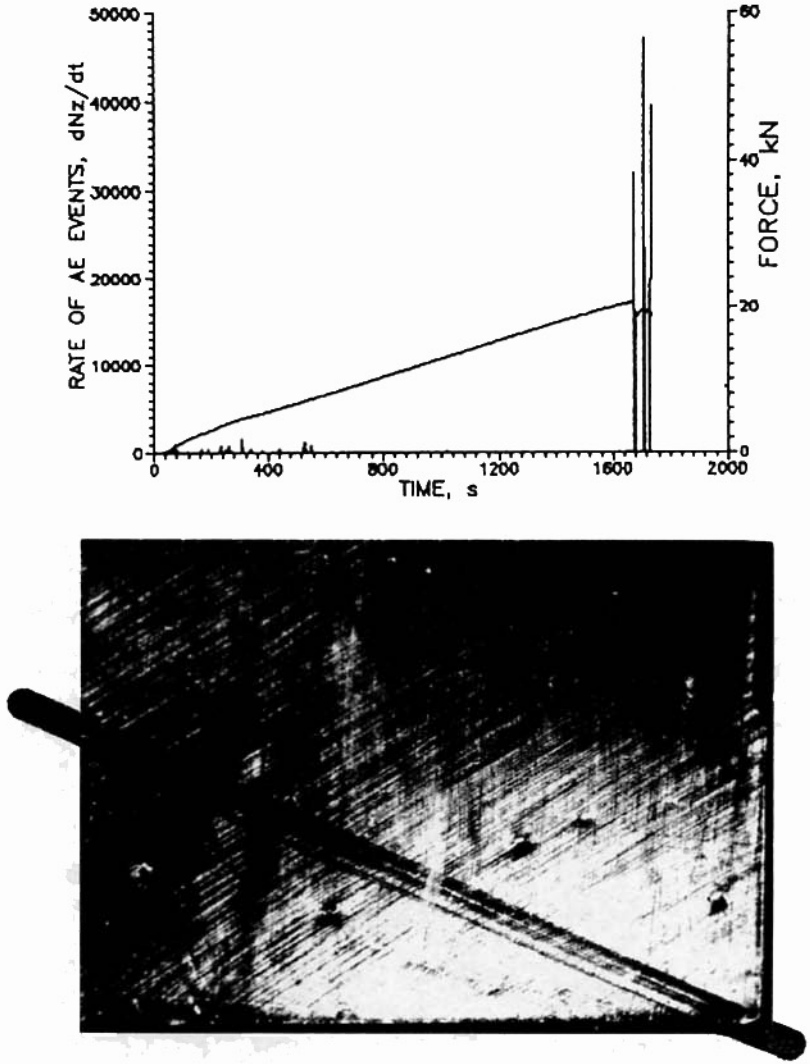

Fig. 9. Acoustic emission (AE), external force (at the top) and the corresponding microstructure (at the bottom) of silver single crystals of {112}⟨111⟩ orientation during channel-die compression at ambient temperature (reduction $z = 11\%$, magnification $\times 10$).

the scheme in Fig. 8) formed due to the escape of the twins to the free surface of the sample are shown. On the other hand, in Fig. 11 it was demostrated that the formation of a primary family of shear bands is related to the creation of the steps at the surface of the sample, the latters being simultaneously strongly correlated to the corresponding AE peaks as well as to the sudden drops of the external compressing force that are accompanying them.

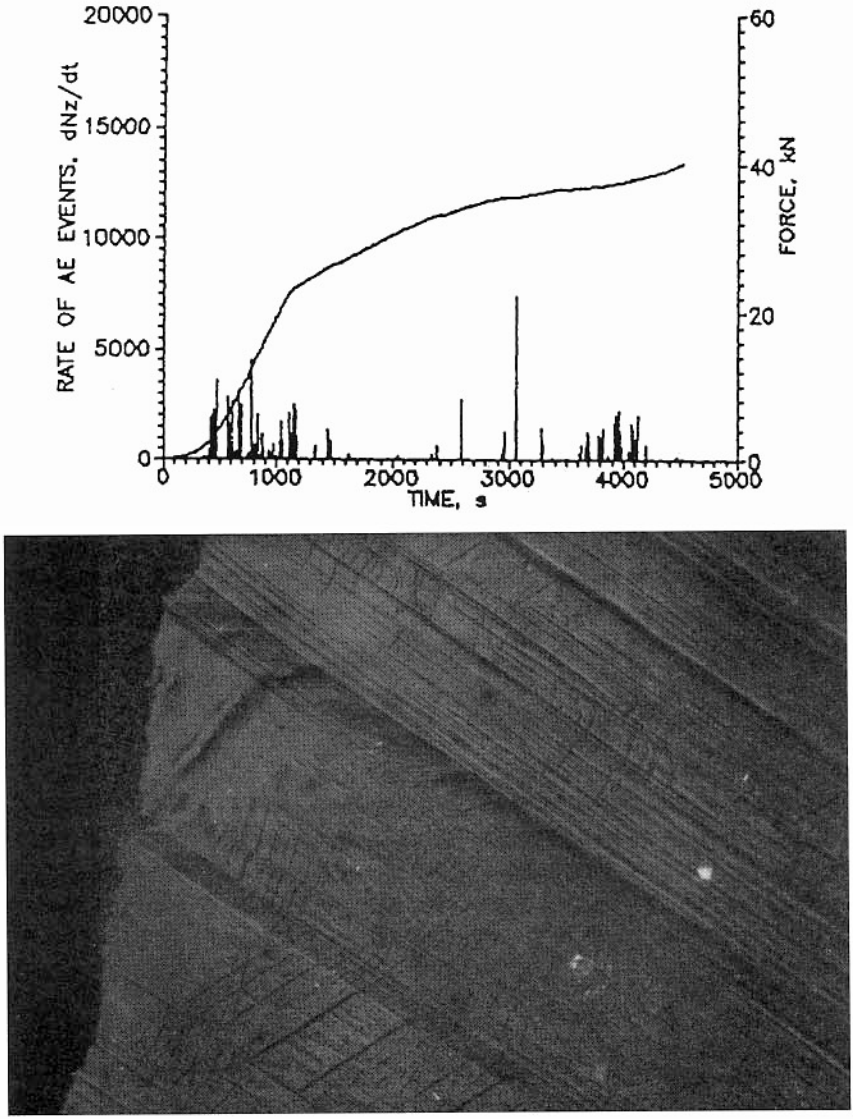

Fig. 10. AE, external force and microstructure of Cu–2% Al single crystals during the channel-die compression ($T = 77$ K, $z = 60\%$, orientation $\{421\}\langle 112\rangle$).

The high rate of the AE events during the formation of the particular plates of twins (Fig. 9), attaining the values even of the order of magnitude significantly above 10^4, is in our opinion caused mainly by the escape of the twins to the crystal surface which results in the formation of characteristic steps like those shown in Fig. 10. If we assume the pole mechanism of the twin formation (Fig. 8), such an interpretation is in a qualitative agreement with formulae (35) and (37).

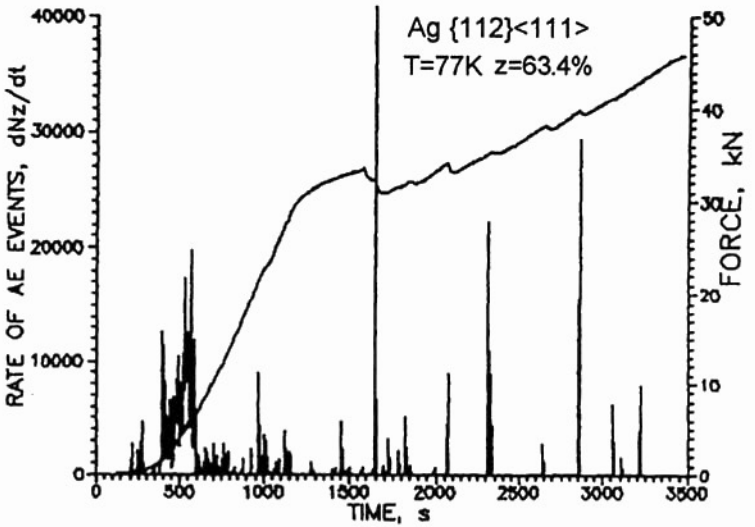

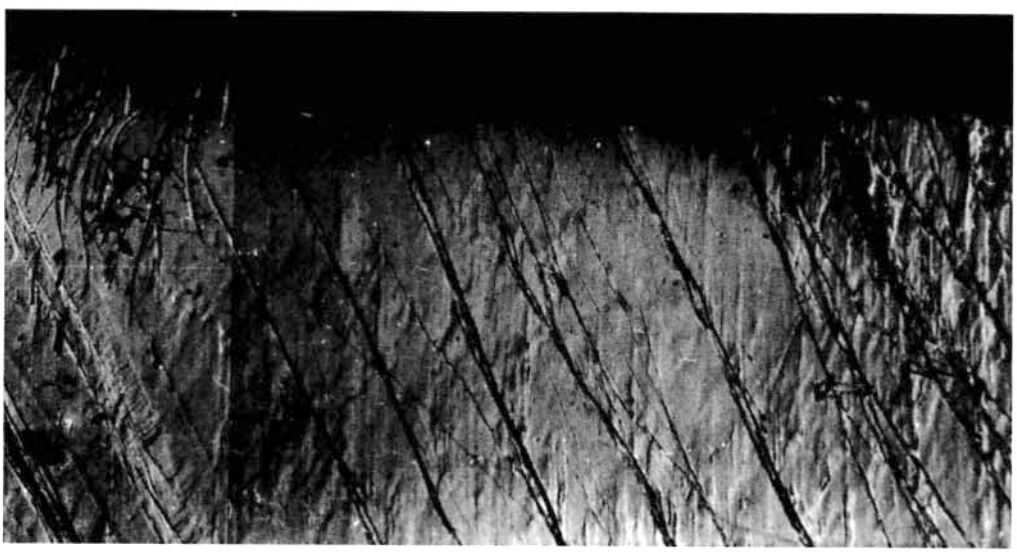

Fig. 11. EA, force and microstructure of Ag single crystals during the channel-die compression ($T = 77$ K, $z = 63\%$, $\times 200$, orientation $\{112\}\langle 111\rangle$).

A following attempt of the quantitative estimation of the rate of AE events during the formation of a single twin plate can be made. Let us assume that an elementary AE event is connected with the escape to the surface of the twinning dislocations moving within the range of one atomic plane. For simplicity, it is assumed that the lattice parameter a is of the order of Burgers vector, i.e. $a \cong b \cong 10^{-4}$ μm (for Cu $b \cong 2.8$ A). The observed width of the twin lamellae oscillates within the limits 10^2 to 10^3 μm which,

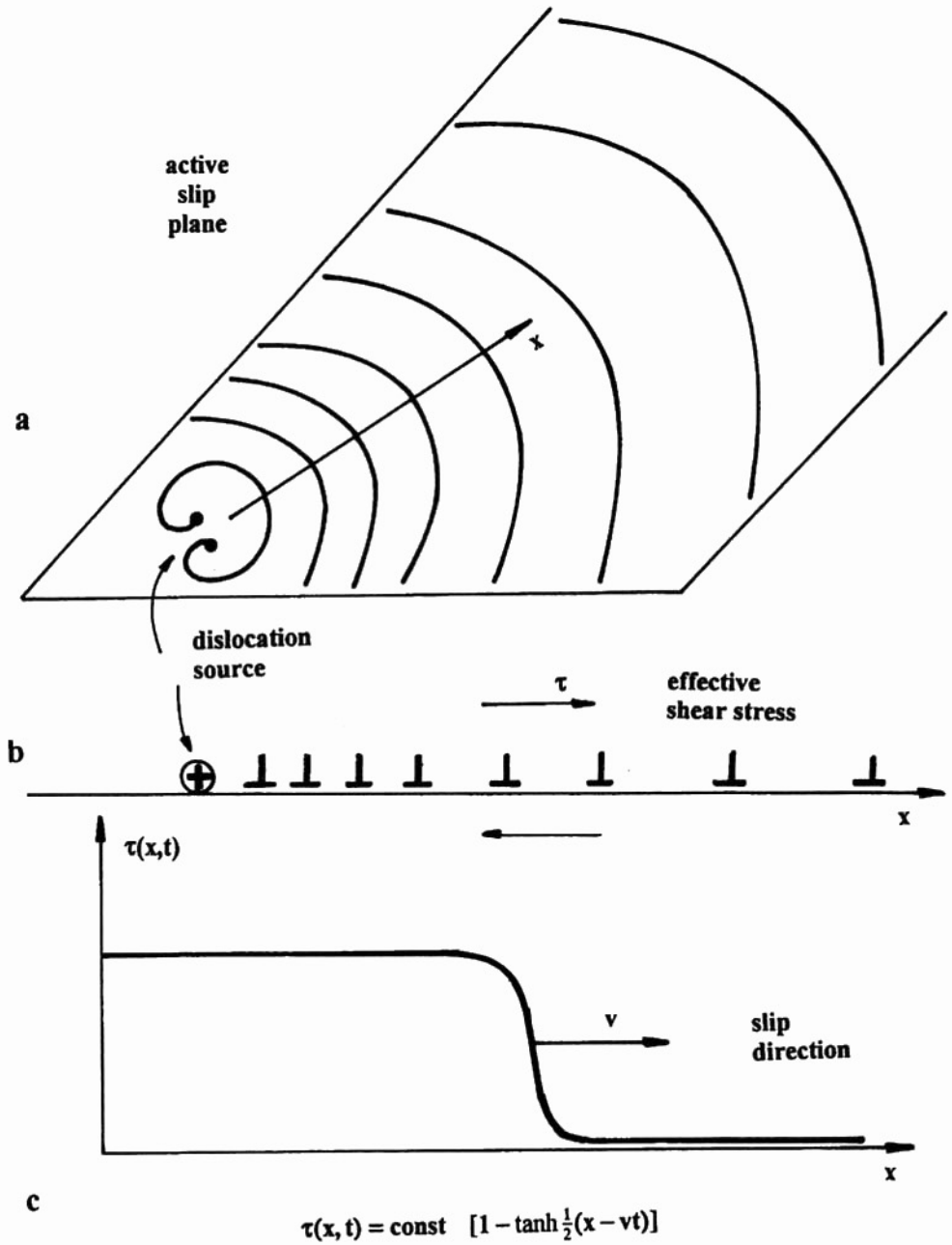

Fig. 12. Schematic illustration of the dynamics of dislocations generated by the source (a), the corresponding dislocation configuration at a one-dimensional approximation (b), and the solitary wave-like character of the dislocation propagation (c).

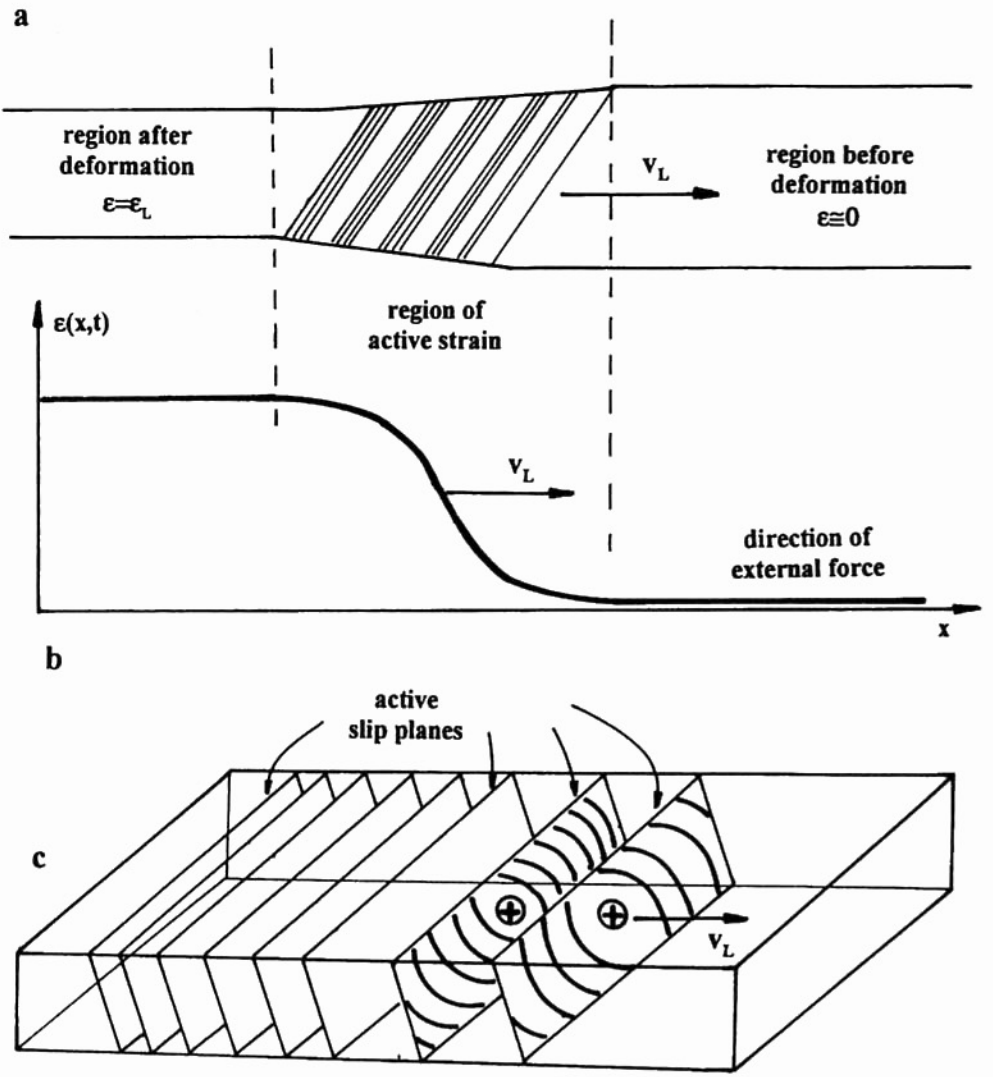

Fig. 13. Schematic illustration of a simple model of slip band propagation (a), its solitary wave representation (b), and the dislocation dynamics in active slip systems (c).

at the applied magnifications of the order of 10 to 100, places the value of the actual width of a twin lamella, at a rough approximation, in the interval from 1 to 100 μm. Hence, the number of engaged atomic planes, and thereby the number of elementary AE events comprising an AE peak originated from a single lamella, is of the order of 10^4 to 10^6 which is satisfactorily consistent with the magnitude of the observed values. As known and has been mentioned earlier, the dislocations may develop very high velocities during the twinning process (of the order of the speed of sound). Thus, it should be

remembered that great dislocation accelerations are also possible which means that the AE sources of the type defined by the formulae (32) or (33) may be of vital importance in the case of the twinning processes.

In consequence, proceeding in a similar way as in the case of the twinning, we can discuss the formation of shear bands (Fig. 11). The steps on the sample surface (clearly seen in the photo) are formed as a result of the strain localization in the generated shear bands, each being accompanied by a rapid drop of the external force and a corresponding AE peak the value of which falls within the limits 10^4 to 4×10^4. Assuming that a single elementary AE event corresponds to the escape of a single gliding dislocation to the surface (a step of the order of magnitude of Burgers vector **b**), it can be estimated that the real size of such steps as shown in Fig. 11 ($\cong$ 2 mm at the magnification $\times 200$) is of the order of 10 μm. Next we assume that the number of dislocations generated by a single FR source, forming a slip line, is of the order of $10^2 - 10^3$ (in the literature values closer to about 10^3 are often assumed [28]; see also [29]). Thus, it can be expected that the formation of a step of size of $\sim$ 10 μm on the sample surface is accompanied by the escape of dislocations from very many slip planes, that can be of the order of 10^2; each single source of the plane (e.g. of the FR type) has produced so many dislocations that nearly 10^3 of them became annihilated on the sample surface. In this way the formation of a step of the order of 1 to 10 μm in size would be associated with the generation of 10^4 to 10^5 elementary acoustic events forming a single AE peak. Such an estimation of the order of magnitude is in accordance with the values observed (from 10^4 to 4×10^4 in Fig. 11).

It should be also pointed out that the contribution to the values of the AE peaks observed may originate also from the annihilation processes during the operation of the FR sources (Figs. 3 and 7) when the dislocation loops are closing as well as from the acceleration of the dislocation loops already generated by these sources. It can be seen that a more significant role of these effects corresponds rather to the beginning stage of the plastic deformation when the yield point (the range of dynamic formation of slip lines) is exceeded. On the other hand, when the shear band formation process is beginning (the creation of the marked steps at the sample surface), the effects of surface annihilation of dislocations are rather prevailing.

To sum up the discussion, it should be emphasized that a new model of dislocation, i.e. the generalized FK model, has been proposed here and that the governing differential equations for the dislocation motion in this model constitute a new class of NLPD equations which, to our knowledge, have not been sufficiently recognized so far in the theory of solitons. Moreover, literature studies of the analytical methods of the solution of NLPD equations have been started, and, at the same time, good progress has been made in preparing a computer programme for their numerical solutions. On the other hand, the FK dislocation model is reconsidered and it has been shown that the basic soliton solutions of the SG equation, being the governing NLPD equation in the model, can be used as basic elements for the dislocation models of the acoustic emission sources since they are very useful for the qualitative understanding of the dislocation annihilation and acceleration processes in a micro-scale. It has also been shown that the proposed dislocation models of the AE sources describe qualitatively the behaviour of AE during

the channel-die compression of fcc metals in a quite satisfactory way. In particular, on the basis of these models the order of magnitude of the values of the peaks of the rate of AE events have been estimated in good agreement with the values observed. Consequently, the most significant results obtained can be formulated in the following final conclusions:

— The differential equations for the dislocation motion, governing in the generalized FK model, are new NLPD equations which can play a role in the theory of the dislocated crystal lattice vibration as well as in the theory of dislocations.

— The SG equation, being the governing NLPD equation in the FK dislocation model, has the analytical solutions which are of the soliton type and which describe the dislocation annihilation processes as well as the vibrating movement of the dislocation kinks.

— The basic soliton solutions of the SG equation, given by Eqs. (29), (30) and (31), as well as the expressions (32) and (37), constitute the main elements of the proposed dislocation models of the acoustic emission (AE) sources related to both the annihilation and acceleration of dislocations.

— The proposed dislocation models of the AE sources allow to estimate the values of the peaks of the rate of AE events accompanying the slip line formation, twinning and shear banding processes during the channel-die compression of fcc metals; the orders of magnitude of these values, are in a quite good agreement with the observed ones for AE peaks.

Acknowledgements

Part of this paper (Sec. 4.4) was financially supported by the State Committee for Scientific Research, Grant No 7 T07B 043 12.

References

[1] R.M. Fisher and J.S. Lally, Can. J. Phys., **45**, 1147 (1967).

[2] R.T. Sedgwick, J. Appl. Phys., **33**, 1728 (1968).

[3] D.R. James and S.E. Carpenter, J. Appl. Phys., **42**, 4685 (1971).

[4] A. Pawełek, J. Appl. Phys., **62**, 2549 (1987).

[5] A. Pawełek, Z. Jasieński, A. Piątkowski, H. Paul and A. Litwora, Proceedings of the 26 Winter School on Molecular and Quantum Acoustics, Ed. Upper Silesian Division of the Polish Acoustical Society, Gliwice – Ustroń, p. 63, 1997.

[6] A. Pawełek, Z. Jasieński, A. Piątkowski, A. Litwora and H. Paul, Materiały XLIV Otwartego Seminarium z Akustyki, OSA'97, Wyd. Polskie Towarzystwo Akustyczne — Oddział Gdański, vol. I, pp. 513, Gdańsk – Jastrzębia Góra 1997.

[7] A. Pawełek, Z. Jasieński, A. Piątkowski, A. Litwora and H. Paul, Materiały Krajowej Konferencji "Dobór i Eksploatacja Materiałów Inżynierskich", pp. 109, Gdańsk – Jurata 1997.

[8] A. Pawełek, A. Piątkowski, Z. Jasieński and S. Pilecki, Archives of Acoustics, **24**, 85 (1999).

[9] A. Pawełek, A. Piątkowski and Z. Jasieński, Akustyka Molekularna i Kwantowa, **18**, 321 (1997).

[10] A. Pawełek, Zeszyty Naukowe AGH, Metalurgia i Odlewnictwo, z. 107, No 1109, Kraków 1987.

[11] A. PAWEŁEK, Acta Phys. Polon., **A68**, 815 (1985).

[12] R. BULLOUGH and V.K. TEWARY, Dislocation in solids, F.R.N. NABARRO [Ed.], vol. 2, p. 1, North-Holland Publ. Co., Amsterdam 1979.

[13] J.N. FLYTZANIS, ST. PREVMATIKOS and M. REMOISSENET, J. Phys. C: Solid State Phys., **18**, 4603 (1985).

[14] A. SEEGER, A. DONTH and A. KOCHENDÖRFER, Z. Physik, **134**, 179 (1953).

[15] J.D. ESHELBY, Proc. Roy. Soc., **A226**, 222 (1962).

[16] A.M. KOSEWICZ, Dislocation in solids, F.R.N. NABARRO [Ed.], vol. 1, p. 33, North-Holland Publ. Co., Amsterdam 1979.

[17] A. PAWEŁEK and A. KORBEL, Phil. Mag., **B61**, 829 (1990).

[18] A. PAWEŁEK, S. PILECKI and Z. JASIEŃSKI, Archives of Mechanics, **47**, 11 (1995)

[19] V.D. NACIK and K.A. CZISZKO, Fiz. Tverd. Tela, **15**, 3126 (1972); **17**, 342 (1975); **20**, 1933 (1978).

[20] A. PAWEŁEK and I. MALECKI, Prace IPPT, No 22, Warszawa 1993.

[21] A.K. HEAD, Phil. Mag., **26**, 43, 65; **27**, 505 (1972).

[22] V. BALAKRISHNAN and C.E. BOTTANI, Phys. Rev., **B33**, 5157 (1986).

[23] A. PAWEŁEK, Archives of Metallurgy, **38**, 245 (1993).

[24] S. PILECKI, Proc. 4-th Int. Conf. on Fracture, vol. 2, p.687, Waterloo (Canada) 1977.

[25] S. PIŁECKI, Engng. Trans., **36**, 269 (1988).

[26] R.K. DODD, J.C. EILBECK, J.D. GIBBON and H.C. MORRIS, *Solitons and nonlinear wave equations*, Academic Press, London 1984.

[27] A.PAWEŁEK and M. JAWORSKI, J. Appl. Phys., **64**, 119 (1988).

[28] A.R. ROSENFIELD and M.F. KANNINEN, Phil. Mag., **22**, 143 (1970).

[29] A. PAWEŁEK, Doctorat Thesis, Academy of Minning and Metalurgy, **A671**, Kraków 1979.

ARCHIVES OF ACOUSTICS
25, 3, 359–368 (2000)

PREVAILING PATTERNS OF THE SOUND SPEED DISTRIBUTIONS IN THE ENVIRONMENT OF THE SOUTHERN BALTIC

G. GRELOWSKA

Naval Academy
(81-919 Gdynia, ul. Smidowicza 71, Poland)
e-mail: grelowska@amw.gdynia.pl

The paper contains the results of experimental and theoretical research aimed at elaborating characteristic features of the acoustic conditions in the Southern Baltic. As there features are fully dependent on the hydrological conditions, the sound speed distribution is influenced by many factors and changes during the year. On the basis of hydrological data recorded from 1979 to 1991 by measurements at stations situated along the deeps of the Southern Baltic, the sound speed has been calculated using the procedure of Chen&Millero recommended by UNESCO. The data were averaged in one-months periods and subjected to a detailed analysis of the speed variations during the year. The patterns of the sound speed distribution characteristic for every month have been determined. Research was also conducted to find to what extent the synoptic patterns of the sound speed distribution differ from the averaged respective data. To solve the problem, several synoptic distributions established in different seasons are compared with the averaged distribution. Difficulties in specifying the acoustical conditions of the Southern Baltic are augmented by the appearance of short-term local phenomena changing considerably the sound speed distribution in certain areas. Examples of such phenomena are presented in the paper. The paper is based on a large number of *in situ* measurement data presented in the form of diagrams.

1. Introduction

Conditions of the acoustic wave propagation in shallow water differ considerably from those prevailing in the ocean. They depend on many factors such as the depth of the water related to the wave length and the boundary conditions specified by the type of the bottom [31, 14, 17] and the state of the sea [2]. Changes in the sound speed distribution in shallow water are the main factor influencing the wave propagation [10, 22]. This fact is often taken into consideration since the range of the action of the devices used in underwater investigation is greatly dependend on it [1, 20, 29].

Numerous publications treated that problem in several aspects confirm its importance. The phenomena having an impact on the wave propagation in the sea are considered in several fundamental monographs, for instance in [4, 8, 30]; the problems concerning the wave propagation in stratified areas are discussed in [3, 5], and the interaction of the atmosphere and the sea in [26, 11]. The matter of acoustic conditions of the Baltic Sea is examined in [15]. Data on the sound speed distribution obtained during cyclical

investigations are published in the annual reports printed inter alia by the Polish Institute of Meteorology and Water Management and in the Reports of the German Baltic Sea Research Institute in Warnemünde. Measurements of the sound speed distribution are often carried out together with other oceanographic investigations and are analyzed jointly [12]. Sometimes they are treated separately and published independently [23, 24. 19].

Numerous underwater investigations conducted concurrently with measurements of the sound speed distribution testify to the recognition of the importance of that problem. However there are very few publications devoted to the general characteristics of the acoustic conditions in the Baltic Sea [13, 18].

Nearly all STD or CTD sounders are presently equipped with a sound speed meter or can offer information on the sound speed distribution calculated on the basis of hydrological parameters. However, in many cases it is necessary to calculate the sound speed having at disposal only the results of measurements of the temperature and salinity as function of depth. It requires an expression that describes adequately the influence of temperature, salinity and static pressure on the sound speed. This aspect is of great importance in view of the standardization of the measuring methods. Several expressions describing the dependence of the sound speed on temperature, salinity and static pressure are known [7, 21]. UNESCO suggests the expression obtained and verified by Chen and Millero [9].

The Baltic Sea can be regarded as a shallow sea at least in two aspects. Its depth is small in comparison with the depth of deep seas. Also assessing its properties from the point of view of the acoustic wave propagation, the Baltic should be treated as a shallow water for many waves of different frequencies, especially for the noise of technical provenance [31].

Because of its low depth, the Baltic is strongly influenced by the wind mechanisms and the changeable distribution of high- and low pressure areas. The acoustical conditions in the Baltic are fully dependent on hydrological conditions. Generally, two main layers can be distinguished in the Baltic Sea: the upper layer and the deep water layer. The acoustical conditions in the upper one are influenced by the inflow of solar energy into the sea surface and its transportation into the deeper parts of the sea, while the acoustical conditions in the deep water layer depend on inflows of highly saline water from the North Sea through the Danish Straits. Though the mechanisms of both of those phenomena are well known, they are not fully predictable. The meteorological phenomena influencing the processes occurring at the ocean — atmosphere border as well as the deep water inflows are carefully observed and monitored. The general trend in their changes during the year is stable, but the randomness factor modulating them plays a significant role in forming the hydrologic-meteorological situation [25, 27]. Additionally, the dynamics of dense bottom currents is strongly dependent on numerous physical factors as well as on the specific bottom topography. Therefore the long-term predictions as well as the short-term ones of the conditions of the acoustic wave propagation are burdened with a certain error.

The aim of the paper is to generalize the knowledge on the sound speed conditions in the southern Baltic Sea. An attempt to characterize the acoustic climate of that

region has been made. Research was also conducted to find an answer to the question to what extent the synoptic patterns of the sound speed distribution, usually dependent on the meteorological conditions prevailing prior to the performed measurements, differ from the averaged respective data. It has also been pointed out that the underwater investigation may be affected by local morphological and hydrological conditions.

2. Material and method of investigations

The various patterns of the sound speed distribution presented in this paper are obtained on the basis of measurements of the temperature and salinity as a function of the depth according to the UNESCO standard. The formula describing the dependence of the speed of sound on temperature, salinity and the static pressure given by Chen and Millero is used in numerical calculation [9].

Results of measurements performed at the stations marked in Fig. 1 in the years 1979–1991 are the base of the investigation. For station P5 — Bornholm Deep and P1 — Gdańsk Deep, the accessible data are from 1960–1997. For each station the average sound speed distribution characteristic for each particular month from March to December was determined. The accessible number of measurements in every month was not identical. In the summer the measurements were done regularly, while in the winter it was not always possible to make them. Thus the distribution for January and February was not determined because of the lack of sufficient data. In Sec. 6 measurements performed by the Sea Fisheries Institute in 1994 and in 1996 were used for exemplifying the impact of local conditions on the patterns of the sound speed.

The averaged distribution of the sound speed c was estimated for each month separately for every station. Because of the scant number of samples being at our disposal, the Student's distribution was applied [16]. It was taken a priori without verification. The confidence interval was evaluated at each measurement depth using the following formula:

$$p(\bar{c} - t_\alpha S < \bar{c} < \bar{c} + t_\alpha S) = 1 - \alpha, \tag{1}$$

where $\bar{c}$ denotes the average value of the sound speed at a fixed depth:

$$\bar{c} = \frac{1}{n} \sum_{i=1}^{n} c_i \tag{2}$$

S — the error mean-square of measurements:

$$S = \sqrt{\frac{1}{n(n-1)} \sum_{i=1}^{n} (c - \bar{c})^2} \tag{3}$$

n — the number of measurements. The value of α depends on the number of measurements and the assumed confidence coefficient. The results of the estimation of the sound speed at every station in each considered month were used as the base for the determination of the averaged vertical distribution of the sound speed along the cross-section over the deeps of the southern Baltic.

Assuming that the distribution obtained in this way is representative for an individual month, the problem of the difference between the averaged distribution and the single synoptic distribution was considered. Apart from that, some phenomena occurring sporadically, but causing an anomaly in the sound speed distribution, were also taken into consideration.

3. Averaged sound speed distribution

The acoustical conditions could be characterized by the vertical sound speed distribution in the main points of the considered area. In the southern Baltic such points were localized at the Gdańsk Deep, the Bornholm Deep and the Słupsk Furrow. The sound speed profiles estimated for the Bornholm Deep and Gdańsk Deep together with the confidence intervals are shown in Fig. 2. They were obtained on the basis of data from 1960 to 1997. The number of accessible data was various in every month.

The confidence interval was evaluated at each measurement depth from the formula (1) applying the t-Student distribution and assuming the confidence coefficient to be equal to 0.9. In the distributions determined for both the stations, seasonal changes characteristic for the southern Baltic are visible. However, a discerning analysis allows to denote several individual features of each of the stations. In the winter-months the distribution in the upper layer is almost uniform. The sound speed increases with the growth of the depth, reaching at the Bornholm Deep values greater by about 7–8 m/s than those at the Gdańsk Deep. This results from the greater salinity in the deep layer that is about 5–6 PSU. Consequently, the difference between the sound speed at the bottom and at the sea surface was equal to about 19 m/s in January and 26 m/s in March at the Gdańsk Deep, while it amounted to about 28 m/s in January and 33 m/s in February at the Bornholm Deep.

Greater values of the sound speed at the bottom in the Bornholm Deep region influence the vertical sound speed distribution during the whole year. There the minimum occurs practically from May to November at depths of about 50 m at the Bornholm Deep and at about 60–70 m at the Gdańsk Deep. The minimal value in both cases increases during the year and is greater at the Bornholm Deep than at the Gdańsk Deep from by about 2 m/s in May to 10 m/s in September. The difference between sound speed at the surface and the minimal value of the sound speed is greater at the Gdańsk Deep than in the Bornholm Deep region by about 3–11 m/s, whereas the difference between the sound speed at the bottom and the minimal value is greater at the Bornholm Deep by about 2–7 m/s.

4. Acoustic climate of the southern Baltic

Results of the estimation of the averaged value of the sound speed at each station marked at Fig. 1 are the base for the determination of the averaged sound speed distribution along the cross-section over the southern Baltic deeps. The next figures illustrate

the estimated distribution in each month from March to December. Because of the lack of sufficient data, the distribution for January and February were not determined. However, the characteristics obtained allow to trace the changes in the acoustical conditions in the southern Baltic throughout the year.

The acoustical conditions in March and April (Fig. 3) could be classified as typical winter conditions in the southern Baltic. A nearly uniform distribution with the smallest yearly values of the sound speed (1415 – 1425 m/s) in the upper layer, and increasing sound speed with growing depth in the deep water layer are typical of them. The values of the sound speed at the Bornholm Deep (> 1450 m/s, at the bottom > 1455 m/s) are greater than in other deeps (1440 – 1450 m/s). The upper border of the area of increased sound speed caused by greater salinity could be illustrated by the isoline 1425 m/s. Its depth depends on the region and varies from about 50 m in the western part to about 60 – 70 m in the eastern one of the southern Baltic. In April the beginning of the process of water warming from the surface is observed, especially in the regions of smaller latitude laying closer to the land.

In May and June heat delivered from the atmosphere creates distributions typical for spring (Fig. 4) in which the minimum appears at the depth of about 50 m in the Bornholm Deep region and of about 60 m in the Gdańsk Deep region. The sound speed at the surface equals from 1445 to 1455 m/s in May and from 1455 to 1465 m/s in June, only close to the estuaries of the Vistula and the Odra it reaches values greater by about 6 – 10 m/s. In spring, in several points of the southern Baltic, the sound speed at the surface and at the bottom is approximately the same. Characteristic for those distribution patterns is the presence of a large volume of decreased sound speed lower than 1430 m/s. It occurs in the middle of the sea and its thickness varies from about 20 m in the western part to about 45 – 50 m in the eastern part of the area. This volume decreases with warming up of the upper layer of the sea.

The next three months: July, August and September could be characterised by the summer sound speed distribution with a well pointed out minimum and a high gradient of the temperature in the upper layer (Fig. 5 and Fig. 6). The difference between the value of the sound speed at the surface and the minimum value reaches 55 – 60 m/s. The depth of the minimum in the sound speed distribution changes from about 50 m at the Bornholm Deep to about 60 – 65 m at the Gdańsk Deep. The volume in which the sound speed is smaller than 1430 m/s decreases, and in August and September occurs only in the environment of the Gotland Deep and the Gdańsk Deep. The gradient of the sound speed in the deep layer is considerably smaller than in the upper one. The lowest value close to the bottom in main deeps is approximately 5 m/s smaller than the spring design.

From October the sound speed distribution changes significantly (Fig. 6 and Fig. 7). The change in the direction of the heat flow at the atmosphere-sea border is reflected also in the acoustical conditions. The value of the sound speed at the surface ranges from 1460 to 1465 m/s and its gradient in the upper layer is smaller than in the summer. A minimum in the vertical distribution still appears and its value is greater than in the summer by about 5 m/s. The configuration of the isoline in October is similar to the spring distributions, but the values are greater by about 5 – 10 m/s. In November and

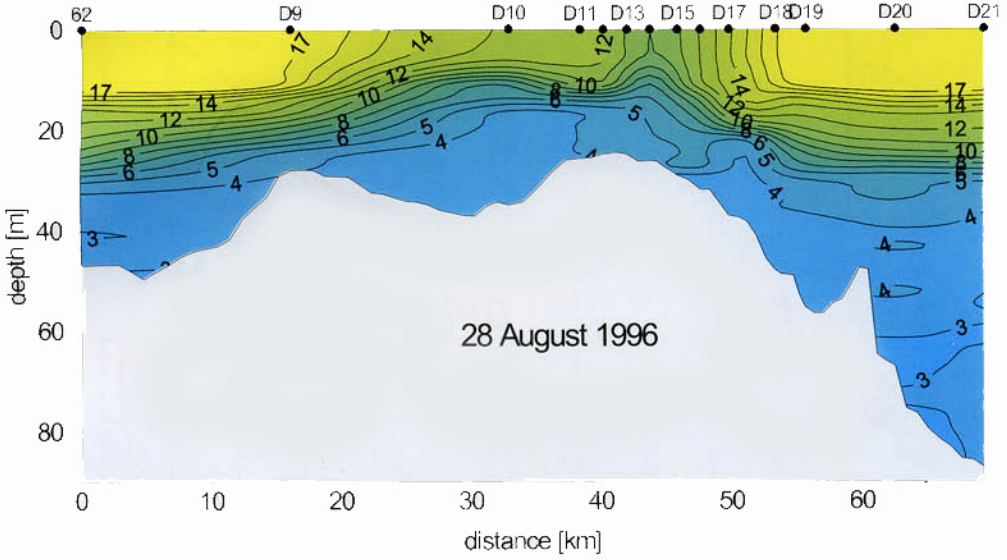

Fig. 13. The vertical temperature distribution at the cross-section shown in Fig. 11.

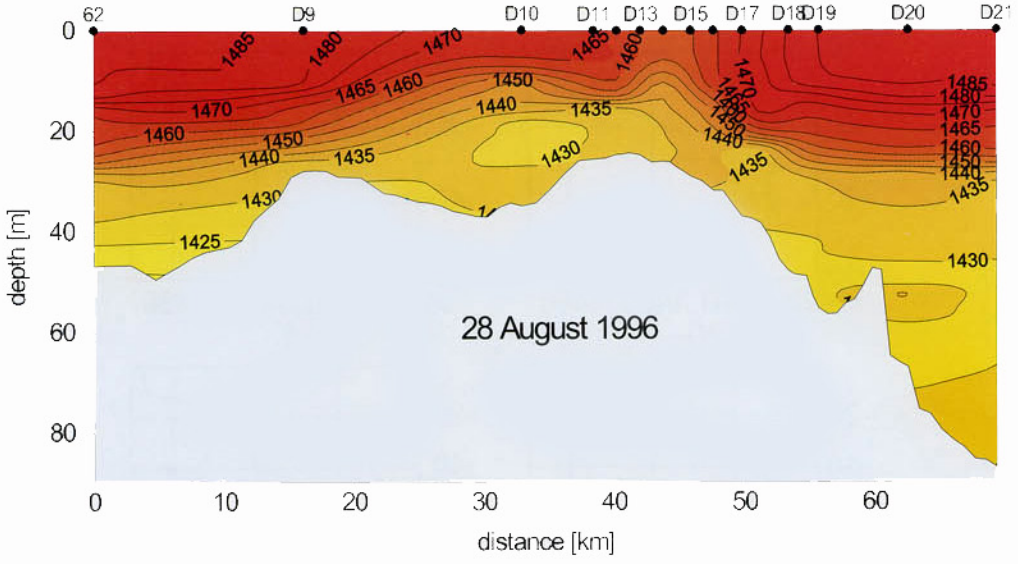

Fig. 14. The vertical sound speed distribution at the cross-section shown in Fig. 11.

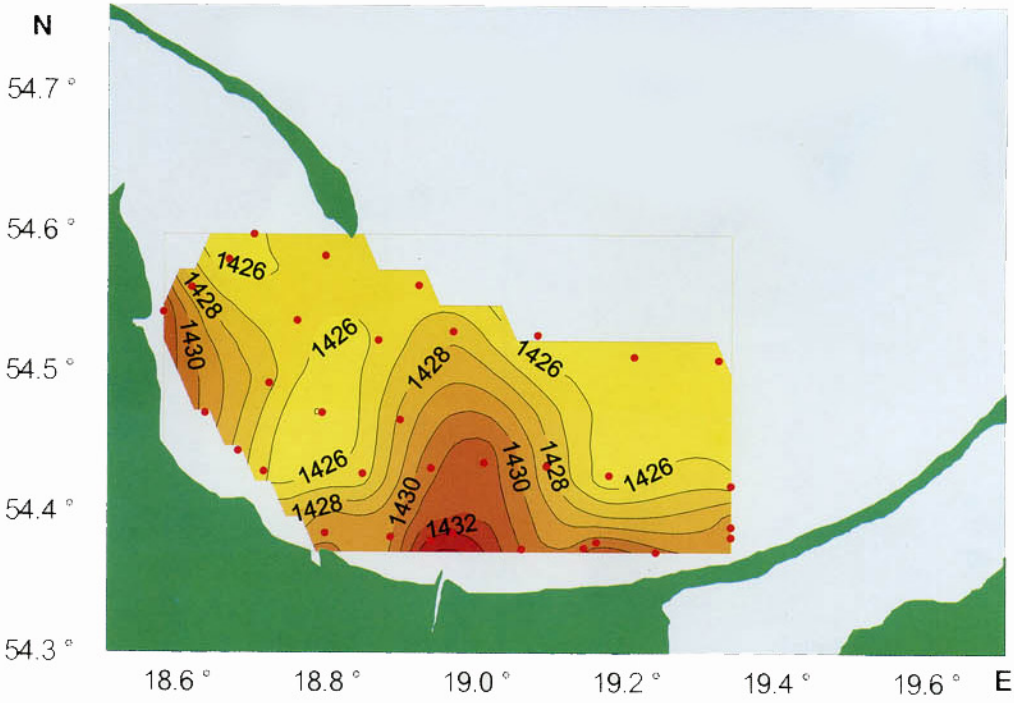

Fig. 15. The sound speed distribution at the surface of the Gulf of Gdańsk in April 1994.

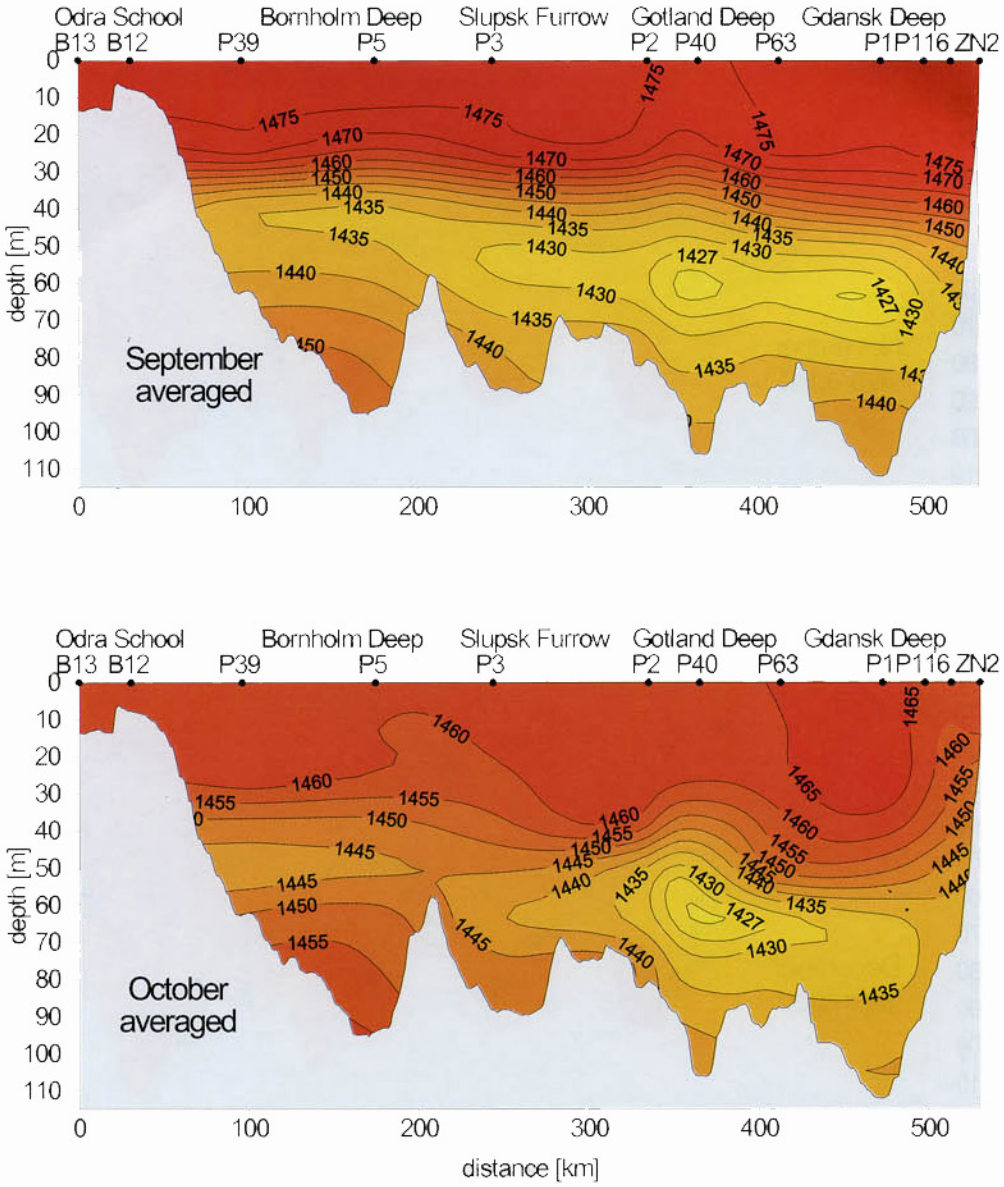

Fig. 6. The averaged vertical sound speed distribution in September and October in the years 1979 – 1991.

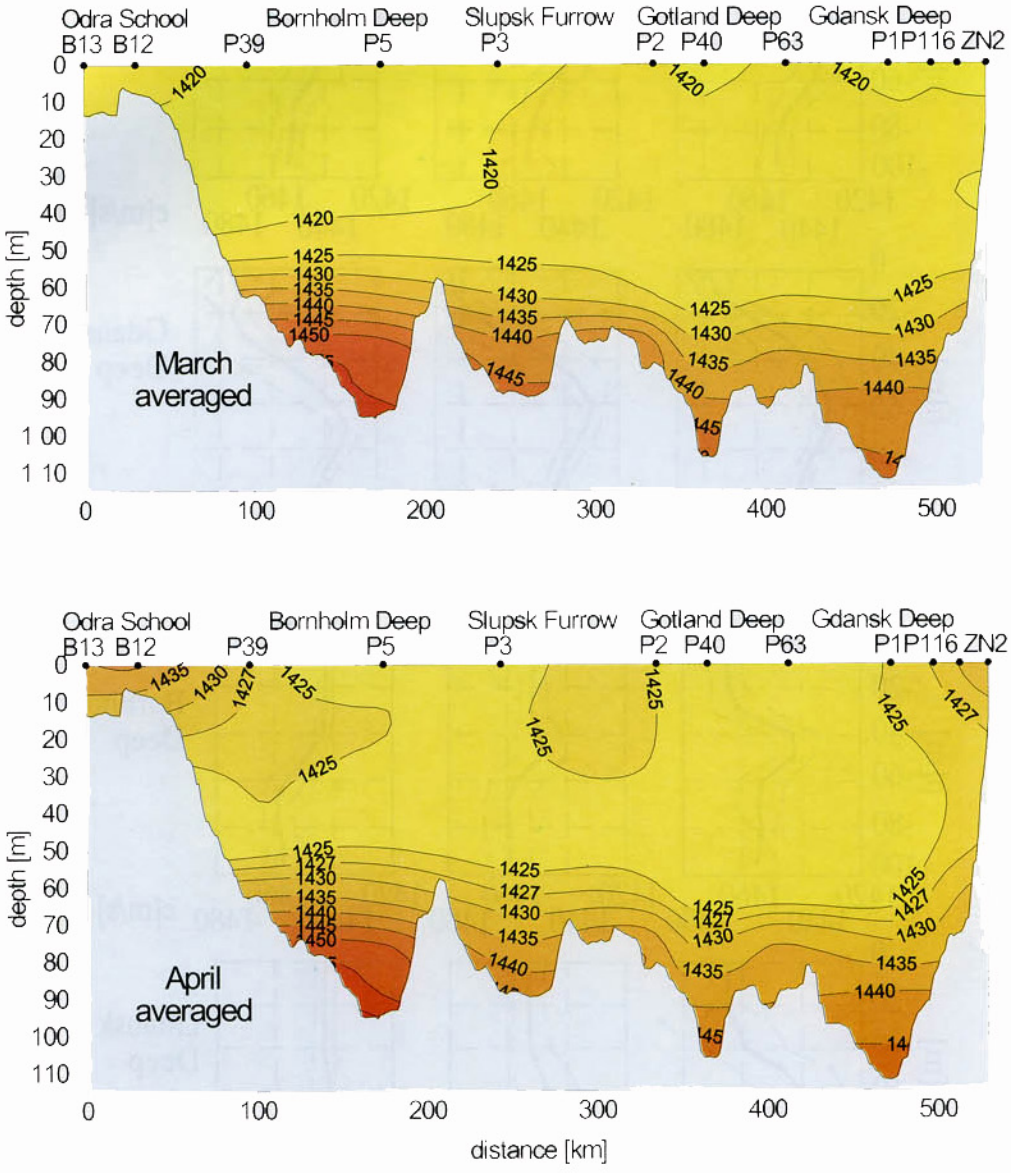

Fig. 3. The averaged vertical sound speed distribution in March and April in the years 1979 – 1991.

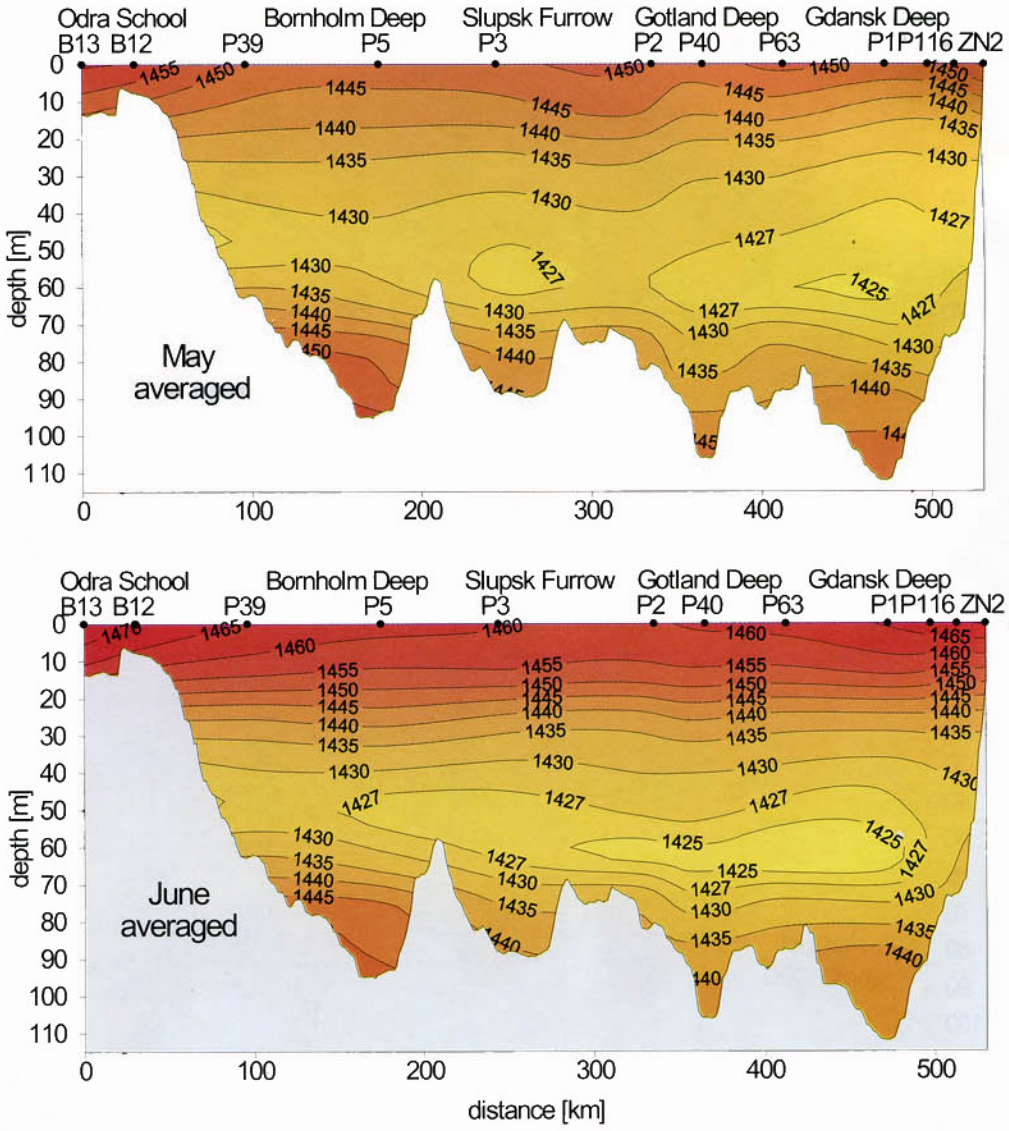

Fig. 4. The averaged vertical sound speed distribution in May and June in the years 1979 – 1991.

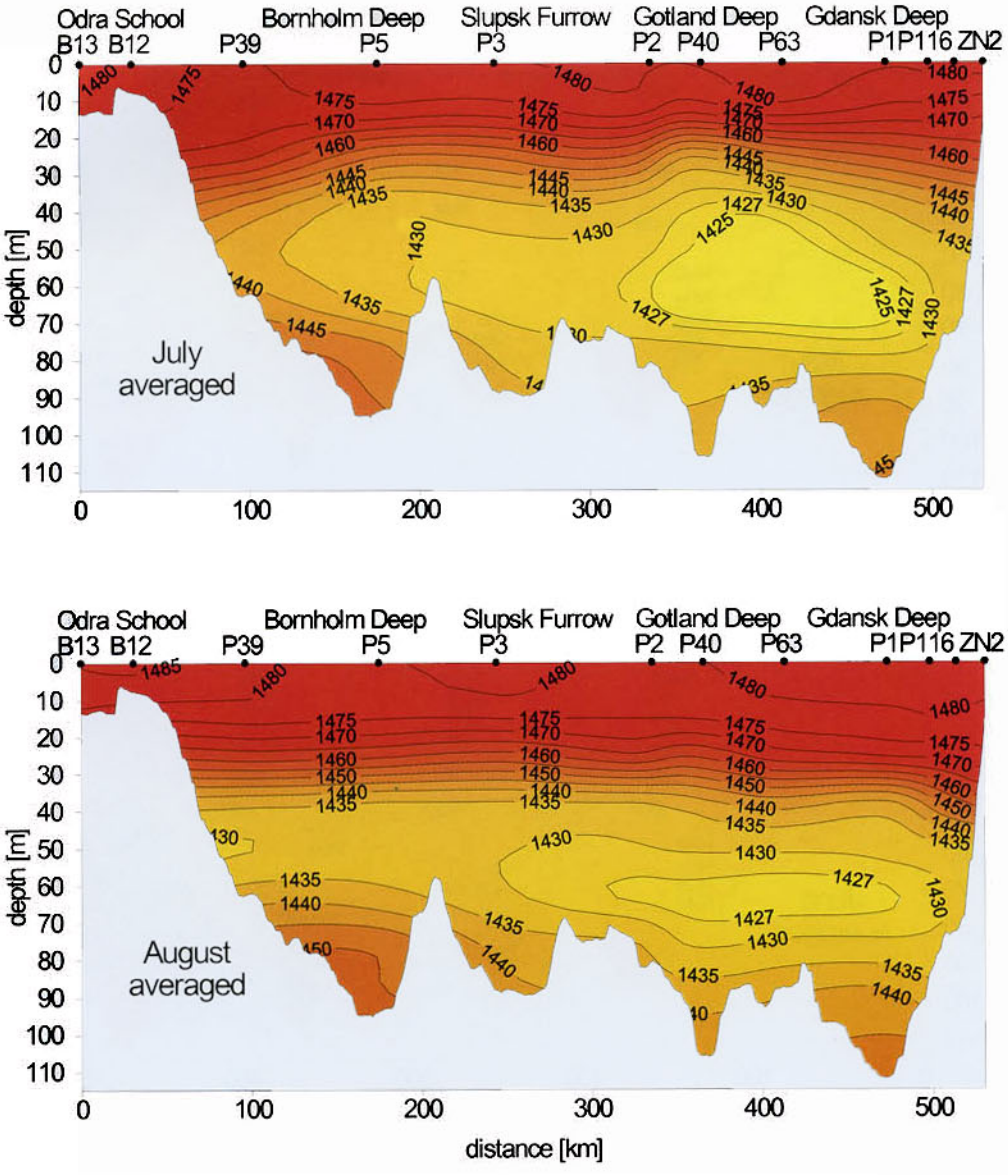

Fig. 5. The averaged vertical sound speed distribution in July and August in the years 1979 - 1991.

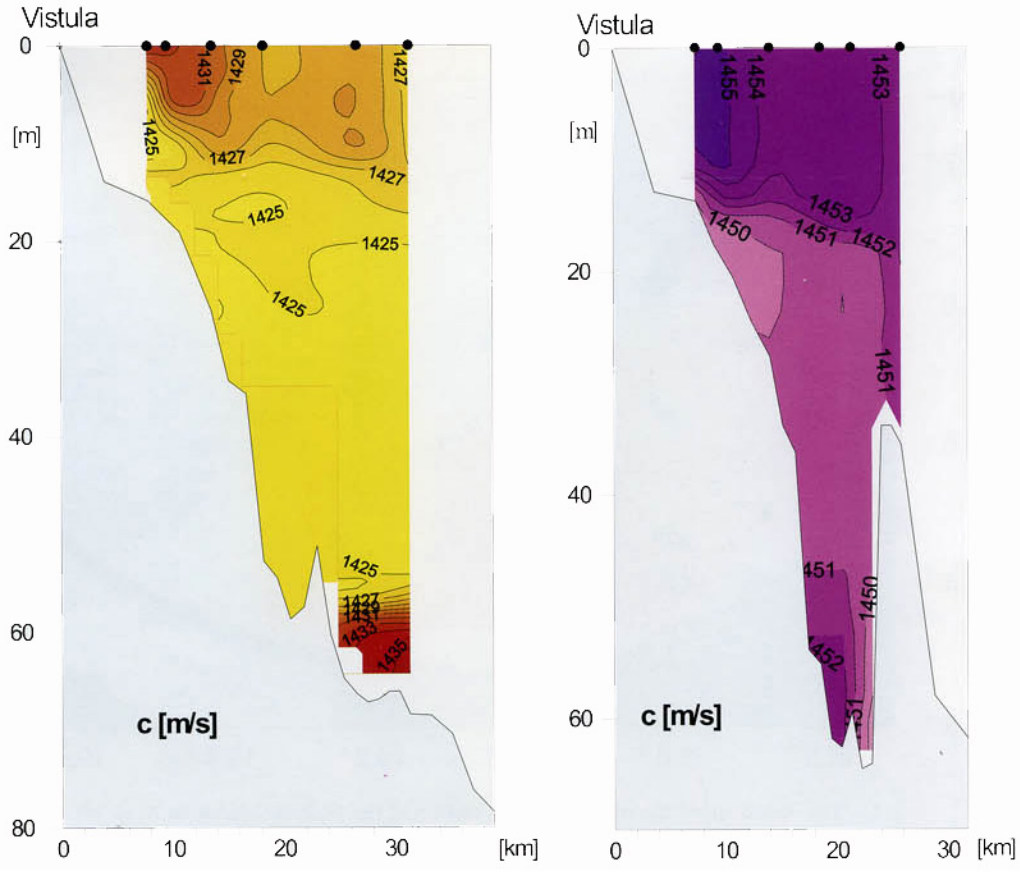

Fig. 16. The vertical sound speed distribution in the Gulf of Gdańsk in April and November 1994.

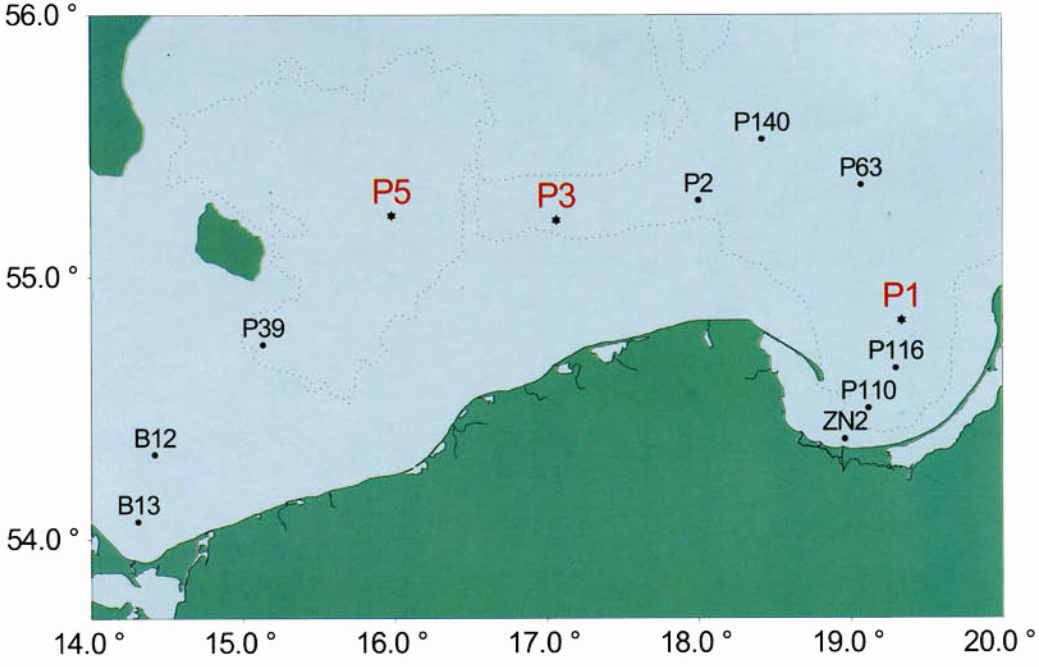

Fig. 1. Distribution of the measurement stations.

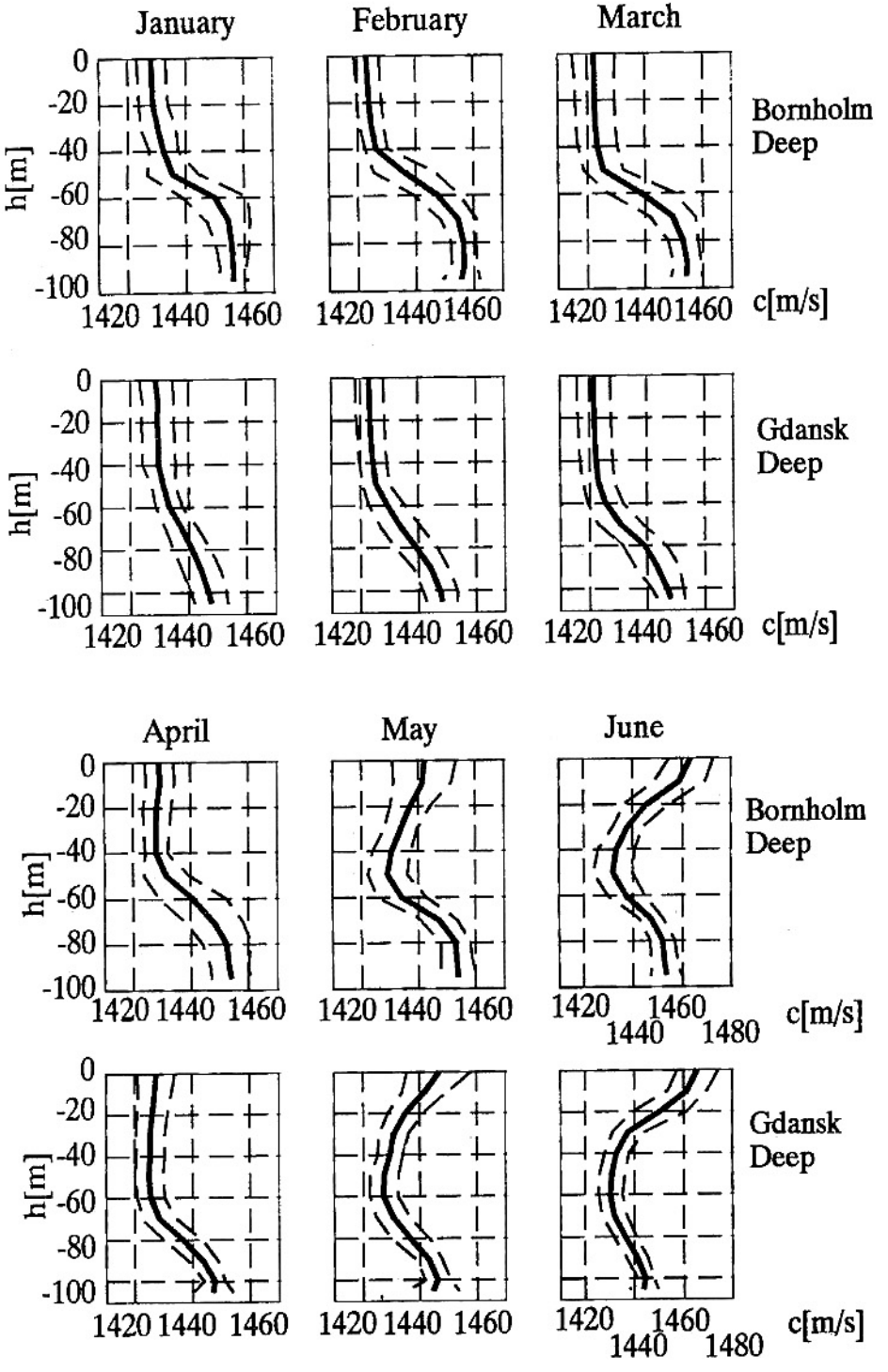
January
February
March
0
-20
-40
-60
-80
-100
h[m]
1420 1440 1460
Bornholm Deep
c[m/s]
Gdansk Deep
April
May
June
1420 1440 1460
1480

[Fig. 2a]

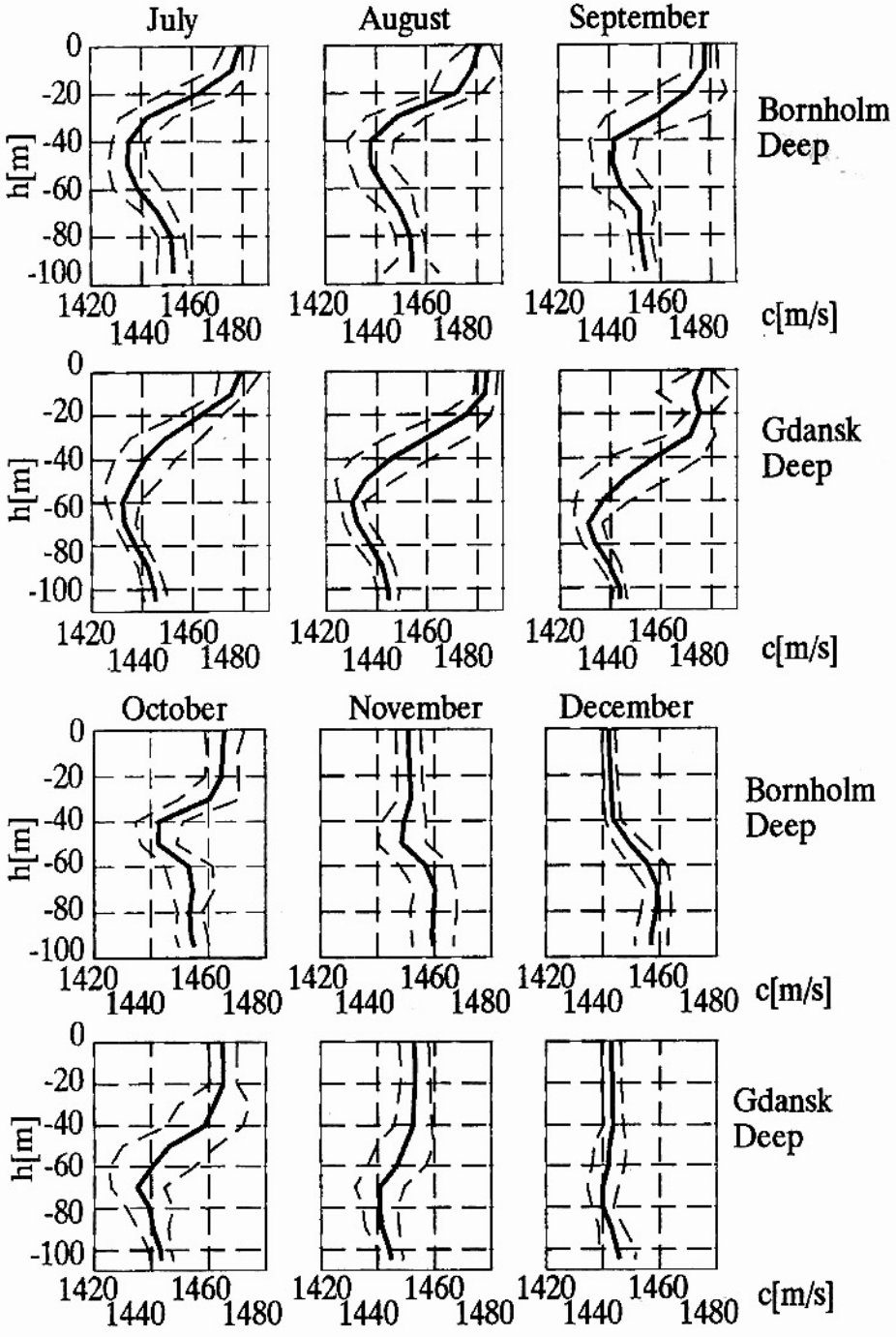

Fig. 2. The vertical sound speed distribution at the Bornholm Deep and at the Gdańsk Deep averaged for the period 1960 – 1997: (—) estimated averaged value, (- - -) confidence interval.

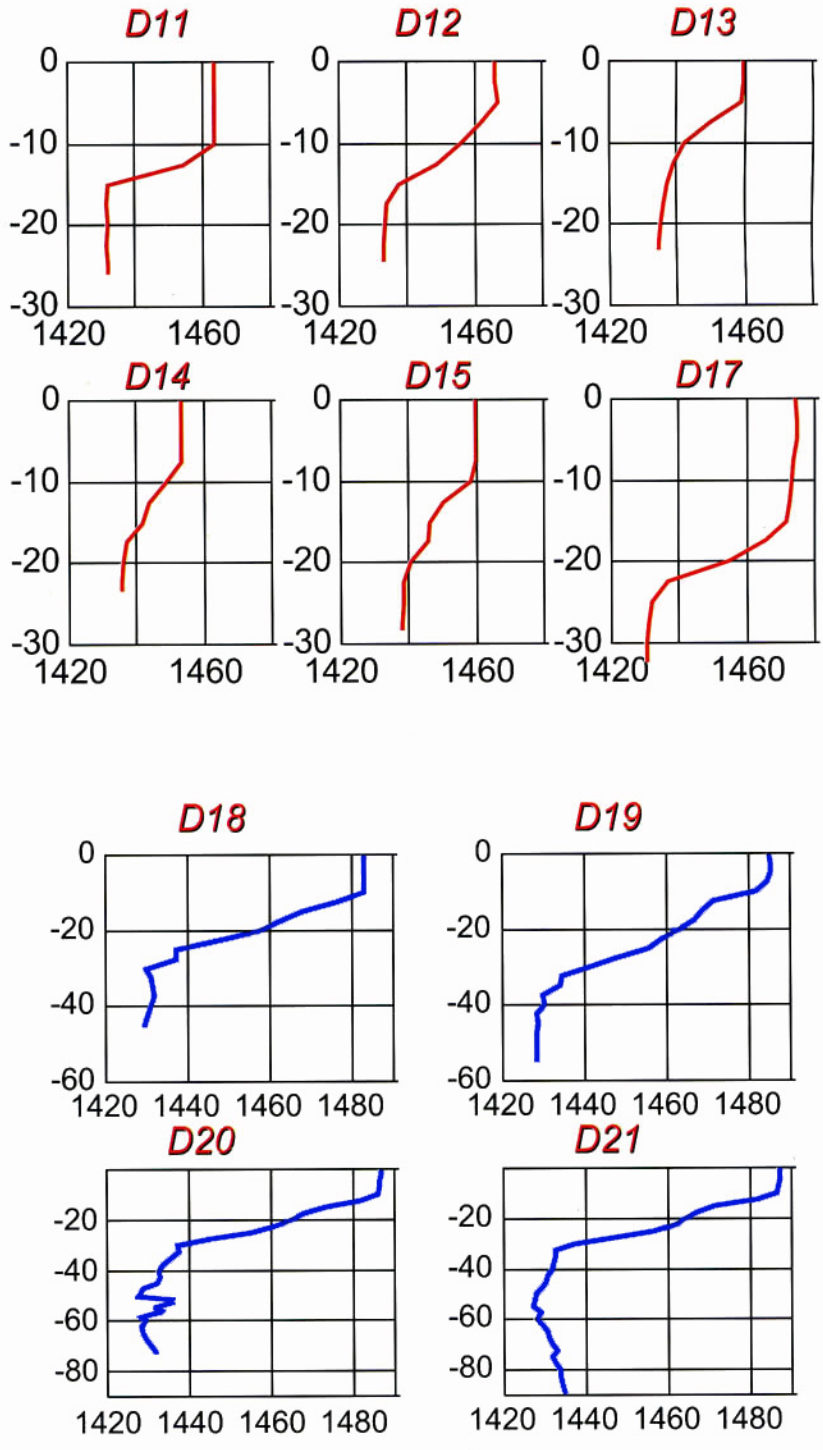

Fig. 12. The sound speed distribution at chosen stations in the vicinity of Rozewie — 28th August 1996.

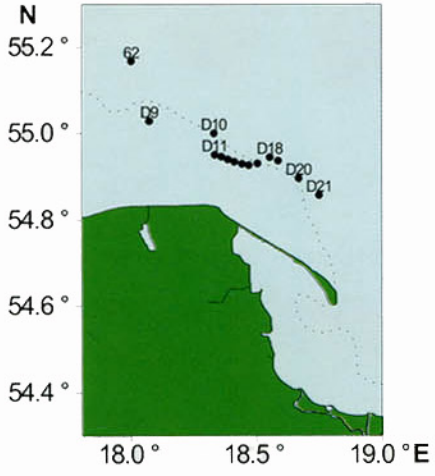

Fig. 11. The distribution of the measurement stations near Rozewie in August 1996.

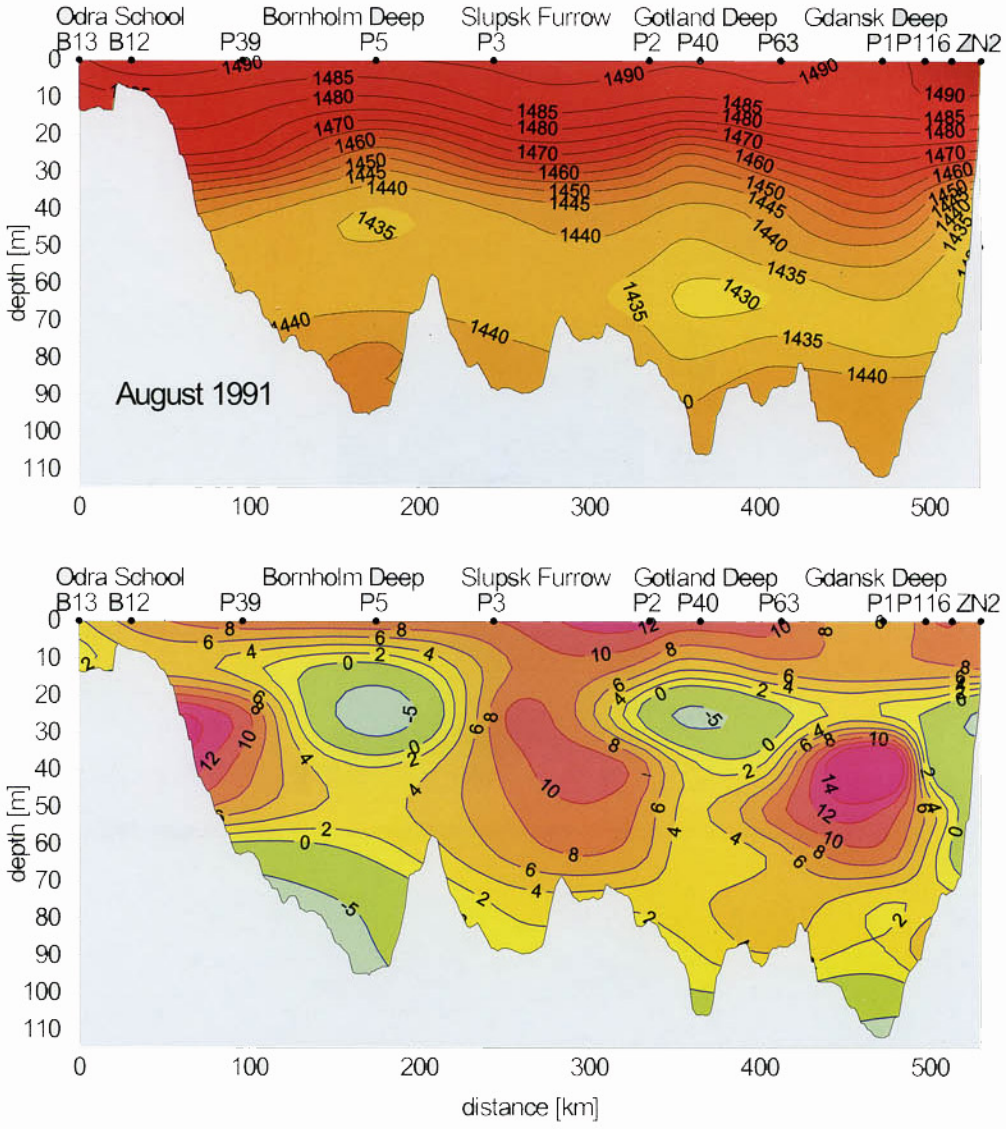

Fig. 10. The vertical sound speed distribution in August 1991 and the difference between it and the averaged distribution in August in the years 1979 – 1991.

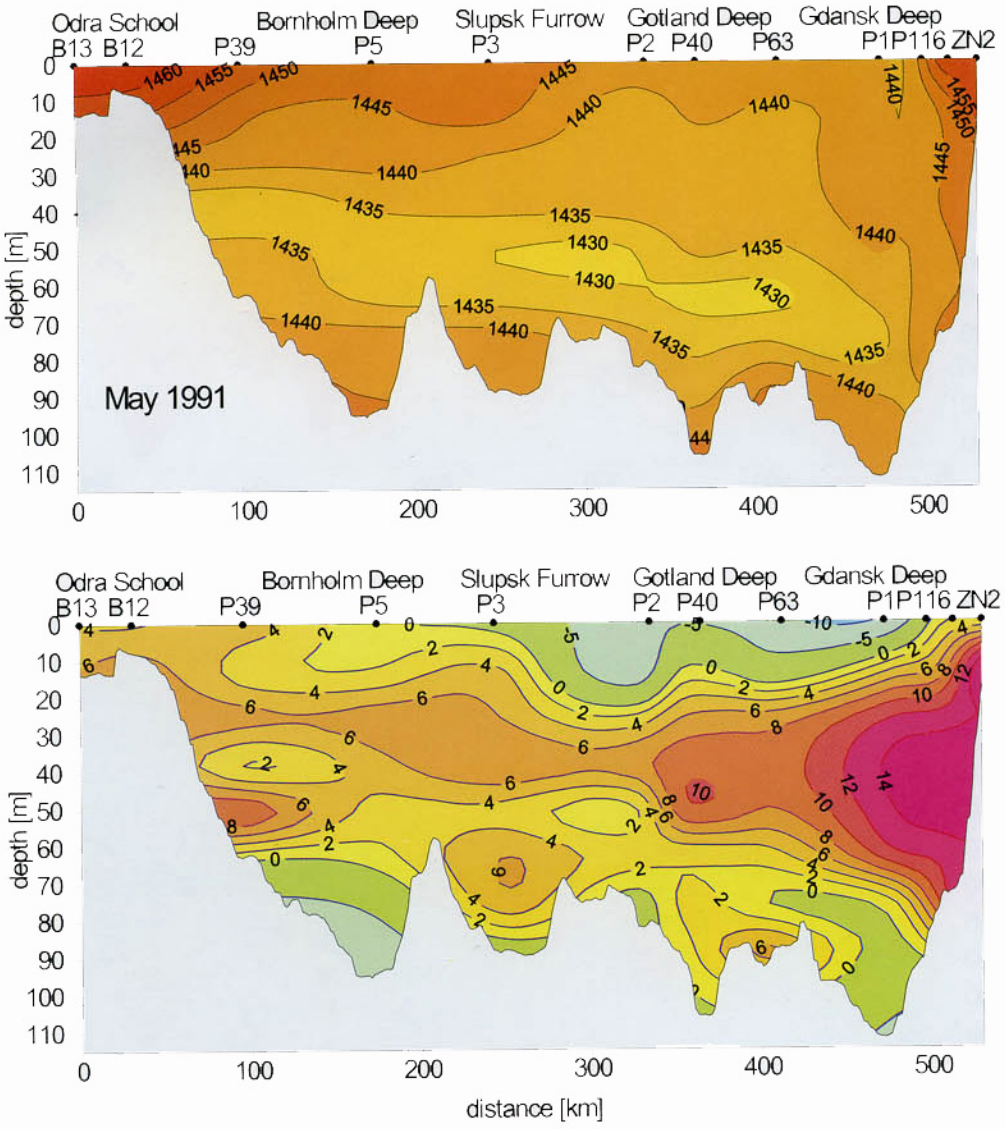

Fig. 9. The vertical sound speed distribution in May 1991 and the difference between it and the averaged distribution in May in the years 1979 – 1991.

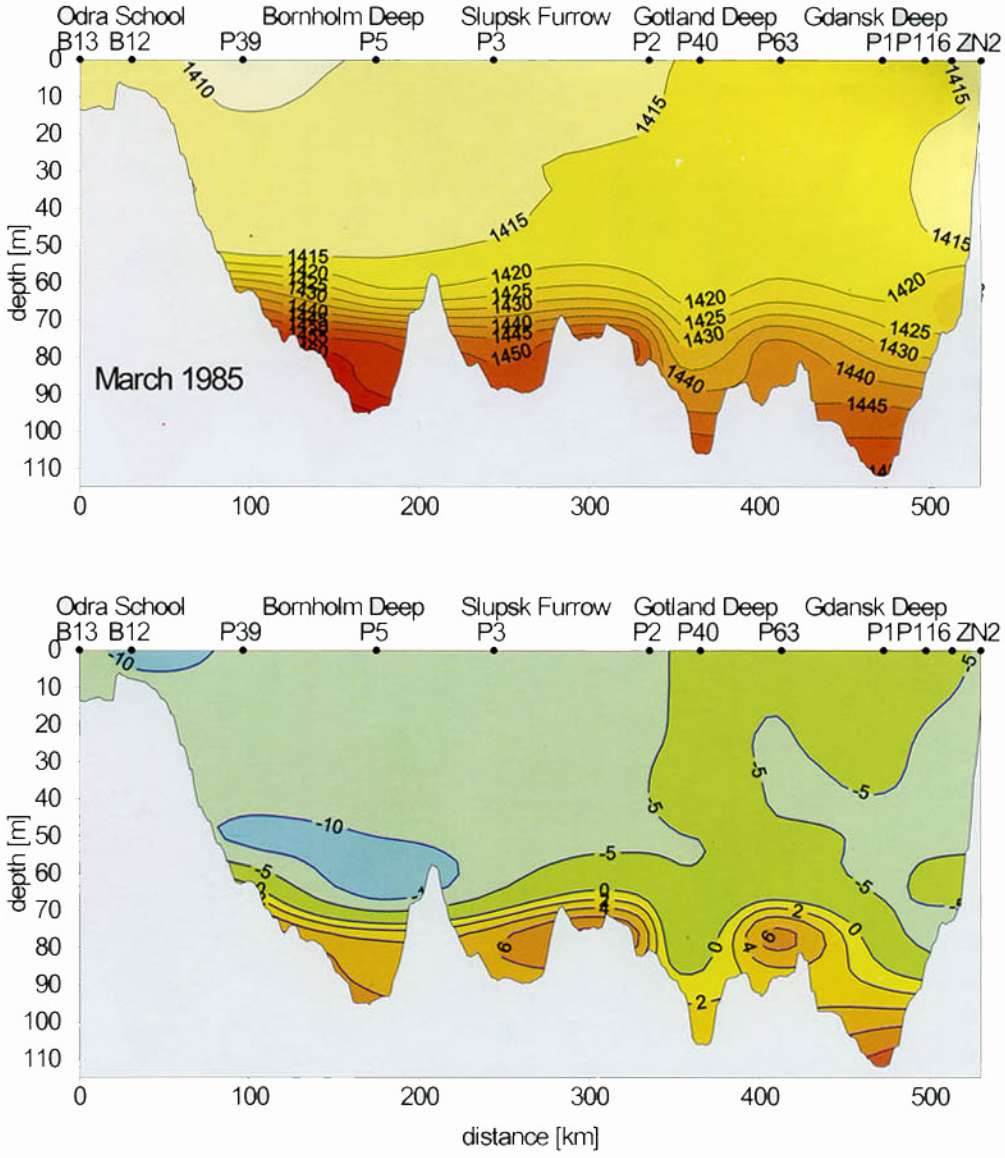

Fig. 8. The vertical sound speed distribution in March 1985 and the difference between it and the averaged distribution in March in the years 1979 – 1991.

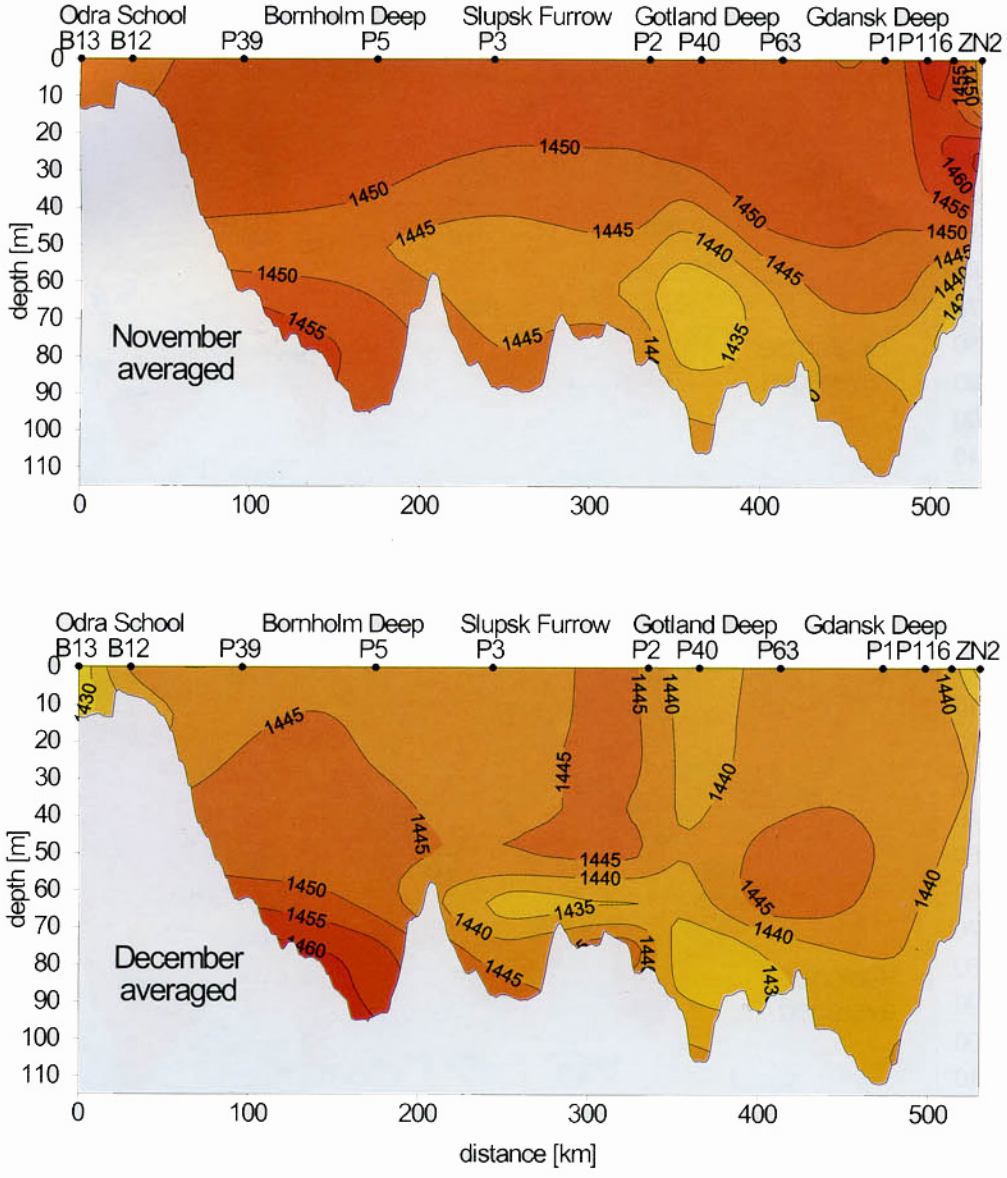

Fig. 7. The averaged vertical sound speed distribution in November and December in the years 1979 - 1991.

December, the distributions are not significantly diversified and the value of the sound speed is relatively considerable. The minimal value is higher than 1445 m/s in the region of the Bornholm Deep, higher than 1440 m/s in the environment of the Gdańsk Deep, and only in the surroundings of the Gotland Deep it is lower than 1435 m/s. In December the sound speed in the deep water layer in the Bornholm Deep increases significantly and at the depth below 60 m reached values greater than 1450 m/s, which comes to about 20 m/s more than in March and to about 10 m/s more than in September in the upper part of the area considered. The value at the bottom exceeded the average in March by about 5 m/s and the average in September by about 10 m/s.

5. Acoustical anomaly in the southern Baltic

In the previous chapter an attempt was made to characterize the acoustic climate of the southern Baltic. It was based on the averaged sound speed distributions. The next step in the search for the specific features of the Baltic treated as a complex environment of sound propagation was to find out how does the particular synoptic sound speed distribution differ from the averaged one. To get the answer, several synoptic distributions established in different seasons are compared with the averaged distribution.

Differences in the winter distribution depend predominantly on two main factors: the anomaly high or low temperature of air and the volume of the inflow of saline water from the North Sea. Both of these factors are reflected in the sound speed distribution in March 1985. During that year the averaged temperature of water in the upper layer at the depth of 10 m was 0.32°C, that is by about 1.16°C lower than the averaged temperature in March at the same depth. The consequence was reflected by the decrease of the sound speed from 5 to 10 m/s in the whole cross-section, with the exception of the areas close to the bottom of the deeps. There, as a result of the inflow which increased the salinity to 16.1 PSU (avg. 15.49 PSU) and the temperature to 7.44°C (avg. 6.42°C) at the Bornholm Deep, the established values were greater by up to 4.92 m/s than the averaged ones. The distribution for March 1985, as well as the difference between it and the averaged distribution (Fig. 3), are shown in Fig. 8.

The situation typical for May (see Fig. 4) could be regarded as the distribution representative for the spring. The influence of the warm winter of 1991 on the acoustical conditions in the next season was confirmed by the distribution pattern in May 1991 presented in Fig. 9. In this case, the middle area of the decreased sound speed is bordered by the isoline 1435 m/s. Only in the northern part of the considered area occurred the residue volumes of water in that the sound speed was below 1430 m/s. In contrast to that, the values at the surface were lower by up to 10 m/s than the average ones. It indicates that the heat delivered from the atmosphere during that spring was smaller than usually. Also in deeps, especially at the Bornholm Deep, the sound speed in the deep water layer was below the average values by up to 10 m/s. It was an effect of the lower salinity at the Bornholm Deep caused by the lack of inflow of saline water in the preceding autumn.

An example illustrating a summer with the generally positive anomaly of the acoustical conditions is the August of 1991 (Fig. 10). Only at the depths of about 20–30 m values below the average ones appeared. It could be the consequence of the negative anomaly near the surface, which was observed in May of that year (Fig. 9). In the deep water in the area of the Bornholm Deep decreased values of the sound speed were observed as a continuation of the situation in the spring.

The above presented examples of the positive and negative anomaly in the whole volume of the southern Baltic or in a part of it were chosen from among those which differed most distinctly. It allows to assess the range of changes of the sound speed in particular seasons.

6. Impact of local morphological and hydrological conditions on the sound speed distribution

Difficulties in specifying the acoustical conditions of the southern Baltic are increased by the appearance of short-term local phenomena changing considerably the sound speed distribution in certain areas [6, 19, 28]. Examples of such phenomena can be seen in the upwelling near Rozewie; the influence of the Vistula waters on the acoustical conditions is visible in the Gulf of Gdańsk.

The shape of the bottom near Rozewie causes in specific hydrological and meteorological conditions the occurrence of upwelling of the colder water. Data shown in the next figures illustrate the influence of upwelling on the acoustical conditions.

The consecutive graphs (Fig. 12) show the sound speed distribution measured on 28th August 1996 at stations marked in the map (Fig. 11). The distances between the stations were relatively small (about 1–2 km), however the distributions differed considerably. The value at the surface varied from 1451 m/s to 1474 m/s, at the bottom from 1431 to 1439 m/s. The difference between the maximal value at the surface and the minimal ones at the bottom changes from 16 m/s at the station D14 to 43 m/s at the station D17. The distance between those two stations equals 5 km.

Patterns of the vertical sound speed distribution at stations the D18, D19. D20 and D21, distant from those mentioned previously by about 3–10 km, were similar to each other. They all had the sound speed of about 1484 m/s at the surface and a high gradient of it within a layer ranging from 10 to 30 m with a sound speed reduction downward by about 1430 m/s.

The upwelling of the mass of cold water with temperatures of about 12°C, being lower by about 6°C in comparison to its environment (Fig. 13), was the cause of the anomaly. The vertical sound speed distribution at the cross-section along the stations marked in Fig. 11 is shown in Fig. 14. It is a phenomenon occurring sporadically, but when it happens it changes the local acoustical conditions to a considerable degree.

Another phenomenon changing the acoustical conditions in the southern Baltic to a certain degree is the inflow of the Vistula waters which influences the acoustic parameters of the Gulf of Gdańsk. This phenomena, described in detail in [19], is the subject of seasonal changes during the year. In propitious circumstances, its impact on the situation

in the Gulf of Gdańsk is clearly visible, as for example in April and November 1994 (Fig. 15, Fig. 16). The situation appeared after a few windless days. The range of the impact of the Vistula waters is up to 20 km from the mouth of the river in a layer of about 15 m thickness from the surface.

7. Conclusions

The acoustical climate of the southern Baltic is difficult to describe because of the many factors influencing it. In the paper, an attempt is made to characterize the acoustical conditions in this region. The characteristics obtained offer much valuable information on the conditions of the sound propagation in the Baltic Sea, on their changes during the year and on the impact of particular physical phenomena on them. However, it must be taken into account that this picture has been created with a limited number of available data.

The averaged distributions allow to assess the general trends and to find specific features for particular seasons. The acoustical conditions in the upper layer, where the salinity is almost invariable, depend on the seasonal changes in the temperature of the water. In the winter temperature, it is nearly stable in the upper layer down to the depth of about 50 – 60 meters. Therefore the spatial distribution of the sound speed is nearly uniform at that season.

In other seasons, the temperature of the water at the surface is higher than in the deeper layers. It involves the vertical gradient of the sound speed and the appearance of the minimum sound speed in its vertical distribution approximately at the border between the upper and the deep water layer. The value of the gradient is the highest in the summer. During the year, the gradient changes seasonally in accordance with the heat exchange between the atmosphere and the seawater. The thermal conditions in the winter exert an influence on the minimal value in the vertical sound speed distribution during successive seasons, whereas the maximal value of the speed at the surface depends on current conditions in each particular season.

The impact of the inflows of highly saline water from the North Sea, causing the increase of the sound speed in the deep water layer, is usually visible in the western part of the Baltic Sea in the autumn, and in the Gdańsk Deep region in the early spring. The inflow appears as a rule in the autumn and the subsequent course of the phenomena depends mainly on when it occurs and on the volume of the inflowing water.

The differences between synoptic and average distributions demonstrate the strength of the impact that physical factors have on them and confirm the necessity of investigating acoustical conditions by hydroacoustic equipment is used in underwater research.

References

[1] G.A. ATHANASSOULIS and E.K. SKARSOULIS, *Arrival-time perturbations of broadband tompgraphic signals due to sound speed disturbances. A wave-theoretic approach*, J. Acoust. Soc. Am., **97**, 6, 3575–3588 (1995).

[2] C. BJERRUM-NIESE and L. BJØRNØ, *A numerical model for time-frequency spreading of acoustic signals scattered from a moving sea surface*, Proc. of the 3rd European Conference on Underwater Acoustics, FORTH-IACM, Heraklion, Crete, 1996, 21–26.

[3] L.M. BREKCHOVSKICH, *Waves in layered media* [in Russian], Nauka, 1973.

[4] L.M. BREKCHOVSKICH, *Ocean acoustics* [in Russian], Nauka, 1974.

[5] C.S. CLAY and H. MEDWIN, *Acoustical oceanography. Principles and applications*, Wiley-Intersci. Publ., New York – London – Sydney – Toronto 1977.

[6] J. CYBERSKI, *Riverine water outflow into the Gulf of Gdańsk*, Oceanological Studies, **26**, 4, 65–76 (1997).

[7] V.A. DEL GROSSO, *New equation for the speed of sound in natural waters (with comparision to other equations)*, J. Acoust. Soc. Am., **56**, 5, 1084–1091 (1974).

[8] J. DERA, *Marine physics*, Elsevier, Amsterdam – Oxford – New York – Tokyo 1992.

[9] N.P. FOFONOFF and R.C. MILLARD, *Algorithms for computation of fundamental properties of seawater*, UNESCO Tech. Papers in Mar. Sci., 44, 1983.

[10] R.P. GILBERT, T. SCOTTI, A. WIRGIN and Y.S. XU, *The unidentified object problem in a shallow ocean*, J. Acoust. Soc. Am., **103**, 3, 1320–1327 (1998).

[11] A.E. GILL, *Atmosphere-ocean dynamics*, Academic Press Inc., Orlando 1982.

[12] D.F. GINGRAS and P. GERSTOFT, *Inversion for geometric and geoacoustic parameters in shallow water: Experiments results*, J. Acoust. Soc. Am., **97**, 6, 3589–3598 (1995).

[13] M. HOLEC and J. RATOWSKI, *Vertical distributions and gradients of the sound speed in the southern Baltic and their changes during the year* [in Polish], Proc. of the XXVth Open Seminar on Acoustics, Poznań 1978.

[14] D.R. JACKSON and K.L. WILLIAMS, *High-frequency sea-bed scattering measurements in shallow water*, Proc. of the 3rd European Conference on Underwater Acoustics, FORTH-IACM, Heraklion, Crete, 1996, 21–26.

[15] Z. KLUSEK, *Sound propagation conditions in the southern Baltic* [in Polish], Institute of Oceanology, Sopot 1990.

[16] G.A. KORN and T.M. KORN, *Mathematical handbook for scientists and engineers*, McGraw-Hill Book Company, New York – San Francisco – Toronto – London – Sydney 1968.

[17] E. KOZACZKA, I. GLOZA, G. GRELOWSKA, T. LESZCZYŃSKI and A. MILEWSKI, *General characteristics of ship noise in shallow water*, Proc. of the 4rd European Conference on Underwater Acoustics, CNR-IDAC, Rome, Italy, 1998, 567–572.

[18] E. KOZACZKA and G. GRELOWSKA, *Nonlinear properties of water* [in Polish], Naval Academy Press, 1996.

[19] E. KOZACZKA, G. GRELOWSKA, P. BITTNER and A. GRELOWSKI, *The influence of Vistula water on the thermodynamic and acoustic parameters of the Gulf of Gdańsk*, Oceanologia, **37**, 2, 277–248 (1995).

[20] X. LURTON and J. MARCHAL, *Long range propagation losses and reverberation levels in shallow water using an averaged intensity model*, Proc. of the 3rd European Conference on Underwater Acoustics, FORTH-IACM, Heraklion, Crete, 1996, 569–574.

[21] K.V. MACKENZIE, *Nine-term equation for sound speed in the ocean*, J. Acoust. Soc. Am., **70**, 807–812 (1981).

[22] D.E. NORRIS, J.L. SPIESBERGER and D.W. MERDES, *Comparison of basin-scale acoustic transmissions with rays and further evidence for a structured thermal field in the north-east Pacific*, J. Acoust. Soc. Am., **103**, 1, 182–194 (1998).

[23] G.V. NORTON and J.C. NOVARINI, *Enhancement of the total acoustic field due to the coupling effects from a rough sea surface and a bubble layer*, J. Acous. Soc. Am., **103**, 4, 1836–1843 (1998).

[24] G.V. NORTON and J.C. NOVARINI, *The effect of sea-surface roughness on shallow water waveguide propagation: A coherent approach*, J. Acous. Soc. Am., **99**, 4, 2013–2021 (1996).

[25] A. ORŁOWSKI, *Acoustic studies of spatial gradients in the Baltic: Implications for fish distribution*, ICES J. Mar. Sci., **56**, 561–570 (1999).

[26] A.H. PERRY and M.J. WALKER, *The ocean-atmosphere system*, Longman London, New York 1977.

[27] J. PIECHURA, *Longterm changes in hydrological conditions of the southern Baltic*, Bull. Sea Fish. Inst., 1, 128, 45–57 (1993).

[28] J. PIECHURA, W. WALCZOWSKI and A. BESZCZYŃSKA-MOLLER, *On the structure and dynamics of the water in the Słupsk Furrow*, Oceanologia, **39**, 1, 35–54 (1997).

[29] C. ROZIER, D. LESSELIER and T. ANGELL, *Optimal shape reconstruction of a perfect target in shallow water*, Proc. of the 3rd European Conference on Underwater Acoustics, FORTH-IACM, Heraklion, Crete, 1996, 21–26.

[30] R.J. URICK, *Principles of underwater sound*, McGraw-Hill Book Company, 1975.

[31] D.E. WESTON, *Range relation in oceanographic acoustics*, J. Sound and Vibration, **18**, 2, 271–287 (1971).

ARCHIVES OF ACOUSTICS
25, 3, 369–376 (2000)

THERMOCHEMICAL PROPERTIES OF BINARY LIQUID SYSTEMS *N*-ALCOHOL/CYCLOHEXANE DETERMINED BY AN ACOUSTIC METHOD

K. BEBEK

Silesian University
Institute of Chemistry
(40-006 Katowice, Szkolna 9, Poland)
e-mail: kbebek@tc3.ich.us.edu.pl

The results of ultrasonic and volumetric measurements were used to obtain the excess molar enthalpies for binary liquid mixtures containing cyclohexane, as the common component, and primary aliphatic alcohols (*n*-propanol, *n*-butanol and *n*-pentanol) at 293.15 K. The excess molar enthalpies of those systems are positive in the whole concentration range and show evidently different concentration dependences. The excess internal pressures of the liquid mixtures, determined in a few different ways, are negative for all the systems. The behaviour of those excesses are discussed in terms of intermolecular interactions in the binaries and the self-association potential of the alcohols.

1. Introduction

The molecules of aliphatic alcohols are highly associated by hydrogen bondings [1, 2]; the self-association in non-polar solvents results in the formation of multimeric ring or chain structures, i.e. the oligomers appearing in the solution are either "open" or "closed" entities [3–7]. Dielectric studies indicate that those various multimeric structures exist in the solution in different proportions depending on the alcohol concentration, its ability to hydrogen-bond formation and the van der Waals type molecular interactions of the non-polar solvent with the alcohol contained in oligomers that are constantly reorganizing [8–12].

The most reliable values of the enthalpies of hydrogen bond formation constants were found by calorimetric measurements in infinitely dilute solutions [13]. The enthalpy of the hydrogen bond formation in solutions of *n*-alcohols in *n*-heptane (23.5 ± 0.5 kJ/mol), determined calorimetrycally, is almost independent of the lengths of the hydrocarbon chain of the aliphatic alcohol [14, 15].

Thermochemical data for aliphatic alcohol solutions (excess molar enthalpy and isobaric heat capacity) determined by calorimetric methods (that are sensitive to changes in the hydrogen bond energy) do not show even a qualitative agreement with those obtained by other thermodynamic methods [16]; the latters seem to reflect variations in the number of hydrogen bonds. Also, the temperature dependences of the thermochemical

quantities of pure aliphatic alcohols and their solutions are considerably more complex than for other organic liquids [17].

The thermochemical data differentiate evidently the homologous series of aliphatic alcohols since they depend on the branching of the alkyl chains [18]; the enthalpy of evaporation of primary alcohols, including those with non-branched hydrocarbon chains (n-alcohols), increase with increasing length of the alkyl chain, while for other alcohols the dependence on the chain length is opposite.

In this paper, we report the concentration dependences of the excess molar enthalpy, $H^E = H^E(x)$, at 293.15 K for binary solutions of n-propanol, n-butanol and n-pentanol in cyclohexane determined from internal pressure values, the latters being obtained in three different ways from ultrasonic and volumetric measurements [19] and the well-known thermodynamic relationships.

2. Experimental

The components, all of analytical grade, were obtained from POCh Gliwice (Poland) and purified by fractional distillation and dried as described previously [19, 20]. The binary mixtures were prepared by weighing immediately before the measurements (the accuracy of the mole fraction was better than 0.25×10^{-4} and the residual water content was less than 0.025%).

The ultrasonic group velocity was measured at a frequency of about 4 MHz by the sing-around method with an accuracy better than 0.5 m/s (the precision of the ultrasonic velocity measurements varied from 0.05 to 0.30 m/s); the measurement device (SA-V/Z) was designed and constructed in our laboratory [21 – 23].

The densities of the systems under test were determined by the Kohlrausch method with an accuracy better than 0.1 kg/m^3. The methods of measurements and calibrations have been already published [19, 20, 24].

The thermal stability of the sample at 293.15 ± 0.01 K was ensured during the ultrasonic velocity and density measurements by a water bath that was heated by a proportional-integrating temperature controller (Unipan 660, Poland) and cooled by water from another thermostat.

3. Measurement results

The molar volumes, V, and excess molar volumes, V^E, of the binary liquid systems were calculated from the measured density, ρ, using the following equations:

$$V = (\mathrm{x}_1 M_1 + \mathrm{x}_2 M_2)/\rho, \tag{1}$$

$$V^E = V - (\mathrm{x}_1 V_1 + \mathrm{x}_2 V_2), \tag{2}$$

where x — mole fraction of the alcohol, M_i — molar masse of the components, the indices "1" and "2" refer to the alcohol (associating component) and to cyclohexane (non-polar component), respectively.

The internal pressure, ¶, was calculated from the following relationship [25–27]:

$$¶ = 2^{1/6}RT/(2^{1/6}V - 2rN^{1/3}V^{2/3}), \tag{3}$$

where R, T, N and r are the gass constant, temperature in K, Avogadro's number and mean molecular radius, respectively.

The mean molecular radii, r, were obtained, according to SCHAAFFS [28], from the density, ρ, and ultrasound velocity, c:

$$r = \left\{3M/(16\pi\rho N)[1 - \gamma RT/(Mc^2)((1 + Mc^2/(3\gamma RT))^{1/2} - 1)]\right\}^{1/3}, \tag{4}$$

where $\gamma = C_p/C_v$ is the ratio of the isobaric heat capacity to the isochoric one; this ratio can be determined from the isentropic and isothermal compressibility coefficients, β_s and β_T, using the well known thermodynamic relation $\beta_T/\beta_s = C_p/C_v$.

The isentropic and isothermal compressibility coefficients were calculated from the following equations:

$$\beta_s = 1/(\rho c^2), \tag{5}$$

$$\beta_T = \beta_s + \alpha^2 VT/C_p, \tag{6}$$

using the isobaric thermal expansion coefficient, α, estimated from the temperature dependence of the densities (measured at 293.15 K in this work and available in the literature for neighbouring temperatures [30–32]) and the isobaric heat capacities, C_p, taken from the literature [30–33].

The molar volumes, molecular radii, coefficients of isothermal compressibility and the cubic thermal expansion coefficients together with the ratio of isobaric and isochoric heat capacities, γ, for the pure components at 293.15 K are collected in Table 1.

Table 1. Molar volumes, molecular radii, isothermal compressibility coefficients, cubic thermal expansion coefficients and the ratios of isobaric to isochoric heat capacities for the pure components at 293.15 K.

	V [m^3 mol^{-1}]×10^5	r [m]×10^{10}	β_T [Pa^{-1}] ×10^{12}	α [kK^{-1}]	$\gamma = C_p/C_v$
n-propanol	7.472	1.89 (8)	1087.5	0.99	1.18
n-butanol	9.145	2.03 (6)	891.3	0.94	1.14
n-pentanol	10.821	2.15 (7)	867.5	0.92	1.18
cyclohexane	10.815	2.15 (2)	1091.1	1.216	1.39

The internal pressures for the pure components and binaries were obtained from the estimated coefficients of thermal expansion and the isothermal compressibility by the following equation [27, 34]:

$$¶ = T\alpha/\beta_T. \tag{7}$$

Because of the lack of α^E data of sufficient accuracy for the binary mixtures, the widely accepted assumption $\alpha^E = 0$ was made. Thus

$$\alpha \approx \alpha^{id} = (1/V^{id})(x_1V_1\alpha_1 + x_2V_2\alpha_2), \tag{8}$$

where $V^{id} = x_1V_1 + x_2V_2$.

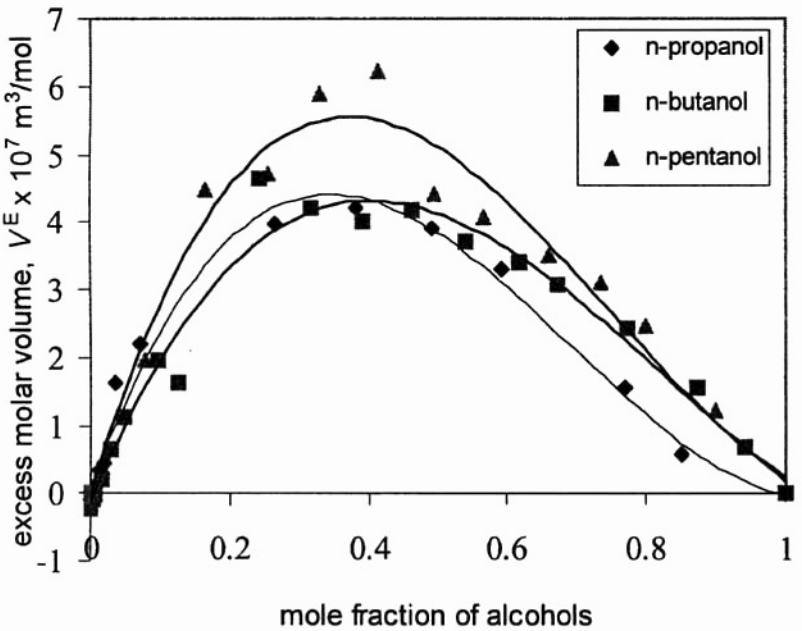

Fig. 1. Excess molar volume isotherms for the binary mixtures of alcohols with cyclohexane at 293.15 K. Points — experimental values.

However, for the binary mixtures under test, the volume effects of mixing are different from zero, $V^E \neq 0$, (the $V^E = V^E(x_1)$ isotherms are shown in Fig. 1) and the excess α^E is most often not small enough to be neglected. The reliable expansion coefficient,

$$\alpha = \alpha^{id} + \alpha^E, \tag{9}$$

can be calculated from the definition [33]:

$$\alpha^E = (1/V)[(\partial V^E/\partial T)_p - V^E\alpha^{id}] \tag{10}$$

using the $(\partial V^E/\partial T)_p$ values calculated as follows [33]:

$$(\partial V^E/\partial T)_p = -(\partial V/\partial T)_p^{id}(V^E/V^{id}) = -V^E\alpha^{id}. \tag{11}$$

Thus, the internal pressure can be obtained either from Eq. (3), or from Eqs. (7) and (8) (assuming $\alpha^E = 0$) or (7) and (9) (using Eqs. (10) and (11)).

The excess molar enthalpies of the solutions under test were determined using the internal pressures calculated in those three different ways and assuming that the mixing is not accompanied by a significant entropy effect [34]:

$$H^E = x_1 ¶_1 V_1 + x_2 ¶_2 V_2 - ¶V. \tag{12}$$

The isotherms of the excess molar enthalpy (calculated in the three ways described above) vs. mole fraction of alcohol ($H^E = HE(x_1)$) are shown in Figs. 2–4, where the points represent values calculated from Eq. (12) using either Eq. (3) (Fig. 2) or Eqs. (7) and (8) (Fig. 3), or (7) and (9) (Fig. 4).

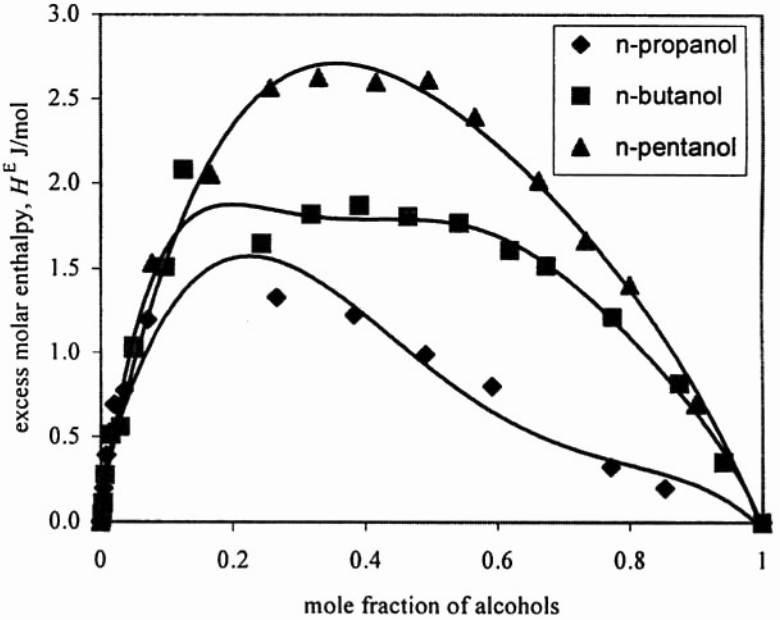

Fig. 2. Excess molar enthalpy isotherms for the binary mixtures of alcohols with cyclohexane at 293.15 K. Points — values calculated from Eq. (3).

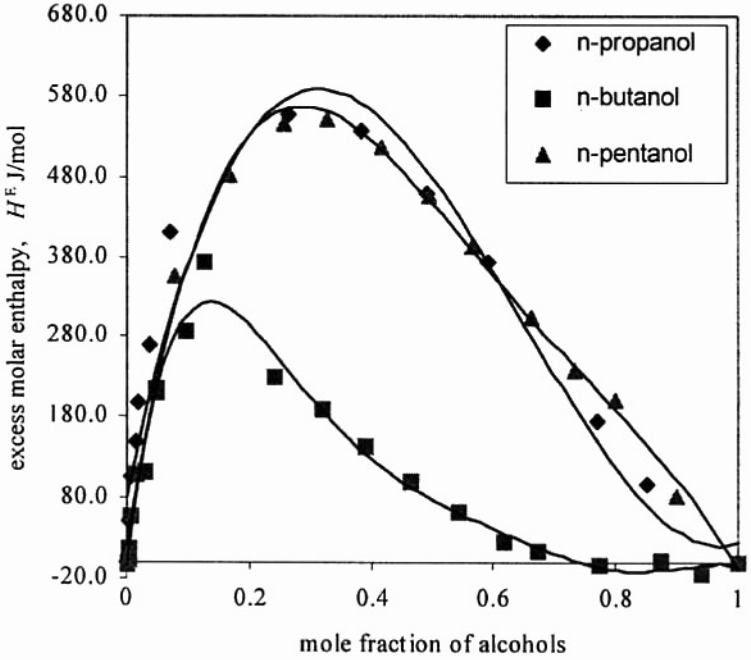

Fig. 3. Excess molar enthalpy isotherms for the binary mixtures of alcohols with cyclohexane at 293.15 K. Points — values calculated from Eq. (12) in connection with Eqs. (7) and (8).

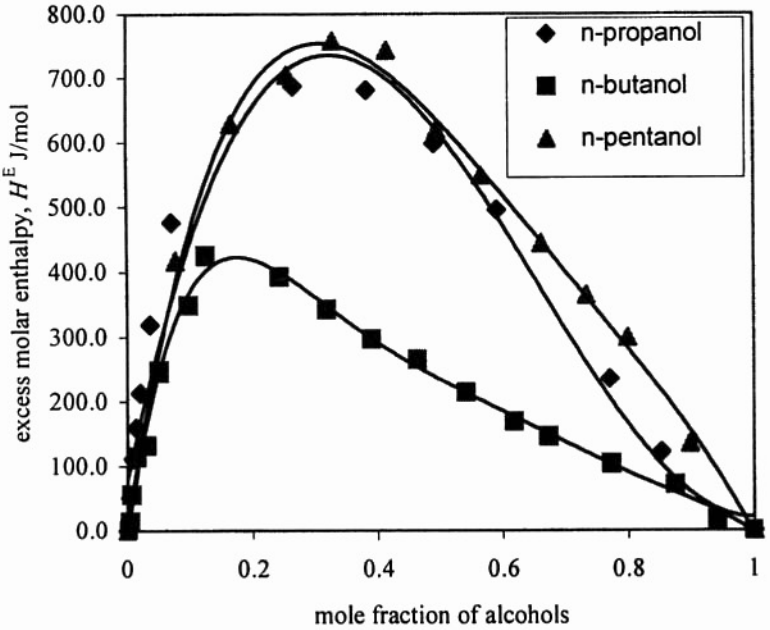

Fig. 4. Excess molar enthalpy isotherms for the binary mixtures of alcohols with cyclohexane at 293.15 K. Points — values calculated from Eq. (12) in connection with Eqs. (7) and (9).

4. Discussion and conclusions

The excess molar volumes for all the systems studied are positive over the whole concentration range and show a similar concentration dependence with a characteristic asymmetry; However, their maximum values are slightly different (Fig. 1). Dilution of the alcohols with cyclohexane results in a gradual decrease of the number of associated species. A more loosely packing of the molecules in solution than in the pure liquids seems to be likely; the solution should be therefore more compressible.

The excess molar enthalpies of the binary mixtures under test, irrespective of how they were determined, are also positive over the entire composition range and show concentration dependences that differ evidently in magnitude and asymmetry (Figs. 2–4).

The minima of the excess internal pressures correlate clearly with the magnitude of the internal pressures of the pure alcohols and their capability of association by hydrogen bonds [19, 20].

The isotherms of $H^E = H^E(x_1)$, calculated from the internal pressures obtained from Eq. (3), increase with increasing length of the hydrocarbon chain of the associating component (alcohol) of the mixture (Fig. 2).

The isotherms of $H^E = H^E(x_1)$ calculated from Eqs. (12) and (7) (Figs. 3 and 4) show a sequence inconsistent with the hydrocarbon chain length of the alcohols. For the n-butanol solutions, the excess enthalpies are lower and their maximum appears at

higher cyclohexane concentrations suggesting a higher capability of self-association of this alcohol in comparison with those of primary propanol and pentanol (Figs. 3 and 4).

From inspection of the isotherms $H^E = H^E(x_1)$ in Figs. 3 and 4, one learns that for all the systems investigated the values calculated by assuming $\alpha^E = 0$ (Fig. 3) are by about 15¬20% lower than those calculated from Eq. (9), i.e. by taking into account the excess thermal expansion coefficients (Fig. 4).

Furthermore, it is worthy of notice that the excess molar enthalpies estimated from Eqs. (12) and (7), by either assuming $\alpha = \alpha^{id}$ or applying approximate $\alpha = \alpha^{id} + \alpha^E$ values, are in good accordance with data determined by other thermochemical methods [35].

Acknowledgement

The author gratefully thanks Professor Stefan Ernst for his interest in this work and the critical reading of the manuscript.

References

[1] W.L. JORGENSEN, J. Phys. Chem., **90**, 1276 (1986).

[2] A. NATH and E. BENDER, Fluid Phase Equilibria, **7**, 275 (1981).

[3] H-H. LIMBACH, *The use of NMR spectroscopy in the study of hydrogen bonding in solution*, [in:] Aggregation Processes in Solution, E. WYN-JONES and J. GORRNALLY [Eds.], Elsevier Scientific Publishing Company, Amsterdam – Oxford – New York 1983.

[4] E.E.TUCKER and E.D. BECKER, J. Phys. Chem., **77**, 1783 (1973).

[5] E.E. TUCKER, T.R. CLEM, J.I. SEEMAN and E.D. BECKER, J. Phys. Chem., **79**, 1005 (1975).

[6] L.M. SWEETING and E.D. BECKER, J. Phys. Chem., **88**, 6075 (1984).

[7] M.A. SUHM, K.J. MÜLLER and H. WEINGÄRTNER, Z. Physik. Chem. Neue Volge, **155**, 101 (1987).

[8] J. MAŁECKI, Acta Phys. Polon., **21**, 13 (1962).

[9] B.B. SWAIN and G.S. ROY, Jpn. J. Appl. Phys., **25**, 2, 209 (1986).

[10] G. ROY and B.B. SWAIN, Acta Chim. Hungarica, **125**, 2, 211 (1988).

[11] J. MAŁECKI, S. BALANICKA and J. NOWAK, J. Chem. Soc. Faraday II, **76**, 42 (1980).

[12] J. MAŁECKI and J. NOWAK, Acta Phys. Polon., **A55**, 55 (1979).

[13] H. BUCHOWSKI, Wiad. Chem., **35**, 11 (1981).

[14] M.K. WÓYCICKA and B. KALINOWSKA, Bull. Acad. Polon. Sci., Ser. Sci. Chim., **23**, 759 (1975).

[15] H.C. VANNESS, C.A. SOCZEK and N.K. KOCHAR, J. Chem. Eng. Data, **12**, 346 (1967).

[16] J. JADŻYN, *Badanie solwatacji molekuł dipolowych w rozpuszczalnikach obojętnych*, Prace Instytutu Fizyki PAN, 61, Warszawa 1975.

[17] V. MAJER, V. SVOBODA and V. HYNEK, J. Chem. Thermodyn., **16**, 1059 (1984).

[18] V. MAJER, V. SVOBODA, V. UCHYTILOVA and M. FINKE, Fluid Phase Equilibria, **20**, 111 (1985).

[19] K. BEBEK and S. ERNST, Akust. Molek. Kwant., **16**, 13 (1995).

[20] K. BEBEK, E. ZORĘBSKI and S. ERNST, *Ultrasonic velocity, molar volume and internal pressure and their correlation with association and molecular interactions in binary liquid mixtures*, Proc. of World Congress on Ultrasonics, Berlin 1995, p. 141.

[21] S. ERNST, R. MANIKOWSKI, W. MARCZAK, E. ZORĘBSKI and M. ZORĘBSKI, Akust. Molek. Kwant., **12**, 65 (1991).

[22] S. ERNST, W. MARCZAK, R. MANIKOWSKI, E. ZORĘBSKI and M. ZORĘBSKI, Acoust. Lett., **15**, 7, 123 (1992).

[23] S. ERNST, W. MARCZAK and R. MANIKOWSKI, Acoust. Lett., **16**, 8, 177 (1993).

[24] K. BEBEK and S. ERNST, Arch. Acoust., **15**, 3-4, 239 (1990).

[25] J.D. PANDEY, N. PANT and B.R. CHATURVEDI, Chem. Scripta, **18**, 224 (1981).

[26] I.L. ACEVEDO, G.C. PEDROSA and M. KATZ, J. Sol. Chem., **19**, 9, 911 (1990).

[27] V. RAJENDRAN, Ind. J. Pure & Appl. Phys., **31**, 812 (1993).

[28] W. SCHAAFFS, *Molekularakustik*, Springer Verlag, Berlin 1963, s. 253.

[29] S. ERNST and J. GLIŃSKI, Acustica, **48**, 109 (1981).

[30] K. TAMURA, K. OHOMURO and S. MURAKAMI, J. Chem. Thermodyn., **15**, 859 (1983).

[31] A. WEISSBERGER, *Technique of organic chemistry*, VII, Interscience Publishers, London 1955.

[32] J.A. RIDDICK and W.A. BUNGER, *Organic solvents*, 3rd Edn., Wiley, NY 1977.

[33] H. OGAWA and S. MURAKAMI, J. Sol. Chem., **16**, 4, 315 (1987).

[34] K. MALAKONDAIAH, V. HYDER KHAN and S.V. SUBRAHMANYAM, Indian J. Chem., **16A**, 733 (1978).

[35] A. CABANAS, B. COTO, C. PANDO and J.A.R. RENUNCIO, Ber. Bunsenges. Phys. Chem., **98**, 6, 777 (1994).

ARCHIVES OF ACOUSTICS
25, 3, 377–385 (2000)

LONGITUDINAL AND SHEAR ULTRASONIC MEASUREMENTS IN VEGETABLE OILS

R. PŁOWIEC and A. BALCERZAK

Polish Academy of Sciences
Institute of Fundamental Technological Research
(00-049 Warszawa, Świętokrzyska 21, Poland)

In this paper the results of ultrasonic longitudinal and shear measurements in vegetable oils are presented and discussed. The run of the ultrasonic attenuation suggests a relaxation process at frequencies below 0.5 MHz. Another one is suggested at low temperature in the vicinity of 1 Hz.

1. Introduction

Vegetable oils play an important role in the diet because of their non-cholesterol nutrition properties. The chemical constituents of oils are triglycerides, i.e. esters of glycerol and three fatty acid molecules. The physico-chemical properties of oils are determined principally by the type and amount of triglycerides which they contain and by their thermal and shear histories.

A general chemical model of triglycerides is shown below:

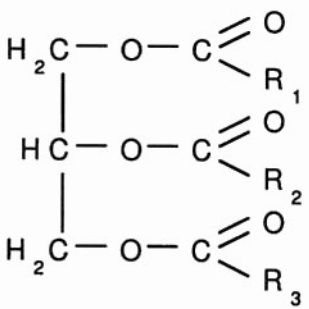

Fig. 1. General chemical model of triglycerides. R_1, R_2, R_3 are the carbon–hydrogen chains.

A variety of techniques have been used to characterise oils, including nuclear magnetic resonance (NMR), refraction measurements (RI), microscopy, X-ray diffraction, density measurements, neutron scattering and differential scanning calorimetry (DSC) [1, 5].

The ultrasonic method was used also to determine the rheological properties of vegetable oils [4, 6]. Ultrasonic spectroscopy has already proved to be a valuable tool for monitoring the dynamic rheology of oils [6] and may have many interesting applications in future in the oil industry. However, the latter is not much interested in the results until now.

The ultrasonic velocity, attenuation of sound and the dynamic viscosity or rheological properties as functions of temperature and frequency are usually measured in oils. The ultrasonic velocities in liquid oils can be related to the concentration of the constituent triglycerides [1]. By measuring the attenuation of longitudinal and shear waves over a wide range of frequencies, it is possible to determine the dynamic bulk and shear moduli as well the viscosities of the oils [6].

It has been proposed that the relaxation of the shear viscosity is due to molecular reorientational changes in the ultrasonic field, whereas the relaxation in the bulk viscosity is due to structural changes [1]. In general, there are two types of motion: viscous movements in which energy is dissipated and elastic deformations without dissipation of energy. In the simplest version of the viscoelastic theory, it is assumed that the viscous and elastic effects may be treated independently and that terms corresponding to the two effects may be added linearly in the equation of motion. Then each relaxation process occurs with a single relaxation time.

In highly viscous oils, such as castor oil, where the interaction between the triglyceride molecules is strong, the bulk and shear viscosities have similar relaxation frequencies, whereas in low viscosity oils, they have different relaxation frequencies [1]. This is probably due to the fact that a strong interaction occurs between the triglycerides in highly viscous oils.

The methods of ultrasonic measurements are typical [2, 4]. The results of ultrasonic measurements of some oils are given below.

2. Theory

The ultrasonic longitudinal waves can be considered as a superposition of pure compression and pure shear. If the period of the sound waves is much longer than the relaxation time of the liquid, the absorption coefficient is [2]

$$\alpha = \omega^2 \eta / 2\rho C^3, \tag{1}$$

where C is the velocity of sound, ω is the frequency, η is the viscosity and ρ is the density.

When the period of the applied stress becomes comparable to the structural relaxation time of the liquid, the attenuation increases rapidly. For a very high alternating stress, the molecules of the liquid do not have time enough to adjust their positions by inelastic (or viscous) movements in the period during which the force is applied, and the molecular motion is that of an elastic deformation. In this region, the viscosity consists of the shear viscosity, η_s, and the bulk one, η_v, and the absorption coefficient is:

$$\alpha = \omega^2 (\eta_s + 4/3\,\eta_v) / 2\rho C^3. \tag{2}$$

The velocity of ultrasonic waves C is connected with the physical properties of the liquid to be measured according to the following equation:

$$C^2 = E/\rho, \tag{3}$$

where E is the elastic modulus and ρ is the density of the liquid. For the longitudinal ultrasonic waves $E = K$, where K is the bulk modulus connected with the adiabatic compressibility. At low temperatures the liquid may have viscoelastic properties; then $E = K + 4G/3$, where G is the shear modulus. Usually all the moduli are complex, i.e. $E^* = E' + jE''$, $K^* = K' + jK''$ and $G^* = G' + jG''$. Shear waves propagate through most solids but they are highly attenuated in liquids and usually do not travel far enough to be detected and measured directly. The shear mechanical impedance is then measured in order to determine the shear modulus.

The shear mechanical impedance ($Z^* = R + jX$) is measured by applying transverse waves. The relation between the mechanical impedance $Z^*_{j\omega}$ and the complex modulus of shear elasticity of a liquid $G^*_{j\omega}$, for the frequency ω is expressed by the equation

$$(Z^*_{i\omega})^2 = \rho G^*_{i\omega}\,, \tag{4}$$

where ρ is the density of the liquid

$$Z^*_{i\omega} = R + iX, \qquad G^*_{i\omega} = G' + iG''. \tag{5}$$

The mechanical shear impedance is determined by measurements of the amplitude reflection coefficient, k, and phase, θ, of the ultrasonic wave on the boundary of two media, i.e. on the boundary between the solid body and the liquid. The mechanical shear impedance of a liquid in the case of a plane wave falling perpendicularly on the boundary surface is

$$Z^*_{i\omega} = Z_Q \frac{1 - k^2 + i2k\sin\theta}{1 + k^2 + 2k\sin\theta}\,, \tag{6}$$

where Z_Q is the impedance of the solid body.

For most of the liquids, the wave phase shift related to the reflection is small, as the impedance of the liquid is $|Z| < 0.1 < |Z_Q|$; therefore, it can be accepted that $\cos\theta = 1$. Then Eq. (6) has the following form:

$$Z^*_{i\omega} \cong Z_Q \left(\frac{1 - k^2}{(1 + k)^2}\right) + i\left(\frac{2k\sin\theta}{(1 + k)^2}\right) = R + iX. \tag{7}$$

The error caused by the assumption $\cos\theta \approx 1$ does not exceed 1%. Using Eq. (8), the real part of the impedance can be calculated if only the amplitude reflection coefficient is known:

$$R = Z_Q \left(\frac{1 - k}{1 + k}\right). \tag{8}$$

Having R and X, the components of the shear modulus of a liquid, $G^*_{i\omega}$, can be determined:

$$G'_\omega = \frac{R^2 - X^2}{\rho}\,, \qquad G''_\omega = \frac{2RX}{\rho} \tag{9}$$

while the dynamic viscosity is expressed by the equation

$$\eta'_\omega = \frac{2RX}{\omega\rho}. \tag{10}$$

The variations of the real and imaginary components of G^*, η^* and Z^* as functions of the normalised frequency are shown in Fig. 2.

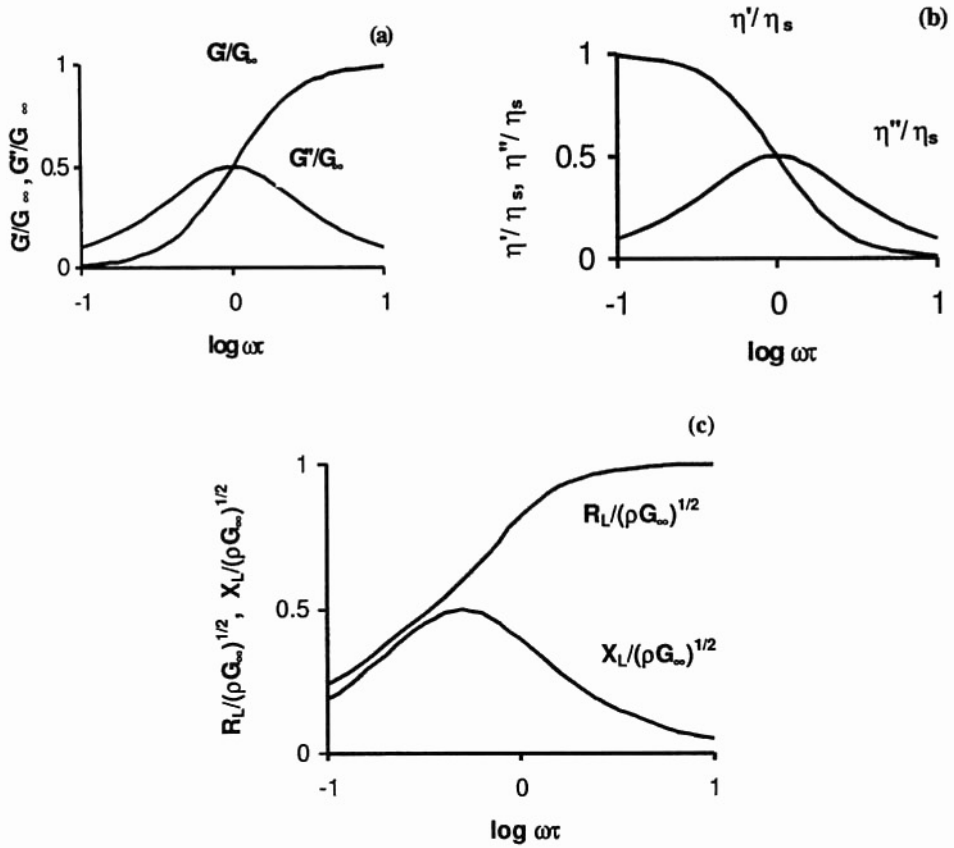

Fig. 2. Variation with frequency of the normalised components of a) the rigidity modulus, b) the dynamic viscosity, and c) the shear mechanical impedance for a single relaxation process [2].

3. Results

Vegetable oils are an interesting object for the investigation of the dynamic viscosity properties because the absorption of longitudinal ultrasonic waves in them has been studied over a wide frequency range, so that with the available data on the shear viscosity it is possible to separate the pure bulk viscosity from the attenuation coefficient.

Our measurement results are reported below and compared with the results of other authors. The chemical components of the rapeseed oil produced by Polish refinery [3] are:

acid	formula	contents in rapeseed oil, % raw	refined
Palmitic	$CH_3(CH_2)_{14}COOH$	5.1	4.9
Oleic	$CH_3(CH_2)_7CH{=}CH(CH_2)_7COOH$	61.8	61.4
Linoleic	$CH_3(CH_2)_4CH{=}CH{-}CH_2{-}CH{=}CH(CH_2)_7COOH$	19.9	20.6
Linolenic	$CH_3(CH_2{-}CH{=}CH_2)_3CH_2(CH_2)_6COOH$	9.2	9.0

The chemical components and specific gravities for edible oils are shown in Table 1 [4].

Table 1. Chemical components (%) and specific gravity (g/cm^3) of edible oils.

	Oil			
Acid	Safflower	Soybean	Peanut	Rapeseed
Myristic	trace	trace	trace	trace
Palmitic	8.8	12.1	13.2	11.3
Palmitoleic	trace	trace	trace	trace
Stearic	3.1	3.7	4.1	4.0
Oleic	14.0	21.0	30.1	21.8
Linoleic	73.6	53.2	44.9	53.4
Linolenic	0.3	7.7	3.8	8.0
Arachidic	—	—	0.7	—
Others	0.2	2.2	3.2	1.5
Specific gravity	0.914	0.913	0.912	0.915

The viscosity of the rapeseed oil measured with an Ubbelohde viscometer as a function of temperature is shown in the Fig. 3. The changes in the ultrasonic velocity for rapeseed oil as a function of frequency are shown in Fig. 4.

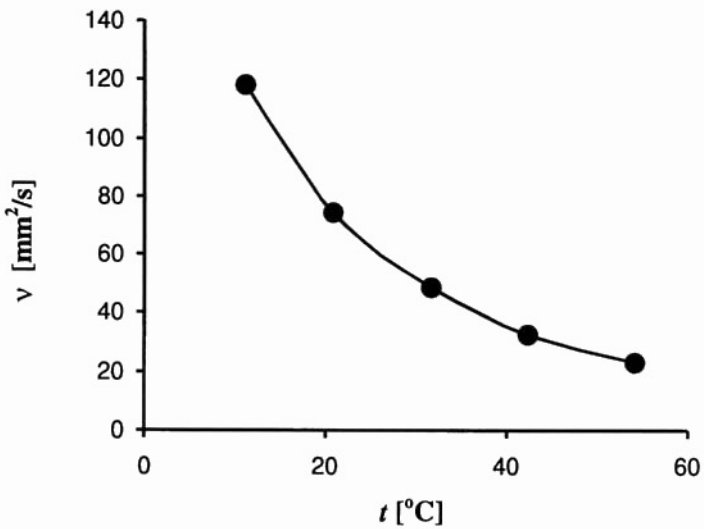

Fig. 3. Viscosity of rapeseed oil vs temperature.

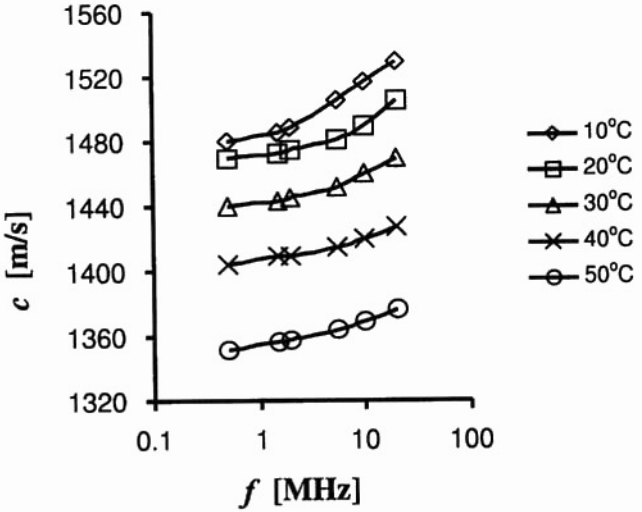

Fig. 4. Velocity of rapeseed oil vs. frequency.

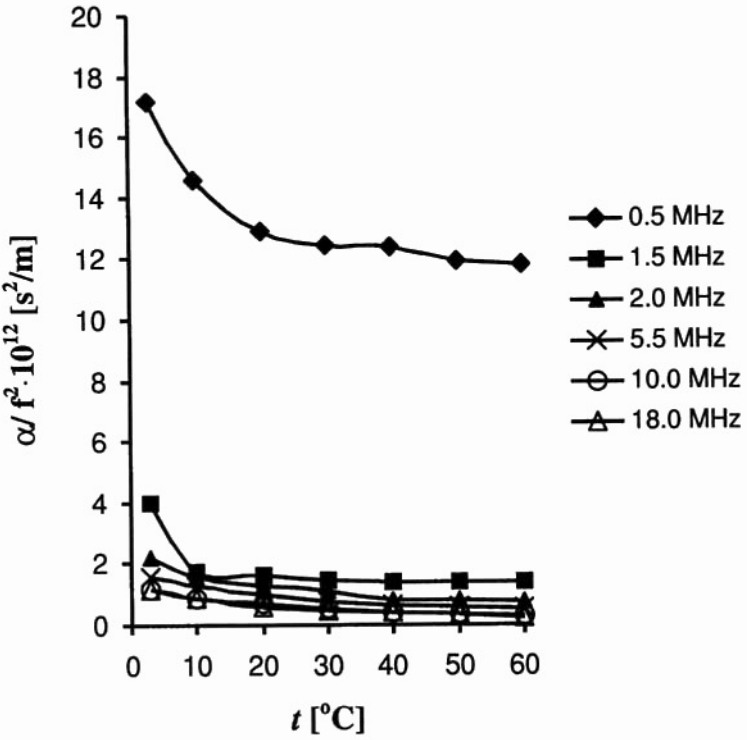

Fig. 5. Ultrasonic attenuation of rapeseed oil vs. temperature.

Many measurements of the ultrasonic velocity in liquids and their temperature dependencies have been reported [7]. In a wide range of liquids, the ultrasonic velocity decreases linearly with increasing temperature over a considerable range of temperature. Deviations from this linear relation occur near the boiling points and the melting points of the liquids, so that an extrapolation of the measured ultrasonic velocities from higher temperatures to the melting point can lead to errors of the order of -2 to -6%. In most of the edible oils, the coefficient dC/dT is close to -3 to -3.4 [1]. The same linear dependence was found for the rapeseed oil.

Considerable changes in ultrasonic attenuation with frequency between 0.5 and 18 MHz are observed in rapeseed oils (Figs. 5 and 6).

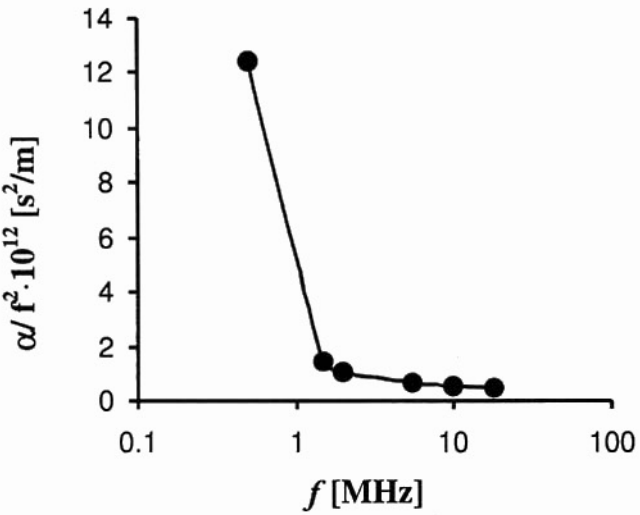

Fig. 6. Ultrasonic attenuation of rapeseed oil vs. frequency. Temperature 30° C.

The run of the attenuation of ultrasonic waves in the rapeseed oil (Fig. 6) measured as a function of frequency suggests a relaxation process at frequencies lower than 0.5 MHz, for which our measurement method can not be applied. The measurements of rapeseed oil performed with DMTA technique [5, 8] using a torsional rheometer signal suggest the possibility of a relaxation process at frequencies around 1 Hz within the temperature limit — 30°C and 0°C.

The shear modulus measured in those temperatures is rather low (circa 30 MPa) and in this range the scale of the equipment was not very accurate. The change of the shear modulus as a function of frequency is shown in Fig. 7a. The curve in Fig. 7b shows the change of the loss angle ($\tan\delta = G''/G'$) and supports the suggestions of a second relaxation process in this range.

The frequency dependence of the dynamic shear viscosity, shear elasticity and effective viscosity in castor oil is shown in Fig. 8.

The shear elasticity measurements of castor oil as a function of frequency show also rather low values and have not been determined within the low frequency range [6].

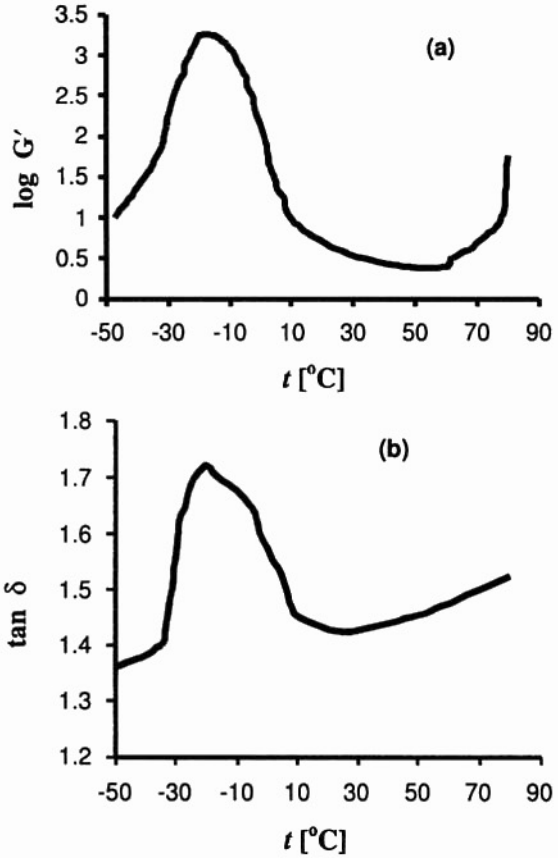

Fig. 7. Changes of the shear modulus (a) and the tan of loss angle (b) vs. temperature for rapeseed oil.

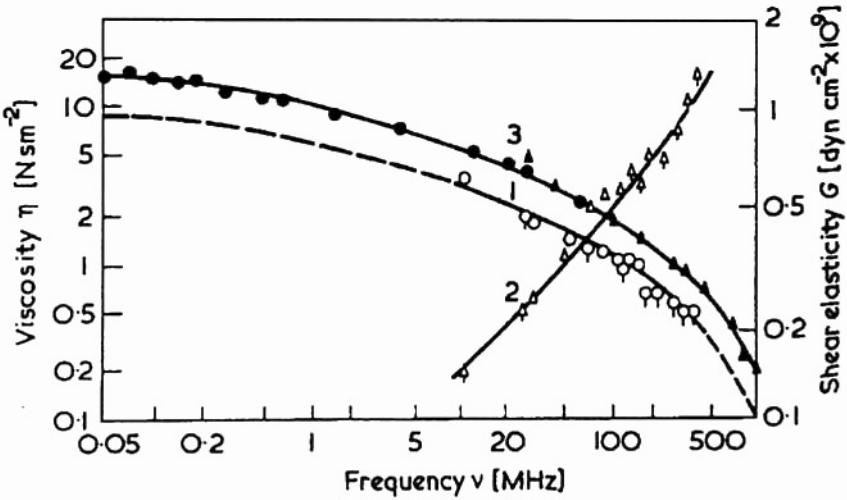

Fig. 8. Frequency dependence of the dynamic shear viscosity (1), shear elasticity (2) and effective viscosity (3) in castor oil [6].

4. Conclusions

The ultrasonic measurements increase the information on vegetable oils because they allow to determine the shear modulus and its changes as a function of temperature, while the attenuation measurements allow to determine the dynamic shear and bulk viscosities and the relaxation processes in oils, and to measure its frequency. Thus the ultrasonic measurements allow to determine the physico-chemical and dynamic properties of vegetable oils.

References

[1] D.J. McClements and M.J.W. Povey, Ultrasonics, **30**, 383 (1992).

[2] R. Płowiec, *Viscosity and elasticity of liquids measured by means of ultrasonic shear waves* [in Polish], PWN, Warszawa – Poznań 1990.

[3] Warsaw Plant of Fatty Industry, Warsaw, Poland.

[4] H.L. Kuo, Jap.J. Appl. Phys., **10**, 167 (1971).

[5] R.E. Wetton, *Developments in polymer characterisation*, Applied Science Publishers, London, 1986, Chap. 5.

[6] I.G. Mikhailov, Yu.S. Manutcharov and O. Khakimov, Ultrasonics, **13**, 66 (1976).

[7] W. Schaaffs, *Molekularakustik*, Berlin – Goettingen – Heidelberg 1962.

[8] R. Płowiec, A. Balcerzak and M. Kurcok, Molecular and Quantum Acoustics, **19**, 217 (1998).

ARCHIVES OF ACOUSTICS
25, 3, 387–392 (2000)

THE INFLUENCE OF GLASS ON THE AIRBORNE SOUND INSULATION OF WINDOWS

J. ZAJAC

Slovak Technical University
Faculty of Civil Engineering
(Bratislava, Slovakia)

From the viewpoint of acoustics, the window is a rather complicated structure and its sound insulation depends upon numerous designing modifications, some of which are of decisive importance. They include glazing, infiltration, the window frame with fixed glass and the window structure itself.

1. Analysis of window desing

From the viewpoint of acoustics, the window is a rather complicated structure and its sound insulation depends upon numerous designing modifications, some of which are of decisive importance. They include glazing, infiltration, the window frame with fixed glass and the window structure itself.

The window structure consists of elements with different acoustic properties and places of contact among the window structural elements. The transition of noise through a window can be classified as follows:

— sound transmission through the glazed area,
— sound transmission through the window frames and wings,
— sound transmission through joints and gaps.

The desing of a window structure corresponding with the basic acoustic evaluation criteria results from the following relation:

$$R_{\mathrm{wo}} = R_{\mathrm{woz}} + \Delta R_{\mathrm{woz}} - \Delta R_{\mathrm{wo\check{s}}} \pm \Delta R_{\mathrm{wor}}\,, \tag{1}$$

where R_{woz} is the sound insulation index of the glass (dB), ΔR_{woz} is the increase resulting from the window desing modifications (dB), $\Delta R_{\mathrm{wo\check{s}}}$ is the decrease resulting from the joints and gaps (dB), ΔR_{wor} is the increase and decrease resulting from the frames and wings (dB).

1.1. Sound transmission through the glazed area

Glass makes 70–80% of a window area (depending upon its surface, frame and wing design) and in general is the decisive element of the window acoustics properties.

Due to its low basis weight, the glazed surface is a thin plate whose sound insulation has numerous negative properties such as resonance and coincidence, depending on frequency. The resonance effect is obvious at low frequencies and at a glass thickness less than 4 mm sound insulation decreases often in the sound insulation area. With glass of thickness below 4 mm, the effect of coincidence is outside the sound insulation sphere.

In the frequency course R (dB) of glass of a thickness above 4 mm the effect of resonance is suppressed at low frequencies. The lowest resonance frequencies are outside of the sound insulation sphere. At higher frequencies, the sound insulation decreases due to the coincidence.

1.2. Single or double glass

Based upon experimental measurements (Measurements were performed by STU SvF Bratislava – acoustic laboratories and the Centre for Civil Engineering, Prague and Zlin [1–5, 9, 10], in accordance with ISO 140-1 and ISO 140-3, the sample glass thickness was 480 mm, weigt 1800 kg · m^{-3} with $R_w = 52$ dB, the window was placed asymetrically with the distance more than 500 mm from the floor, ceiling and walls, the window jamb was lined by material with absorptance less than 0.1, the rough jamb dimensions usually used in Slovakia is 1200/1200 mm) of sound insulation of sample windows with single or double glass of various thickness (weight) and distance between the glass layers, the following relationship for R_{woz} (dB) has been derived:

$$R_{\mathrm{woz}} = 26.4 + 14 \log d/d_0 + 24 \log h/h_0 \ \ (\mathrm{dB}), \tag{2}$$

where d is the distance between the glass layers in mm ($d = 10 - 200$ mm), $h = h_1 + h_2$ is the thickness of the first and second glass layers (from the interior) in mm ($h = 6 - 14$ mm), d_0, $h_0 = 10$ mm.

Basing upon experimental measurements, the following glass thicknesses has been chosen:

$h_1 \geq 1.5$ to $2h_2$ for the insulation double glass,

$h_1 \geq 1.5$ to $2h_2$ for the double and coupled windows.

Different glass thicknesses result in the suppression of the resonance and coincidence effects. Thicker glass shows higher sound insulation from the exterior side and makes up a barrier for noise from outside, the inner glass, due to lower weight, emits less sound energy.

For a glass system in that the air gap between the glass layers is joined with the outside environment and makes a de-compression cavity, from the viewpoint of sound insulation it is better to have an inner glass of higher thickness (weight).

It can be stated that

— for a larger gap between the glass layers d (mm), R_{woz} increases,

— for a higher glass thickness, R_{woz} increases.

Beside acoustic requirements, a glazed system must also meet thermal engineering requirements. They have therefore to be considered when designing the distance between the glass layers.

1) PVC window with double glass 4/16/4 Planitherm $R_w = 33\,\mathrm{dB}$
2) Wooden window with doubles glass 9/12/6 $R_w = 37\,\mathrm{dB}$
3) Wooden window with triple glass 4/8/4/8/4 $R_w = 32\,\mathrm{dB}$

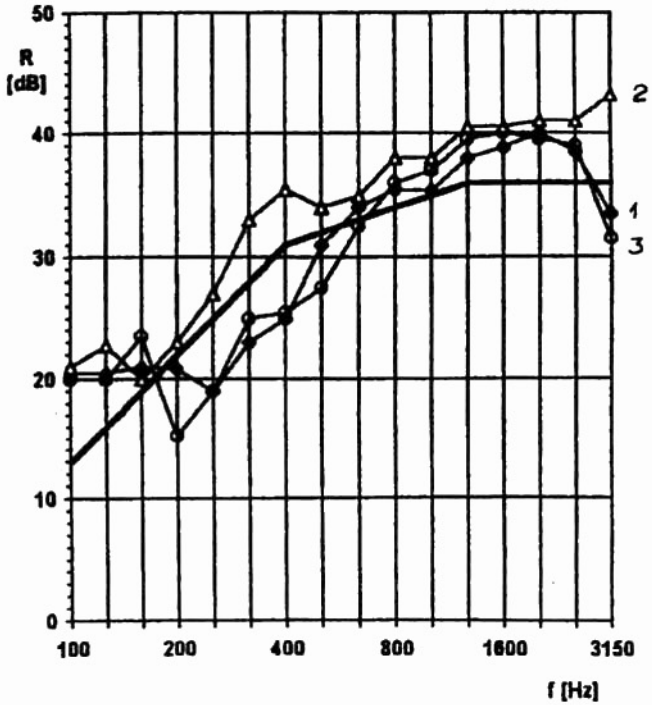

Fig. 1. Results of meassuring.

1.3. Multiple glass

The energy requirements related to the window quality require multiple glazing. The adding of another glass layer results in increased glazing weight and sound insulation, correspondingly. The sound insulation improvement will not be very high — adding another glass divides the air gap into two narrower spaces whose resonance frequency causes reduction at low and medium frequencies. The effect of the higher glazing weight will be obvious at high frequencies.

Experimental measurements of glazed systems indicate that from the viewpoint of acoustics it is better to use two glass layers of different thickness than a triple glazing of equal weight (factory produced triple glazing).

The use of multiple glass is reasonable

— if the gaps between the glass layers are different $d_1 \geq 3d_2$ (mm),

— if the gap is wider $d_1 \geq 50\,\mathrm{mm}$,

— if glass thicknesses are highly different, the following glass thicknesses are suitable: $h_1 \geq h_3$ and $h_2 \geq 1.5 - 2h_3$,

Department of Building Structures, Faculty of Civil Engineering, Slovak University of Technology, Radlinského 11, SK-81368 Bratislava

Composition of tested specimen:

Plastic window with thermal insulated double glazing

composition of double glazing: 9 + 16 +6 (mm)

KONTRANITTERM+AR.KW31/44/1,3

Protocol No.: A30-2/98

Specimen: No.2

Customer: Lignotesting a.s.
Lamačská cesta č.1
841 05 Bratislava

Date of adoption: 9.12.1998

Date of testing: 21.12.1998

Testing method: STN 730516

Acoustic chambers:

Receiving chamber: Volume V= 57 m^3

Sending chamber: Volume V= 53 m^3

Testing sound: noise generator

Filters: 1/3 of octave

Testing area: S = 1,4 m^2

Tested specimen:

Name: Plastic window

Dimensions: 1180x1180 mm

Weight related to the area: 43.6 kgm^{-2}

Measurement conditions:

Temperature: 20 °C

Pressure: 997 mB

Relative humidity: 33 %

Air sound insulation STN 730513
Air sound insulation index:
R_{W1} = 37 dB
R_{W2} = 38 dB

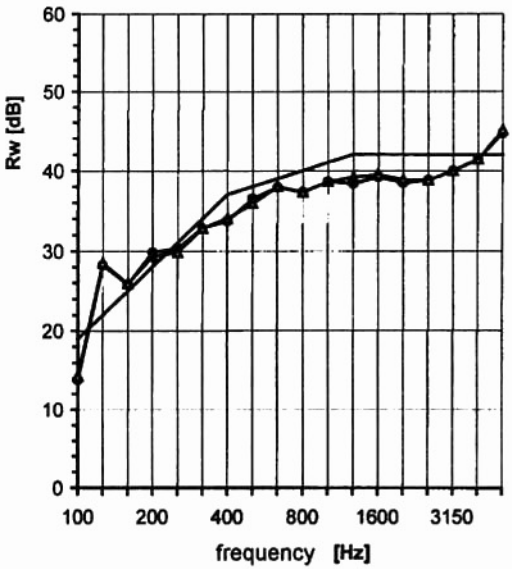

Date: 7.1.1999

Measured by: Mgr.Daniel Szabó

Approved by: Prof.Ing.Jozef Zajac,DrSc.

Fig. 2. Measure protocol.

Building Acoustics Analyzer B&K 4418

RECORD NO. 325
OPTION NO. 93

NRM. LEVEL DIFF.
V= 57 S= 1.4

HZ CODES	DB
100	13.8
125	28.2
160	25.8
200	29.8
250	30.3
315	32.8
400	33.7
500	36.5
630	37.9
800	37.3
1000	38.6
1250	38.4
1600	39.2
2000	38.5
2500	38.8
3150	40.0
4000	41.4
5000	44.7
6300	44.8
8000	46.2

RECORD NO. 326
OPTION NO. 93

NRM. LEVEL DIFF.
V= 57 S= 1.4

HZ CODES	DB
100	14.3
125	28.5
160	25.9
200	29.3
250	29.8
315	32.8
400	34.0
500	35.9
630	38.0
800	37.3
1000	38.6
1250	39.2
1600	39.5
2000	38.9
2500	38.8
3150	40.0
4000	41.4
5000	45.1
6300	44.7
8000	46.4

Fig. 3.

— for insulation double glass design,

— for glazing with a pre-set glass and with a insulation double glass, whereas d_i = gap width and h_i = glass highness.

Insulation double glass is used from the interior side, as the space between the pre-set glass and insulation double glass makes a de-compression cavity.

1.4. Desing modifications of glazing

a) It is good to use a noise absorbent along the air gap circumference:

— At a larger distance between the glass layers.

— The noise absorbent use is governed by functional possibilities valid for the desing of the absorbing lining.

— The R_{woz} (dB) increase along the air gap circumference resulting from the of noise absorbent is +2 to +3 dB, [11, 12].

b) Desing of separate window frames:

— The decrease of the noise insulation is influenced by the glazing and mounting.

— Depends upon the shape and number of window wings, and the way of joining the wings and frames of coupled and doubled windows.

c) Gas filled insulation double glass:

— In heavy gases, sound propagates at a lower rate.

— In the gas filling, forced oscillation does not occur so easily, and thereby, its level is lower.

d) Thermo-insulating double glass

— The glazed system weight increases, and thus the resonance at low frequencies will be suppressed.

e) Glass mounting

— Elastic mounting increases the transfer of sound waves of high wavelength, therefore the sound insulation decreases at low frequencies.

— With fixed glazing, the sound insulation decreases at medium and high frequencies.

— The glazing materials used at present do not affect the acoustic parameters significantly.

References

[1] J. ZAJAC, *Window and the quality of living*, 11th International Conference on Noise Control '98, Krynica, In.Zb., 477–482.

[2] J. ZAJAC, *Pohoda interiéru s normovými požiadavkami* [in Slovak], 57. Akustický seminár ČR '98, In. Zb., 93–96.

[3] J. ZAJAC, *Pokles indexu vzduchovej nepriezvučnosti R_w vplyvom dĺžky škáry* [in Slovak], Konferencia 60. Cýročie SvF STU Bratislava 1998, In. Zb., 158–161.

[4] J. SCHWARZ and M. MĚLLER, *Návrh a overenie aproksimačných metód pre stanovenie doby dozvuku* [in Czech], 57. Akustický Seminár ČR 1998, In. Zb., 47–54.

[5] M. MIROWSKA, *The influence of low frequency noise on the healt of exposed inhabitans*, 11th International Conference on Noise Control '98, Krynica, In. Zb., 289–296.

[6] J. ZAJAC, *Ochrana proti hluku a jej zlepšenie v obytných domoch* [in Slovak], Coneco '97 Bratislava, SR In. Zb., 45.

[7] J. ZAJAC, *Vplyv škáry na nepriezvučnosť* [in Slovak], 50. Akustický Seminár, ČR 1995, In. Zb., 257–261.

[8] J. ZAJAC, *Interakcia stykovej škáry a vzduchovej nepriezvuçnosti* [in Slovak], Coneco '95 Bratislava, In. Zb., 24–25.

[9] J. ZAJAC, *Einfluss der Schwartentiefe auf akustische Eigenschaften ausgewählter Schwartenrepresentanten*, 17th AICB Congres Prague 1992, In. Zb., 424–429.

[10] J. ZAJAC, *The interaction of loggia envelopes and in door enviroment*, Traffic Effects on Structures and Enviroment — TESE '94 The High Tatras 1994, In. Zb., 177–181.

[11] Laboratory measurement results, Faculty of Civil Engineering, Bratislava, Slovak Republic.

[12] Laboratory measurement results, Centre for Civil Engineering, Prague and Zlin, Czech Republic.